COMILLAS
UNIVERSIDAD PONTIFICIA
ICAI

GRADO EN INGENIERÍA EN TECNOLOGÍAS INDUSTRIALES

TRABAJO FIN DE GRADO

STUDY OF AERODYNAMIC BEHAVIOR OF DIFFERENT TYPES OF VEHICLE BEHIND WINDBREAK FENCES UNDER CROSSWIND

Autor: Íñigo Andrés Tagliavia Ramírez

Director: Paolo Schito

Madrid

Julio de 2020

Declaro, bajo mi responsabilidad, que el Proyecto presentado con el título

Study of aerodynamic behavior of different types of vehicle behind windbreak fences under crosswind

en la ETS de Ingeniería - ICAI de la Universidad Pontificia Comillas en el curso académico 2019/2020 es de mi autoría, original e inédito y no ha sido presentado con anterioridad a otros efectos. El Proyecto no es plagio de otro, ni total ni parcialmente y la información que ha sido tomada de otros documentos está debidamente referenciada.

Fdo.: Iñigo Andrés Tagliavia Ramírez Fecha: 24 / 07 / 2020

Autorizada la entrega del proyecto

EL DIRECTOR DEL PROYECTO

Fdo.: Paolo Schito Fecha: 24 / 07 / 2020

COMILLAS
UNIVERSIDAD PONTIFICIA
ICAI

GRADO EN INGENIERÍA EN TECNOLOGÍAS INDUSTRIALES

TRABAJO FIN DE GRADO

STUDY OF AERODYNAMIC BEHAVIOR OF DIFFERENT TYPES OF VEHICLE BEHIND WINDBREAK FENCES UNDER CROSSWIND

Autor: Íñigo Andrés Tagliavia Ramírez

Director: Paolo Schito

Madrid

Julio de 2020

Acknowledgements

I would like to thank my project supervisor Paolo Schito for guiding me in this work during this very complicated year and teaching me that important branch of engineering that is aerodynamics.

ESTUDIO DEL COMPORTAMIENTO AERODINÁMICO DE DIFERENTES TIPOS DE VEHÍCULOS TRAS VALLAS CORTAVIENTOS BAJO VIENTO CRUZADO

Autor: Tagliavia Ramírez, Íñigo Andrés.
Director: Schito, Paolo.
Entidad Colaboradora: ICAI – Universidad Pontificia Comillas, Politecnico di Milano

RESUMEN DEL PROYECTO

1. Introdución

Según la DGT, el viento es la tercera causa de accidentes por mal tiempo en España, causando un total de 270 accidentes y 30 muertes por año. Pero estos datos son de los accidentes en los que el viento se considera la principal y única causa, ya que si consideramos los accidentes relacionados con el viento, como las situaciones con viento y lluvia o con viento, nieve y niebla, las cifras son mucho mayores. Según datos de (Edwards 1999) en el Reino Unido, el 3,7% de los accidentes anuales están fuertemente relacionados con el viento, lo que significaría unos seis mil accidentes anuales causados por el viento.

El viento en la carretera es un peligro real, ya sea una ligera ráfaga de viento, que en presencia de un conductor desprevenido puede hacer que el vehículo se mueva de lado con el riesgo que ello conlleva y pueda producirse un accidente, o una fuerte ráfaga de viento capaz de volcar un camión.

Los traumatismos causados por el tránsito son un problema de salud pública mundial. Según datos de la Organización Mundial de la Salud, 1,3 millones de personas mueren en las carreteras cada año y entre 20 y 50 millones de personas sufren lesiones no mortales.

Más allá de los daños humanos inmediatos causados por los vehículos de carretera que acabamos de comentar, el sector del transporte, según los datos de la AEMA de 2016, es el que más contribuye a las emisiones de gases de efecto invernadero en la UE, generando el 27% de las emisiones, lo que supone 1205 millones de toneladas de CO2 equivalente, siendo los coches y las furgonetas responsables de la mitad de estas. Y el viento cruzado, además de la evidente fuerza lateral que provoca en el vehículo, aumenta la fuerza de arrastre con respecto a la que se tendría con el viento totalmente de frente cuando este impacte en el vehículo con un ángulo mayor de 0° a 30°. Esto se traduce directamente en un mayor consumo de combustible, que también se ve incrementado por la fuerza lateral debido a la necesidad de estar rectificando constantemente la trayectoria del vehículo que lucha contra este viento. Por lo tanto, dado que la reducción de las emisiones de gases de efecto invernadero es una prioridad urgente a nivel mundial, también debe considerarse y estudiarse cualquier solución que pueda mejorar esta situación.

Por lo tanto, en vista de la necesidad de resolver estos dos problemas a nivel mundial, y entendiéndolos como un gran desafío para la ingeniería, este trabajo presentará lo que podría disminuir las cifras que se acaban de presentar, las vallas cortavientos.

Durante este Proyecto se tratará de desarrollar una barrera contra el viento que colocada a un lado de la carretera será capaz de proteger cualquier tipo de vehículo de la acción del viento cruzado, y sus fatales consecuencias. Aunque la prioridad de la investigación será reducir las fuerzas laterales a las que se ve sometido un vehículo por el viento, y su riesgo de desplazarse lateralmente o incluso de volcarse, también se tratará de desarrollar estos cortavientos de manera que sean capaces de reducir al máximo la fuerza de arrastre del vehículo.

Las prioridades del sector de la aerodinámica del automóvil a lo largo de su historia han sido: limitar la resistencia del aire frontal, ya sea en la búsqueda de eficiencia o en la búsqueda de mayor velocidad, y, en el caso de los vehículos de competición, aumentar su adherencia.

Pero obviamente hay otra fuerza causada por el viento en un vehículo, la fuerza lateral. Desde hace algunos años, esta acción del viento cruzado sobre los vehículos ha sido estudiada más a fondo, aunque solo sea de forma académica, siendo más extenso su estudio en los trenes que en los vehículos de carretera.

El principal objeto de estudio en esta área es la preocupación por el efecto que el viento lateral puede tener sobre los vehículos pesados en zonas muy expuestas a estas fuertes ráfagas de viento, como viaductos y terraplenes.

En los trabajos de (Cheli, Corradi, et al. 2011) y (Cheli, Ripamonti, et al. 2011) se estudian en profundidad las cargas inducidas por el viento transversal desde un ángulo de incisión de 0° a uno de 90° en un túnel de viento para vehículos pesados de carretera, estudiando este fenómeno para un vehículo en un terreno plano y para vehículos en zonas de alta exposición como viaductos o terraplenes. Una vez realizados numerosos estudios sobre el comportamiento aerodinámico de los vehículos pesados de transporte por carretera, se ha comenzado a estudiar también el peligro que corren estos vehículos ante las estelas de viento que pueden generar elementos estructurales, como los pilones de los puentes, que pueden provocar estelas turbulentas que pueden generar un riesgo para estos vehículos, como se ha desarrollado en (Salati, et al. 2018).

Una vez conocidos y estudiados los riesgos de seguridad que puede provocar el viento cruzado en los vehículos, especialmente los pesados y de gran superficie lateral, se ha buscado una solución a este fenómeno, y es aquí donde aparecen las barreras de viento en el campo automovilístico. El trabajo (Alonso-Estébanez, et al. 2017) trata de encontrar la mejor configuración posible (geometría, porosidad, distancia y altura) para una barrera de viento cuya tarea es proteger un camión de los vientos laterales mientras está parado. Este trabajo profundiza en el desarrollo de las barreras de viento introduciendo para ello una geometría diferente, con placas que forman un ángulo con la vertical, además de las convencionales con zonas abiertas en forma de agujeros circulares y rectangulares. Por lo tanto, esta investigación será tomada como referencia para el desarrollo de las vallas.

Lo que se pretende con este Proyecto es marcar la diferencia con lo que ya se ha hecho en esta área de estudio, es estudiar diferentes geometrías y configuraciones para barreras de viento como (Alonso-Estébanez, et al. 2017), pero para diferentes ángulos de ataque del viento que puedan simular situaciones reales, ya que la mayoría de los estudios realizados hasta la fecha se realizan con un ángulo de ataque de 90° respecto a la trayectoria del vehículo, lo que supondría un vehículo parado, caso que no merece estudio. Además de las diferencias mencionadas anteriormente, este trabajo pretende estudiar la acción de los vientos cruzados y la eficacia de las barreras de viento no solo en los vehículos más expuestos (grandes vehículos pesados), sino en todos los vehículos que se encuentran en la carretera. Por lo tanto, se ha decidido probar un camión, un coche y una motocicleta, los tres grupos de vehículos más comunes en la carretera.

Por último, otra gran diferencia que se pretende con respecto a los estudios anteriores es analizar el beneficio que pueden tener las barreras de viento en la fuerza de arrastre que experimentan los vehículos debido al viento, y comprobar así los beneficios que pueden tener las barreras de viento en cuanto al consumo de combustible.

2. Metodología

Para llevar a cabo el estudio aerodinámico que se pretende para comprender el comportamiento que tienen diferentes tipos de vehículos ante el viento cruzado y el desarrollo del diseño de una valla

cortavientos se usará la tecnología de las simulaciones CFD a traves del software de código abierto OpenFoam. En este trabajo se simularán diferentes casos de ángulo de ataque del viento entre 10° y 50° para tres tipos de vehículos, un camión, una motocicleta y un coche. El camión que se utilizará será una réplica del usado en (Cheli, Corradi, et al. 2011), trabajo que se usará para la validación del modelo numérico, la geometría de la moto se extraerá del repositorio de OpenFoam y el coche será el modelo DrivAer desarrollado por la Universidad Técnica de Múnich.

Para el desarrollo del prototipo final de valla de viento se estudiará la influencia de cada variable a la hora de diseñar este tipo de vallas en su eficiencia para proteger el camión de la acción del viento, donde se buscará poder anular el coeficiente de momento (de balanceo o vuelco) y el coeficiente fuerza lateral y reducir el coeficiente de resistencia aerodinámica. Las variables a estudiar serán la de la geometría de la valla, su porosidad, su altura, su distancia respecto al vehículo y la efectividad de la incorporación de un deflector en lo alto de la valla y la influencia del ángulo de este deflector.

Las geometrías de valla que se van a estudiar están basadas en las estudiadas en (Alonso-Estébanez, et al. 2017):

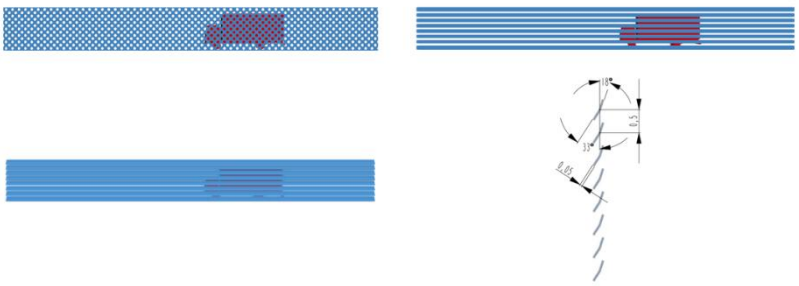

Figura 1: Geometrías de las vallas.

Para resolver las simulaciones CFD se utilizará el solucionador de OpenFoam simpleFoam, ya que se simularán flujos incompresibles en régimen estable, además para resolver las ecuaciones de RANS se van a incluir las dos ecuaciones del modelo turbulencia SST k-omega, por su buen funcionamiento en casos de bajo número de Reynolds y gradientes adversos de presión.

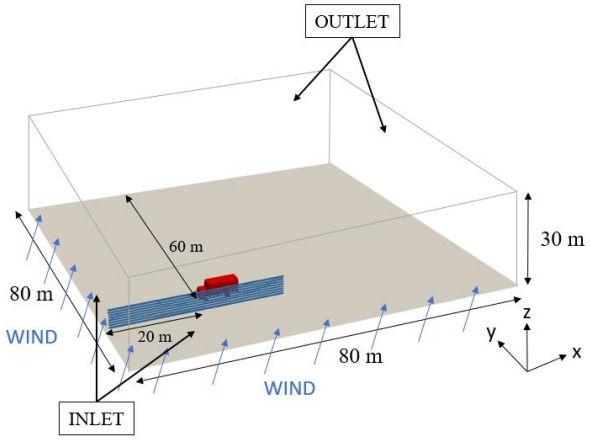

Figura 2: Dominio comupacional.

El dominio computacional será el mostrado en la Figure 2, donde el largo y ancho de este dominio se han fijado, acorde con el estudio bibliográfico que se ha realizado, en diez veces el largo del camión y el alto en ocho veces la altura del camión, para así conseguir un dominio lo suficientemente grande como para que se desarrolle plenamente la estela provocada por el camión y la valla y que las condiciones de contorno impuestas no influencien en los resultados numéricos. Siendo las condiciones de contorno las siguientes:

- ENTRADAS: Flujo con velocidad fija y ángulo de ataque.
- SALIDAS: Una condición de contorno entrada-salida.
- CAMIÓN: Condición de no deslizamiento.
- VALLA y PARED INFERIOR: Velocidad fija igual a la del vehículo en el eje x.
- PARED SUPERIOR: Condición de deslizamiento.

Para el mallado del dominio y las geometrías se usará la utilidad de OpenFoam SnappyHexMesh, y se hará una malla diferente para cada ángulo de ataque de viento.

Una vez mallados los casos se ha validado exitosamente el modelo numérico de cada vehículo utilizando como referencias (Cheli, Corradi, et al. 2011) para el modelo del camión, (Fintelman, et al. 2015) para la motocicleta y (Heft, Indinger and Adams 2012), (Heft, Indinger and Adams 2012) y (Peters, et al. 2015) para la validación del modelo del camión.

Una vez validado el modelo se ha comenzado el desarrollo del prototipo de valla cortavientos.

3. Resultados y conclusiones

A la hora de desarrollar la valla cortavientos se ha centrado este trabajo en optimizar esta para la protección del camión, ya que se ha hipotizado que si una valla es capaz de proteger del viento cruzado al vehículo más voluminoso también será capaz de proteger del a vehículos de menores dimensiones.

En primer lugar se ha estudiado la influencia que tienen la geometría y la porosidad en la efectividad de la valla cortavientos, donde se ha podido concluir que no existe una geometría idónea para reducir los coeficientes de momento y fuerza lateral del vehículo sino que para cualquier geometría se puede encontrar la porosidad para la cual estos coeficientes se ven anulados. En este trabajo se ha optado por elegir la valla con aperturas rectangulares, ya que para una porosidad del 20% reduce hasta casi hacer despreciables estos coeficientes para cualquier ángulo de guiñada y además es la geometría más capaz de reducir el coeficiente de resistencia al aire, por lo que, como lo que se busca era encontrar una valla capaz de proteger al camión del viento cruzado para cualquier ángulo de ataque esta ha sido la elegida.

Tras este estudio sobre la geometría y la porosidad se ha estudiado la influencia que tienen en el comportamiento aerodinámico del camión la altura de la valla y la distancia de la valla al camión, estudio en el que se ha visto que a mayor altura se consigue una mayor protección en las fuerzas laterales que experimenta el vehículo ante la acción del viento para cualquier ángulo de ataque, y en cuanto la distancia entre valla y vehículo se ha podido comprobar que el comportamiento al variar este parámetro no es el mismo para todos los ángulos de ataque, sino que para ángulos medios y grandes (30° y 50°) a mayor distancia se consigue una mayor protección, y en cambio para ángulos pequeños (10°) a menor distancia se produce una mayor reducción de las fuerzas laterales. Este estudio se ha realizado para alturas de dos, tres y cuatro metros y para distancias entre valla y camión también de dos, tres y cuatro metros, utilizando una valla opaca, ya que esta es el punto en común entre las tres geometrías de valla presentadas. Rápidamente se ha podido descartar la valla de 2 m de altura al no ser suficiente para reducir notablemente los coeficientes de momento y fuerza lateral, y también se ha comprobado que la mejor opción en cuanto a distancia es la de 3 m, por lo que la decisión final ha estado entre la elección de la valla de 3 m y la de 4 m. La gran ventaja de la valla de 3 m opaca era que pese a reducir en menor medida los coeficiente de momento y fuerza lateral era

más capaz de reducir el coeficiente de resistencia aerodinámica del camión, pero al comprobar este suceso para una valla con aperturas rectangulares y un 20% de porosidad se ha comprobado que la protección para el coeficiente de resistencia no era mayor. Por lo tanto la decisión final en cuanto a altura y distancia ha sido la de una valla de 4 m de altura y una distancia entre esta y el camión de 3 m.

El último parámetro que se ha estudiado ha sido la influencia de la incorporación de un deflector y su ángulo, estudio del que se ha podido concluir que la influencia del deflector en el comportamiento aerodinámico del vehículo no es grande, también se ha comprobado que para conseguir una reducción de los coeficientes de momento y fuerza lateral por medio de la incorporación de un deflector el ángulo de este con la horizontal debe ser amplio (60°-80°).

Una vez realizados todos estos estudios se ha llegado a un prototipo final de una valla cortavientos con aperturas rectangulares con porosidad del 20%, 4 m de altura, 3 m entre valla y camión y un deflector con un ángulo de 80° con respecto a la horizontal.

Tras elegir la configuración final de la valla cortavientos más indicada para proteger al camión de la acción del viento cruzado se ha probado su efectividad para los tres vehículos para los cinco casos propuestos de ángulo de guiñada:

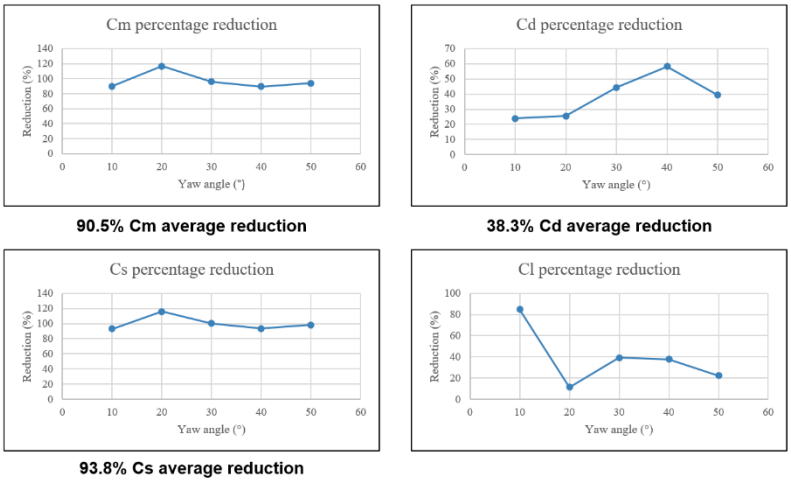

Figura 3: Eficiencia de la valla para el camión.

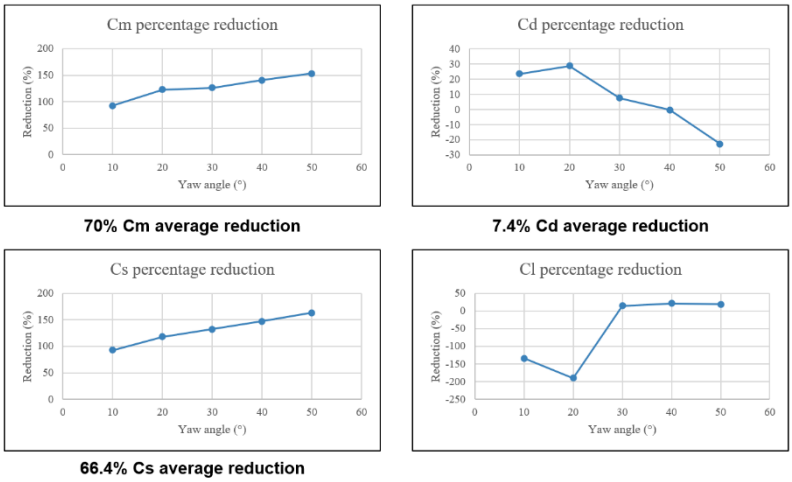

Figura 4: Eficiencia de la valla para la motocicleta.

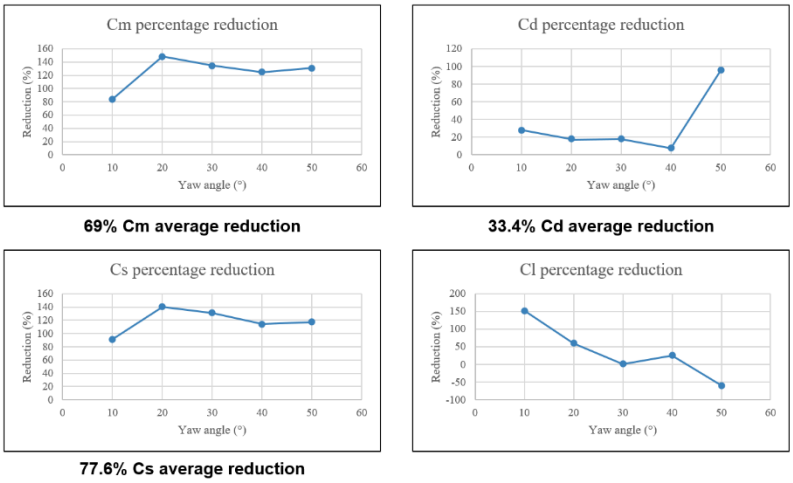

Figura 5: Eficiencia de la valla para el coche.

Como se puede ver en los gráficos recién mostrados para el camión se ha conseguido una reducción muy notable de los coeficientes de momento y fuerza lateral, y al mismo tiempo se ha conseguido también una reducción en el coeficiente de resistencia aerodinámica por lo que los objetivos han sido alcanzados.

Por su parte la eficiencia de la valla en el caso de la motocicleta y el coche es menor que para la del camión, debido a que se ha buscado optimizar la valla para el caso del camió. La explicación a que la eficiencia sea menor en el caso del camión y de la moto es que para estos vehículos la altura relativa de la valla y la distacia entre el vehículo y la valla es mayor que para el camión, por lo que, como ya se ha comentado, a mayor altura y distancia se obtiene una mayor reducción de los coeficientes de momento y fuerza lateral. Para el caso de la moto y el coche la reducción de los coeficientes de momento y fuerza lateral ha sido tal que estos han cambiado de signo, por lo que el vuelco del vehículo se produciría hacia la valla y la fuerza lateral es de atracción entre la valla y el vehículo, provocando que los valores absolutos de estos coeficientes sigan siendo notables aunque con una reducción considerable.

Por otro lado la reducción del coefiente de resistencia aerodinámica para la motocicleta ha disminuido con el aumento del ángulo de ataque hasta que se ha llegado a incrementar este valor, suceso que ha podido sucederse por la interacción del flujo entre la valla y la motocicleta con el carenado de la misma.

Por ultimo para el coeficiente de resistencia del coche se ha dado un fenómeno extraño por el que este coeficiente ha sido casi anulado gracias a la valla cuando el ángulo de ataque del viento es de 50°, este suceso se ha dado como fenómeno casual por las condiciones de la simulación, la geometría del coche y el ángulo de ataque, pero del estudio de este fenómeno se podrían sacar conclusiones que ayudarían a la mejora de la efectividad de las vallas cortavientos a la hora de reducir el coeficiente de resistencia del vehículo.

Con los estudios realizados en este proyecto y los resultados finales se puede concluir la gran efectividad que pueden tener las vallas cortaviento para la reducción de los coeficientes aerodinámicos de los vehículos (en especial los coeficientes de momento y fuerza lateral), por lo que, como se planteaba en la introducción, esta técnica puede contribuir a dos problemas de urgencia global, como son los accidentes de tráfico y las emisiones de gases de efecto invernadero.

Además se ha podido comprobar que no exixte una solución unica para este problema, ya que se pueden dar numerosa configuraciones de valla cortavientos capaces de proteger con buenos resultados a los vehículos de la acción del viento.

Por último se concluye que esta técnica es digna de estudio para ser incorporada a las carreteras, siendo este proyecto solo una primera toma de contacto con la técnica los estudios que pueden derivar de este pueden ser de gran utilidad para su implementación.

4. **Referencias**

Alonso-Estébanez, A., J. J. Del Coz Díaz, F. P. Álvarez Rabanal, and P. Pascual-Muñoz. 2017. "Performance analysis of wind fence models when used for truck protection under crosswind through numerical modeling." *Journal of Wind Engineering and Industrial Aerodynamics* 168 (April): 20-31.

Cheli, F., R. Corradi, E. Sabbioni, and G. Tomasini. 2011. "Wind tunnel tests on heavy road vehicles: Cross wind induced loads-Part 1." *Journal of Wind Engineering and Industrial Aerodynamics* (Elsevier) 99 (10): 1000-1010.

Fintelman, D., H. Hemida, M. Sterling, and F. X. Li. 2015. "A numerical investigation of the flow around a motorbike when subjected to crosswinds." *Engineering Applications of Computational Fluid Mechanics* 9 (1): 528-542.

Heft, A.I., T. Indinger, and N.A. Adams. 2012. "Experimental and numerical investigation of the drivaer model." *American Society of Mechanical Engineers, Fluids Engineering Division (Publication) FEDSM.* 41-51.

Heft, Angelina I, Thomas Indinger, and Nikolaus A Adams. 2012. "Introduction of a New Realistic Generic Car Model for Aerodynamic Investigations." *SAE 2012 World Congress & Exhibition.* SAE International.

Peters, Brett C, Mesbah Uddin, Jeremy Bain, Alex Curley, and Maxwell Henry. 2015. "Simulating DrivAer with Structured Finite Difference Overset Grids." SAE International.

STUDY OF AERODYNAMIC BEHAVIOR OF DIFFERENT TYPES OF VEHICLE BEHIND WINDBREAK FENCES UNDER CROSSWIND

Author: Tagliavia Ramírez, Íñigo Andrés.
Supervisor: Schito, Paolo.
Collaborating Entity: ICAI – Universidad Pontificia Comillas, Politecnico di Milano

ABSTRACT

1. Introduction

According to the DGT, wind is the third largest cause of accidents in bad weather in Spain, causing a total of 270 accidents and 30 fatalities per year. But these data are of the accidents in which the wind is considered to be the main and only cause, since if we consider the accidents related to the wind, such as situations with wind and rain or with wind, snow and fog, the numbers are much higher. According to (Edwards 1999) data in the UK, 3.7% of annual accidents are strongly wind related, which would mean about six thousand accidents per year caused by wind.

Wind on the road is a real danger, whether it is a light gust of wind, which in the presence of an unsuspecting driver can cause the vehicle to move sideways with the risk that this entails and an accident can occur, or a strong gust of wind capable of overturning a truck.

Road traffic injuries are a global public health problem. According to World Health Organization data, 1.3 million people die on the roads each year and between 20 and 50 million people suffer non-fatal injuries.

Beyond the immediate human damage caused by the road vehicles just discussed, the transport sector according to EEA data from 2016 is the largest contributor of greenhouse gas emissions in the EU, generating 27% of emissions, which is 1205 million tons of CO2 equivalent, with cars and vans being responsible for half of these. And the cross wind, in addition to the obvious lateral force it causes in the vehicle, increases the drag force with respect to the one that would be had with the wind totally face when this impact in the vehicle with an angle greater than 0 to 30. This translates directly into higher fuel consumption, which is also increased by the lateral force due to the need to be constantly rectifying the trajectory of the vehicle fighting against this wind. Therefore, since the reduction of greenhouse gas emissions is an urgent priority at global level, any solution that can improve this situation must also be considered and studied.

Therefore, in view of the need to solve these two problems at a global level, and understanding them as a great challenge for engineering, this thesis will present what could diminish the numbers just presented, the windbreak fences.

During this thesis the aim will be to develop a wind barrier that placed on the side of the road will be able to protect any type of vehicle from the action of the cross wind, and its fatal consequences. Although the priority in the research will be to reduce the lateral forces to which a vehicle is subjected to the wind, and its risk of moving sideways or even overturning, it will also be a matter of developing these wind breakers in such a way that they are capable of reducing the dragging force of the vehicle as much as possible.

The priorities of the automotive aeodynamics sector throughout its history have been: limiting frontal air resistance, either in the search for efficiency or in the search for greater speed, and ,in the case of competition vehicles, increasing their grip.

But obviously there is another force caused by the wind in a vehicle, the lateral force. For some years now, this action of the cross wind on vehicles has been studied more in depth, even if only in an academic way, being more extensive its study on trains than road vehicles.

The main object of study in this area is the concern about the effect that side wind can have on heavy vehicles in areas which are very exposed to these strong gusts of wind, such as viaducts and embankments.

In the work of (Cheli, Corradi, et al. 2011) and (Cheli, Ripamonti, et al. 2011) the loads induced by the cross wind from an angle of incision of 0° to one of 90° are studied in depth in a wind tunnel for heavy road vehicles, studying this phenomenon for a vehicle in a flat ground (in the first work) and for vehicles in zones of high exposure like viaducts or embankments (in the second work). (Cheli, Corradi, et al. 2011).Once numerous studies about the aerodynamic behaviour of heavy road vehicles have been carried out, it has also started to study the danger to which these vehicles are subjected to the wind wakes that can generate structural elements, such as bridge pylons, which can cause turbulent wakes that can generate a risk for these vehicles, as developed in (Salati, et al. 2018).

Once the safety risks that can be caused by the cross wind on vehicles, especially those that are heavy and have a large lateral surface, have been known and studied, a solution to this phenomenon has been sought, and this is where wind barriers appear in the automotive field. Work (Alonso-Estébanez, et al. 2017) seeks to find out the best possible configuration (geometry, porosity, distance and height) for a wind barrier whose task is to protect a truck from side winds while it is stationary. This work goes deeper into the development of wind barriers by introducing a different geometry for it, with plates that form an angle with the vertical, in addition to the conventional ones with open areas in the form of circular and rectangular longitudinal holes. Therefore, this research will be taked as a reference for the development of the fences.

What is intended to make a difference in this thesis, to what has already been done in this area of study, is to study different geometries and configurations for wind barriers like (Alonso-Estébanez, et al. 2017), but for different angles of attack of the wind that can simulate real situations, since most of the studies made to date are made with an angle of attack of 90° with respect to the trajectory of the vehicle, which would suppose a stopped vehicle, case that does not deserve of study. In addition to the differences mentioned above, this thesis aims to study the action of crosswinds and the efficiency of wind barriers not only on the most exposed vehicles (large heavy vehicles), but on all vehicles that can be found on the road. Therefore, it has been decided to test a truck, a car and a motorcycle, the three most common groups of vehicles in the road.

Finally, another major difference that is intended with respect to previous studies is to analyse the benefit that wind barriers can have in the drag force experienced by vehicles due to the wind, and thus check the benefits that wind barriers can have in terms of fuel consumption.

2. Methodology

To carry out the aerodynamic study that is intended to understand the behavior of different types of vehicles in cross wind and the development of a wind fence design will use the technology of CFD simulations through open source software OpenFoam. In this work different cases of wind yaw angle between 10° and 50° will be simulated for three types of vehicles, a truck, a motorcycle and a car. The truck will be a replica of the one used in (Cheli, Corradi, et al. 2011), work that will be used for the validation of the numerical model, the geometry of the motorbike will be extracted from the OpenFoam repository and the car will be the DrivAer model developed by the Technical University of Munich.

For the development of the final prototype of the wind fence, the influence of each variable in the design of this type of fence on its efficiency in protecting the truck from the action of the wind will

be studied, where the aim will be to be able to annul the moment coefficient (of roll or overturn) and the side force coefficient and to reduce the drag coefficient. The variables to be studied will be the geometry of the fence, its porosity, its height, its distance from the vehicle and the effectiveness of the incorporation of a deflector at the top of the fence and the influence of the angle of this deflector.

The fence geometries to be studied are based on those studied in (Alonso-Estébanez, et al. 2017):

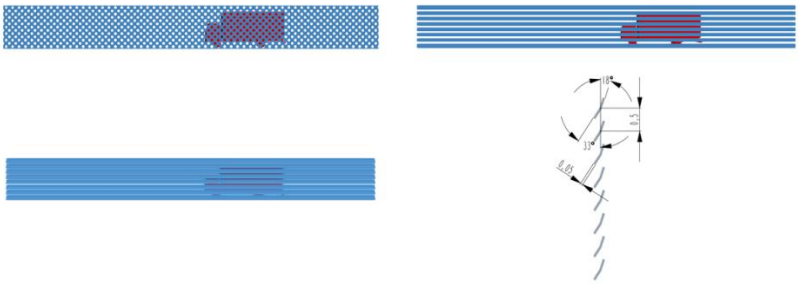

Figure 1: Fence geometries.

To solve the CFD simulations the OpenFoam solver simpleFoam will be used, since incompressible steady-state flows will be simulated, in addition to solve the RANS equations the two equations of the turbulence model SST k-omega will be included, because of its good operation in cases of low Reynolds number and adverse pressure gradients.

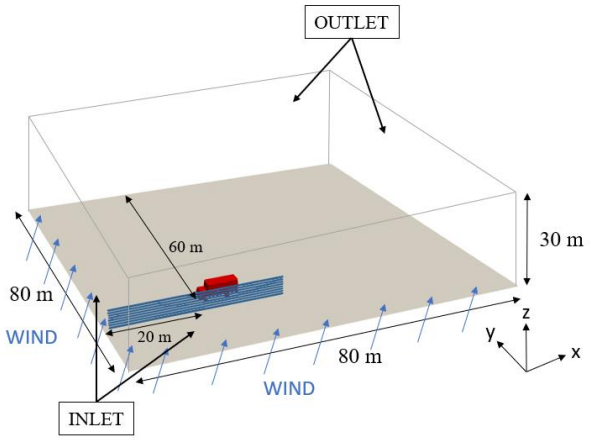

Figure 2: Computational domain.

The computational domain will be as shown in Figure 2, where the length and width of this domain have been set, in accordance with the literature study that has been carried out, at ten times the length of the truck and the height eight times the height of the truck, in order to achieve a domain large enough so that the wake caused by the truck and the fence develops fully and that the imposed boundary conditions do not influence the numerical results. The boundary conditions are as follows:

- INLET: Fixed flow velocity and yaw angle.
- OUTLET: An inlet-outlet boundary condition.
- TRUCK: A no-slip condition.
- FENCE and LOWER WALL: Fixed vehicle velocity in the x-direction.
- UPPER WALL: Slip condition.

The OpenFoam SnappyHexMesh utility will be used to mesh the domain and geometries, and a different mesh will be made for each yaw angle of wind.

Once the cases have been meshed, the numerical model of each vehicle has been successfully validated using as references (Cheli, Corradi, et al. 2011) for the truck model, (Fintelman, et al. 2015) for the motorcycle and (Heft, Indinger and Adams 2012), (Heft, Indinger and Adams 2012) and (Peters, et al. 2015) for the validation of the truck model.

Once the model has been validated, the development of the prototype wind breaker has begun.

3. Results and Conclusions

When developing the windbreak fence, this work has been focused on optimizing it for the protection of the truck, since it has been hypothesized that if a fence is capable of protecting the largest vehicle from cross winds, it will also be capable of protecting smaller vehicles.

In the first place, the influence of geometry and porosity on the effectiveness of the windbreak has been studied, where it has been possible to conclude that there is no ideal geometry for reducing the torque and lateral force coefficients of the vehicle, but that for any geometry the porosity for which these coefficients are cancelled can be found. In this work we have chosen the fence with rectangular openings since for a porosity of 20% it reduces up to almost negligible these coefficients for any yaw angle and also it is the geometry more capable of reducing the drag coefficient, so, as what we were looking for was to find a fence capable of protecting the truck from the cross wind for any yaw angle this has been the chosen one.

After this study on geometry and porosity, the influence of the height of the fence and the distance between the fence and the truck on the aerodynamic behaviour of the truck was studied. This study showed that the higher the height, the greater the protection of the lateral forces experienced by the vehicle against the action of the wind at any yaw angle, and in all the distance between fence and vehicle it has been possible to behave in varying this parameter is not the same for all the yaw angles, but for medium and large angles (30° and 50°) at a greater distance greater protection is achieved, and on the other hand for small angles (10°) at a shorter distance there is a greater reduction in lateral forces. This study has been carried out for heights of two, three and four metres and for distances between fence and truck also of two, three and four metres, using an opaque fence, as this is the common point between the three fence geometries presented. The 2 m high fence was quickly discarded as it was not sufficient to significantly reduce the moment and lateral force coefficients, and it was also found that the best option in terms of distance was the 3 m fence, so the final decision was between choosing the 3 m and 4 m fences. The great advantage of the opaque 3 m fence was that despite reducing to a lesser extent the moment and lateral force coefficients it was more capable of reducing the truck's drag coefficient, but when testing this event for a fence with rectangular openings and 20% porosity it was found that the protection for the drag coefficient was not greater. Therefore the final decision in terms of height and distance was that of a 4 m high fence and a distance between it and the truck of 3 m.

The last parameter that has been studied was the influence of the incorporation of a deflector and its angle, study from which it has been possible to conclude that the influence of the deflector in the aerodynamic behavior of the vehicle is not great, also it has been verified that to obtain a reduction

of the coefficients of moment and lateral force by means of the incorporation of a deflector the angle of this with the horizontal one must be ample (60°-80°).

Once all these studies have been carried out, a final prototype of a windbreak fence with rectangular openings with 20% porosity, 4 m high, 3 m between fence and truck and a deflector with an angle of 80° with respect to the horizontal has been reached.

After choosing the final configuration of the wind fence most suitable to protect the truck from the action of the cross wind, its effectiveness has been tested for the three vehicles for the five proposed cases of yawing angle:

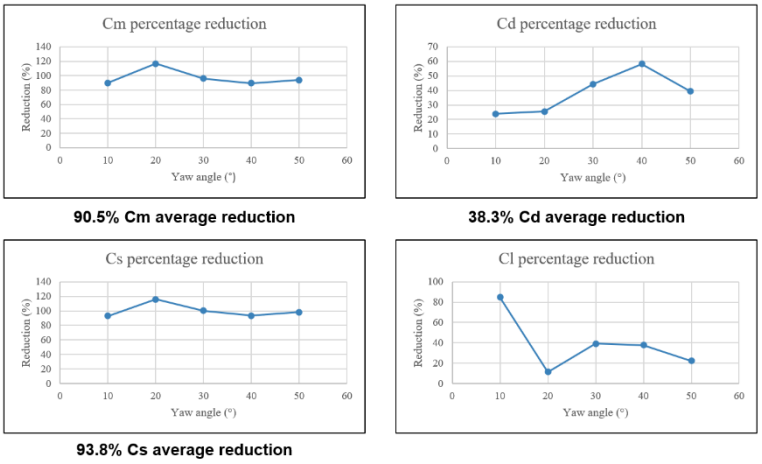

Figure 3:Efficiency of the fence for the truck.

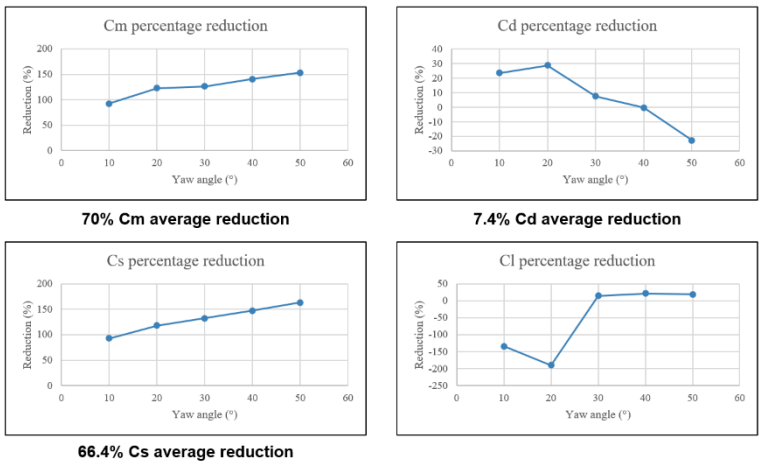

Figure 4:Efficiency of the fence for the motorbike.

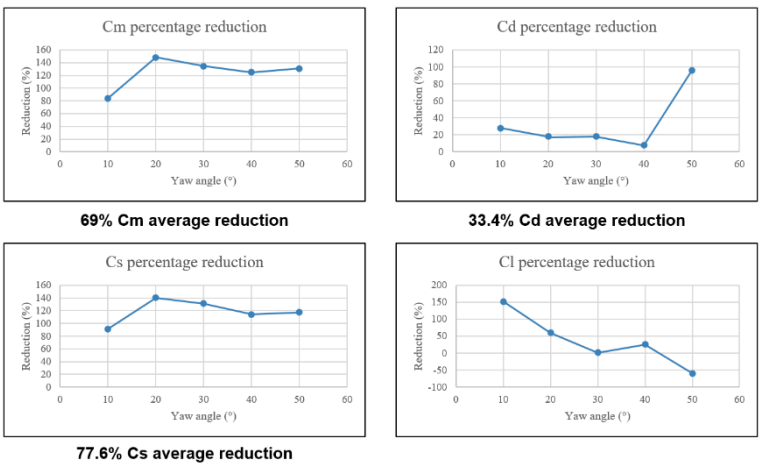

Figure 5:Efficiency of the fence for the car.

As can be seen in the graphs just shown for the truck, a very noticeable reduction in the moment and lateral force coefficients has been achieved, and at the same time a reduction in the drag coefficient has been achieved, so the objectives have been met.

On the other hand, the efficiency of the fence in the case of the motorcycle and the car is lower than for the truck, because we have sought to optimize the fence for the case of the truck. The explanation for the lower efficiency in the case of the truck and the motorcycle is that for these vehicles the relative height of the fence and the distance between the vehicle and the fence is greater than for the truck, so, as already mentioned, the greater the height and distance, the greater the reduction in the moment and lateral force coefficients. In the case of the motorbike and the car, the reduction of the moment and lateral force coefficients has been such that they have changed sign, so that the vehicle would roll over towards the fence and the lateral force is of attraction between the fence and the vehicle, causing the absolute values of these coefficients to continue to be notable, although with a considerable reduction.

On the other hand the reduction of the drag coefficient for the motorcycle has decreased with the increase of the angle of attack until this value has been increased, event that has been possible to happen by the interaction of the flow between the fence and the motorcycle with the fairing of the same one.

Finally for the car resistance coefficient there has been a strange phenomenon by which this coefficient has been almost annulled thanks to the fence when the yaw angle of the wind is 50°, this event has occurred as a casual phenomenon due to the conditions of the simulation, the geometry of the car and the yaw angle, but from the study of this phenomenon we could draw conclusions that would help to improve the effectiveness of wind barriers when reducing the drag coefficient of the vehicle.

With the studies carried out in this project and the final results, it can be concluded that wind barriers can be very effective in reducing the aerodynamic coefficients of vehicles (in particular the moment and lateral force coefficients). Therefore, as stated in the introduction, this technique can contribute to two problems of global urgency, as road accidents and greenhouse gas emissions.

Furthermore, it has been shown that there is no single solution to this problem, as there are many different configurations of windbreaks that can successfully protect vehicles from the action of the wind.

Finally it is concluded that this technique is worthy of study to be incorporated into the roads, being this project only a first contact with the technique the studies that can derive from it can be very useful for its implementation.

4. References

Alonso-Estébanez, A., J. J. Del Coz Díaz, F. P. Álvarez Rabanal, and P. Pascual-Muñoz. 2017. "Performance analysis of wind fence models when used for truck protection under crosswind through numerical modeling." *Journal of Wind Engineering and Industrial Aerodynamics* 168 (April): 20-31.

Cheli, F., R. Corradi, E. Sabbioni, and G. Tomasini. 2011. "Wind tunnel tests on heavy road vehicles: Cross wind induced loads-Part 1." *Journal of Wind Engineering and Industrial Aerodynamics* (Elsevier) 99 (10): 1000-1010.

Fintelman, D., H. Hemida, M. Sterling, and F. X. Li. 2015. "A numerical investigation of the flow around a motorbike when subjected to crosswinds." *Engineering Applications of Computational Fluid Mechanics* 9 (1): 528-542.

Heft, A.I., T. Indinger, and N.A. Adams. 2012. "Experimental and numerical investigation of the drivaer model." *American Society of Mechanical Engineers, Fluids Engineering Division (Publication) FEDSM*. 41-51.

Heft, Angelina I, Thomas Indinger, and Nikolaus A Adams. 2012. "Introduction of a New Realistic Generic Car Model for Aerodynamic Investigations." *SAE 2012 World Congress & Exhibition*. SAE International.

Peters, Brett C, Mesbah Uddin, Jeremy Bain, Alex Curley, and Maxwell Henry. 2015. "Simulating DrivAer with Structured Finite Difference Overset Grids." SAE International.

INDEX

LIST OF FIGURES

LIST OF TABLES

CHAPTER 1: Introduction

According to the DGT, wind is the third largest cause of accidents in bad weather in Spain, causing a total of 270 accidents and 30 fatalities per year. But these data are of the accidents in which the wind is considered to be the main and only cause, since if we consider the accidents related to the wind, such as situations with wind and rain or with wind, snow and fog, the numbers are much higher. According to (Edwards 1999) data in the UK, 3.7% of annual accidents are strongly wind related, which would mean about six thousand accidents per year caused by wind.

Wind on the road is a real danger, whether it is a light gust of wind, which in the presence of an unsuspecting driver can cause the vehicle to move sideways with the risk that this entails and an accident can occur, or a strong gust of wind capable of overturning a truck. Given the relevant side wind conditions, a wind of 13 m/s is sufficient to deflect a large vehicle considerably from its path and a side wind of 20 m/s may be able to overturn it.

Road traffic injuries are a global public health problem. According to World Health Organization data, 1.3 million people die on the roads each year and between 20 and 50 million people suffer non-fatal injuries. Road traffic accidents are a leading cause of death in all age groups, and the first in people aged between 15 and 29. So any solution that can reduce these fatal numbers must be considered and studied.

Beyond the immediate human damage caused by the road vehicles just discussed, the transport sector according to EEA data from 2016 is the largest contributor of greenhouse gas emissions in the EU, generating 27% of emissions, which is 1205 million tons of CO2 equivalent, with cars and vans being responsible for half of these. And the cross wind, in addition to the obvious lateral force it causes in the vehicle, increases the drag force with respect to the one that would be had with the wind totally face when this impact in the vehicle with an angle greater than 0 to 30. This translates directly into higher fuel consumption, which is also increased by the lateral force due to the need to be constantly rectifying the trajectory of the vehicle fighting against this wind. Therefore, since the reduction of greenhouse gas emissions is an urgent priority at global level, any solution that can improve this situation must also be considered and studied.

Therefore, in view of the need to solve these two problems at a global level, and understanding them as a great challenge for engineering, this thesis will present what could diminish the numbers just presented, the windbreak fences.

During this thesis the aim will be to develop a wind barrier that placed on the side of the road will be able to protect any type of vehicle from the action of the cross wind, and its fatal consequences. Although the priority in the research will be to reduce the lateral forces to which a vehicle is subjected to the wind, and its risk of moving sideways or even overturning, it will also be a matter

of developing these wind breakers in such a way that they are capable of reducing the dragging force of the vehicle as much as possible. In order to reach the point of developing this solution with criteria, first of all what will be dealt with in this work is to study and understand the aerodynamic behaviour of the vehicles in crosswinds, in order to find a solution.

1.1 Objectives

The primary objective of this thesis, as already mentioned, is to develop a wind barrier capable of protecting vehicles from side winds. But this objective could be expanded into several intermediate points necessary to reach this final goal:

- To understand the aerodynamic behaviour of a vehicle when faced with a cross wind and its peculiarities.
- To develop several types of barriers with different geometries and configurations and to understand how they affect the wind when it affects them and the benefits of these on the behaviour of the vehicle.
- To find the geometry and configuration for the barrier that is capable of almost completely cancelling out the lateral forces produced by the wind in the vehicle and to reduce the drag force on the vehicle.
- To present a final prototype of a windbreak fence that is capable of considerably protecting all types of vehicles present on the road from crosswinds and reducing their drag. And in this way be able to reduce the wind related traffic accidents and the fuel consumption of vehicles, with its consequent reduction in the emission of greenhouse gases into the earth's atmosphere. Thus, collaborating in the resolution of two of the world's highest priority problems.
- That this study may serve as a reference for possible future research on automotive aerodynamics in the face of side winds and may serve as a starting point for the development of wind barriers. Having thus contributed to the world of engineering.

1.2 Methodology

The methodology followed to achieve the objectives just presented will be presented below:

Stage 1. Bibliographic study of the subject under discussion and about CFD simulations.

Stage 2. Aerodynamic study of the three most representative types of vehicles in road traffic (truck, car and motorcycle) in different cross wind configurations, and the relevant analysis of the results obtained.

Stage 3. 3D CAD design of the wind barriers that will be used during the research, with their different geometries, porosities and heights (adjustments and changes to the designs will be made as the research progresses).

Stage 4. Aerodynamic study of the wind barriers and the behaviour of the vehicle when faced with these for the different geometries and when the porosity varies. Analysis of the results obtained and preliminary choice of the most effective geometry and porosity.

Stage 5. Aerodynamic study of the optimum distance between vehicle and barrier, and the height of the barrier. Analysis of the results obtained and preliminary choice of the optimum distance and height.

Stage 6. Aerodynamic study of the benefits that can be achieved by incorporating a deflector at the top of the fender and the search for its optimum angle. Analysis of the results obtained and choice of the deflector angle.

Stage 7. Analysis of the results as a whole and choice of the configuration, in terms of geometry, porosity, distance, height and deflector, most suitable and effective for the final barrier prototype.

Stage 8. Aerodynamic study of the final barrier prototype for the three types of vehicles in different crosswind configurations.

Stage 9. Final analysis of the results and the benefits of the final barrier prototype in the behaviour of the vehicles when faced with side winds.

Stage 10. Conclusions of the work carried out, the results and possible future studies

In addition, each aerodynamic study will have the same structure: meshing, validation and simulation of the case.

Finally, to close this introduction, the structure of the present report should be commented. Following this, in CHAPTER 2: State of the art, a brief review will be made of the history of automotive aerodynamics and the current state of development of wind fences. After that, in CHAPTER 3: Numerical method, the theoretical basis of aerodynamics and CFD will be reviewed. With CHAPTER 4: Numerical setup, the research work of the thesis will start, where the geometries of the vehicles and windbreak fences to be tested will be presented, as well as the preparation of the cases and their respective validations. Then, in CHAPTER 5: Results, the results obtained from the simulations will be shown and analyzed, and finally, in CHAPTER 6: Conclusions, the conclusions reached about the methodology used, the results and the future studies that could be made from this work will be presented. The last chapter

of this report, CHAPTER 7: Sustainable Development Goals, shows how far and according to which objectives this work can help to achieve the SDGs of 2030.

CHAPTER 2: State of the art

It is well known that aerodynamics has been a fundamental part of the automotive sector for decades, but its influence, methodology and objectives have varied from its beginnings in the early 20th century to the present day.

The study of air resistance predates the appearance of the automobile, and before the first car, due to studies of birds and fishes, the ideal shape for moving around in fluids had already been revealed.

However, the air resistance of cars was not a concern in the first models because they moved at very low speed, and it was not until the 30s when the bodies began to be developed with the idea of "penetrating" the air, thus developing drop-shaped bodies with a great inspiration in naval and aeronautical design.

After the Second World War with the collapse of the price of oil, aerodynamics took a back seat and was only considered in racing cars, where it advanced notably until the 60s and 70s, when the force of the wind began to be used by means of spoilers and skirts to improve the adherence of the car. This advance could have led to the production vehicles and changed the automotive history notably, but because of the 1973 oil crisis, with the increase of the oil price that this supposed, the aerodynamics returned to enter full in the production vehicles to look for the maximum efficiency with a low consumption of fuel. This new interpretation of aerodynamics brought a trend of sharp noses and rounded sides that continued until the 1990s.

From the 1990s until today the importance of aerodynamics and its effectiveness has only grown and grown, which is largely due to the improvement of tools used to study aerodynamics, such as wind tunnels and computer simulations. It should be noted that wind tunnels have existed since the 19th century, where they were used to study the flow of air over the first aircrafts, and began to be used to study the efficiency of cars after World War II. But in the last decades both wind tunnels and computer simulations have become the main tools in the study of vehicle aerodynamics, and as these tools improve, vehicle aerodynamics improves with them.

With this overview of the history of automotive aerodynamics, it is easy to see what the priorities of this sector have been: limiting frontal air resistance, either in the search for efficiency or in the search for greater speed, and ,in the case of competition vehicles, increasing their grip.

But obviously there is another force caused by the wind in a vehicle, the lateral force. For some years now, this action of the cross wind on vehicles has been studied more in depth, even if only in an academic way, being more extensive its study on trains than road vehicles.

The main object of study in this area is the concern about the effect that side wind can have on heavy vehicles in areas which are very exposed to these strong gusts of wind, such as viaducts and embankments.

In the work of (Cheli, Corradi, et al. 2011) and (Cheli, Ripamonti, et al. 2011) the loads induced by the cross wind from an angle of incision of 0° to one of 90° are studied in depth in a wind tunnel for heavy road vehicles, studying this phenomenon for a vehicle in a flat ground (in the first work) and for vehicles in zones of high exposure like viaducts or embankments (in the second work). (Cheli, Corradi, et al. 2011) due to its depth of experimental study in the behavior of a truck in the cross wind for different angles of incision will be the work of reference for the validation of the numerical model of the truck of this study, which will be similar to the one used in (Cheli, Corradi, et al. 2011) and in the European aerodynamic investigations (W.P.2.2.1 2005) and (W.P.2.3.2 2005).

Once numerous studies about the aerodynamic behaviour of heavy road vehicles have been carried out, it has also started to study the danger to which these vehicles are subjected to the wind wakes that can generate structural elements, such as bridge pylons, which can cause turbulent wakes that can generate a risk for these vehicles, as developed in (Salati, et al. 2018).

Once the safety risks that can be caused by the cross wind on vehicles, especially those that are heavy and have a large lateral surface, have been known and studied, a solution to this phenomenon has been sought, and this is where wind barriers appear in the automotive field.

But wind barriers are nothing new or innovative, as they have been used at least since the beginning of the 20th century, and probably much earlier, to protect crops from wind and the malicious particles it can carry. Although this has been the main purpose of wind barriers since their inception, they are also widely used for other purposes such as containing sand dunes or snow, and now also to protect vehicles from the wind.

Again, as with cross wind studies, the implementation of wind barriers has been studied much more to protect trains than road vehicles. But these studies are equally useful for road vehicles as for trains when it comes to understanding the effect wind barriers have on wind and how barriers should be geometrically designed to have an optimal effect on the vehicle to be protected. In the (Bocciolone, et al. 2008) study, the behaviour of the trains against cross wind is studied in an experimental way in a wind tunnel, and the protection of wind barriers with and without porosity is introduced. Another research on this subject is (Gu, et al. 2020), where the benefit of porous wind barriers with round holes in the behaviour of trains against side wind is studied both experimentally and computationally.

Returning to the research on the risk of heavy road vehicles in areas of high exposure to crosswinds, in the study (Kozmar, et al. 2012) an experimental study of the efficiency of wind barriers on bridges was carried out as well as in study (Chen, et al. 2015) in an experimental and computational way and in study (Chu, et al. 2013) only in a computational way. In this works, the behavior of porous wind barriers with square or circular holes for perpendicular angles of wind attack, or almost, on the trajectory of the vehicle is studied.

Work (Alonso-Estébanez, et al. 2017) seeks to find out the best possible configuration (geometry, porosity, distance and height) for a wind barrier whose task is to protect a truck from side winds while it is stationary. This work goes deeper into the development of wind barriers by introducing a different geometry for it, with plates that form an angle with the vertical as shown in Figure 1, in addition to the conventional ones with open areas in the form of circular and rectangular longitudinal holes. Therefore, this research will be taked as a reference for the development of the fences.

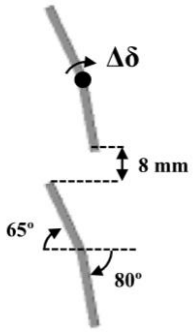

Figure 1: Lungitudinal plates of a wind fence (Alonso-Estébanez, et al. 2017)

It has also been investigated with original shapes for barriers such as those presented in study (Çoşkun, et al. 2017), where the benefit of fractal forms such as those in Figure 2 is studied. However, it has been shown that these shapes do not benefit in protecting the wind by not being more efficient than barriers with round holes and even because of their peculiar shapes can produce turbulences not desirable to protect a vehicle from the action of crosswind on it.

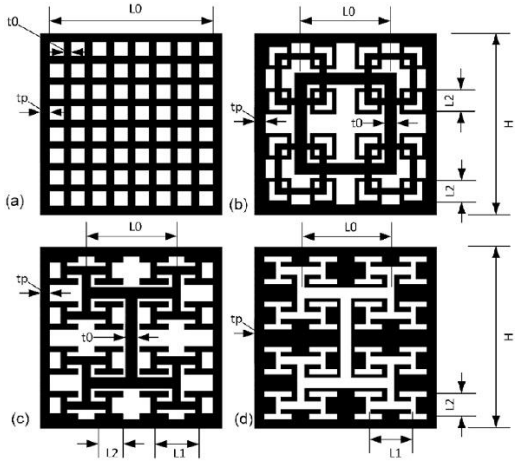

Figure 2: Wind fence witch fractal forms (Çoşkun, et al. 2017)

Although the protective barriers are beginning to be seen on some stretches of road, mainly viaducts, such as those of the Črni Kal Viaduct in Slovenia shown in Figure 3, it is still not a very widespread technique and the advantages that these can bring to road traffic may not yet have been fully considered.

Figure 3:Črni Kal Viaduct Slovenia (Jaka Ivancic)

The last work to mention is (Fintelman, et al. 2015), since it is the aerodynamic study of a motorcycle against crosswind, so it will be taked into account when validating the numerical model of the motorcycle case in this thesis.

After all this bibliographic study, what is intended to make a difference in this thesis, to what has already been done in this area of study, is to study different geometries and configurations for wind barriers like (Alonso-Estébanez, et al. 2017), but for different angles of attack of the wind that can simulate real situations, since most of the studies made to date are made with an angle of attack of 90° with respect to the trajectory of the vehicle, which would suppose a stopped vehicle, case that does not deserve of study. In addition to the differences mentioned above, this thesis aims to study the action of crosswinds and the efficiency of wind barriers not only on the most exposed vehicles (large heavy vehicles), but on all vehicles that can be found on the road. Therefore, it has been decided to test a truck, a car and a motorcycle, the three most common groups of vehicles in the road.

Finally, another major difference that is intended with respect to previous studies is to analyse the benefit that wind barriers can have in the drag force experienced by vehicles due to the wind, and thus check the benefits that wind barriers can have in terms of fuel consumption.

CHAPTER 3: Numerical method

Aerodynamics is the science of air in motion and its impact on solid bodies placed in the flow field as an obstacle. Being a subfield, most of the equations of fluid dynamics also apply to aerodynamics, including all the equations of steering, turbulence, boundary layer theory and the ideal gas assumption.

The airflow studied in automotive aerodynamics is almost entirely turbulent flow. Therefore, the great challenge in studying this field is to solve the equations of the turbulent model, which will be modeled throughout this report using the approach of Reynolds-averaged Navier-Stokes equations (RANS).

Turbulence modeling is an attempt to conceive several differential equations for calculating turbulent flow, based on appropriate approximations of the exact Navier-Stokes equations. At the Reynolds-averaged Navier-Stokes (RANS) equation approach the starting point is Reynolds decomposition of the flow variables in the mean and fluctuating parts, where the insertion of Reynolds decomposed variables into the Navier-Stokes, followed by an average of the equations themselves, give rise to Reynolds stress tensor, an unknown term that has to be modeled for the RANS equations to be solved. The problem of the closure of system of Navier-Stokes equations consists essentially of this operation.

Throughout this chapter an introduction to these equations governing the movement of fluids will be made, developing them, and indicating their possible resolution models, developing the models used and needed for this thesis.

3.1 Reynolds-Average Navier-Stokes Equations

The flow of an incompressible viscous fluid with constant properties is governed by the Navier-Stokes equations (Einstein summation convention applies to repeated indices):

$$\frac{\partial u_i}{\partial t} + \frac{\partial}{\partial x_j}\left(u_i u_j\right) = -\frac{\partial p}{\partial x_i} + v\frac{\partial^2 u_i}{\partial x_j \partial x_j} \tag{1}$$

$$\frac{\partial u_i}{\partial x_i} = 0 \tag{2}$$

(u_i is the fluid velocity, p is the pressure (divided by the density ρ), v is the fluid kinematic viscosity, and body forces do not appear explicitly), where the convective term of Eq. (1) is expressed in conservative form.

According to Reynolds concept of decomposition, the dependent variables of Eq. (1) and Eq. (2) are decomposed into mean and fluctuating parts:

$$u_i = \bar{u}_i + u_i', \qquad p = \bar{p} + p' \tag{3}$$

By replacing Eq. (3) into Eqs. (1) and(2), taking an average ensemble, and the relevant properties of the average operator, the system of partial differential equations that governs the mean velocity and pressure fields of the incompressible turbulent flow is obtained:

$$\frac{\partial \bar{u}_i}{\partial t} + \frac{\partial}{\partial x_j}\overline{(u_i u_j)} = -\frac{\partial \bar{p}}{\partial x_i} + \nu \frac{\partial^2 \bar{u}_i}{\partial x_j \partial x_j} \tag{4}$$

$$\frac{\partial \bar{u}_i}{\partial x_i} = 0 \tag{5}$$

Regarding the non-linear term of Eq. (4) , there is:

$$\overline{u_i u_j} = \bar{u}_i \bar{u}_j + \overline{u_i' u_j'} \tag{6}$$

that gives:

$$\frac{\partial \bar{u}_i}{\partial t} + \frac{\partial}{\partial x_j}(\bar{u}_i \bar{u}_j) = -\frac{\partial \bar{p}}{\partial x_i} + \nu \frac{\partial^2 \bar{u}_i}{\partial x_j \partial x_j} - \frac{\partial}{\partial x_j}(\overline{u_i' u_j'}) \tag{7}$$

And finally, the RANS equations are obtained (Speziale 1991):

$$\frac{\partial \bar{u}_i}{\partial t} + \bar{u}_j \frac{\partial \bar{u}_i}{\partial x_j} = -\frac{\partial \bar{p}}{\partial x_i} + \nu \frac{\partial^2 \bar{u}_i}{\partial x_j \partial x_j} - \frac{\partial \tau_{ij}}{\partial x_j} \tag{8}$$

$$\frac{\partial \bar{u}_i}{\partial x_i} = 0 \tag{9}$$

where the convective term of Eq. (8) is now expressed in a non-conservative form, and:

$$\tau_{ij} = \overline{u_i' u_j'} \tag{10}$$

is the term Reynolds-stress (the Reynolds-stress tensor divided by density) which incorporates the effects of turbulent movements on mean stresses. The Reynolds-stress is symmetrical, the diagonal components are normal stresses, and the components outside the diagonal are shear stresses. The system of Eqs (8) and (9) is not a closed system for the calculation of the four dependent variables u_i and p in the sense that the Reynolds stress tensor contains six additional independent unknowns. The problem of the closure of the Reynolds averaged Navier-Stokes equations consists in expressing mainly through models the Reynolds stress tensor as a function of the mean field and/or other variables. This can be done directly, as in the case of eddy viscosity models, or indirectly, as in the case of models based on the resolution of additional partial equations. Which in this case will be done through the linear eddy viscosity models.

After the introduction of Eq. (3), by subtracting Eq. (8) from Eq. (1) and Eq. (9) from Eq. (2), the system of partial differential equations governing the fluctuating field of incompressible turbulent flow is obtained:

$$\frac{\partial u_i'}{\partial t} + \bar{u}_j \frac{\partial u_i'}{\partial x_j} = -u_j' \frac{\partial u_i'}{\partial x_j} - u_j' \frac{\partial \bar{u}_i}{\partial x_j} - \frac{\partial p}{\partial x_j} + v \frac{\partial^2 u_i'}{\partial x_j \partial x_j} + \frac{\partial \tau_{ij}}{\partial x_j} \tag{11}$$

$$\frac{\partial u_i'}{\partial x_i} = 0 \tag{12}$$

3.2 Linear eddy viscosity models

These are turbulence models in which the Reynolds stresses, as obtained from a Reynolds averaging of the Navier-Stokes equations, are modelled by a linear constitutive relationship with the mean flow straining field, as:

$$-\rho(u_i u_j) = 2\mu_t S_{ij} - \frac{2}{3}\rho k \delta_{ij} \tag{13}$$

where:

- μ_t is the coefficient termed “viscosity" (also called the eddy viscosity).
- k is the mean turbulent kinetic energy.
- $S_{ij} = \frac{1}{2}\left[\frac{\partial U_i}{\partial x_j} + \frac{\partial U_j}{\partial x_i}\right] - \frac{1}{3}\frac{\partial U_k}{\partial x_k}\delta_{ij}$ is the mean strain rate.

The inclusion of $\frac{2}{3}\rho k \delta_{ij}$ in the linear constitutive relation is required by tensorial algebra purposes when solving for two-equation turbulence models (or any other turbulence model that solves a transport equation for k).

This linear relationship is also known as the Boussinesq hypothesis.

There are several subcategories for linear eddy viscosity models, depending on the number of (transport) equations solved to calculate the eddy viscosity coefficient: Algebraic models, One equation models and Two equation models. In this work, a model of two equations will be used.

Two equation turbulence models are one of the most common types of turbulence models. Models such as the k-epsilon model and the k-omega model have become industry standard models and are commonly used for most types of engineering problems. Two equation turbulence models also remain a very active area of research and new refined two equation models continue to be developed.

By definition, two-equation models include two additional transport equations to represent the turbulent properties of the flow. This allows a two-equation model to consider historical effects such as convection and diffusion of turbulent energy.

Most often one of the transported variables is turbulent kinetic energy, k. The second transported variable varies according to the type of two-equation model. The most common options are turbulent dissipation, ε, or specific turbulence dissipation rate, ω. The second variable can be considered as the variable that determines the scale of the turbulence (length scale or time scale), while the first variable, k, determines the energy in the turbulence.

3.2.1 Boussinesq eddy viscosity assumption

The basis of the two equation models is the Boussinesq eddy viscosity assumption, Eq. (13), which proposes that the Reynolds stress tensor, τ_{ij}, is proportional to the mean stress rate tensor, S_{ij}.

Boussinesq assumption is both the strength and weakness of two equation models. This assumption is an enormous simplification that allows us to think of the effect of turbulence on average flow in the same way that molecular viscosity affects laminar flow. The assumption also allows us to introduce intuitive scalar turbulence variables such as turbulent energy and dissipation and to relate these variables to even more intuitive ones such as turbulence intensity and turbulence length scale.

The weakness of Boussinesq hypothesis is that it is not generally valid. There is nothing to say that Reynolds stress tensor should be proportional to the stress rate tensor. It is true that in simple flows such as straight boundary layers and wakes, but in complex flows such as strongly curved flows, or strongly accelerated or decelerated flows, Boussinesq assumption is simply not valid. This gives two equation models inherent problems in predicting strongly rotating flows and other flows where the effects of curvature are significant.

3.2.2 Near-wall treatments

When using CFD there are two ways to take the boundary layer into account: Solve the flow near the wall by applying an increasing layer of cells and calculate the boundary layer profile, which is computationally very expensive. Or by applying wall functions in the turbulent model.

The structure of the turbulent boundary layer exhibits large velocity gradients and quantities that characterize turbulence, compared to flow in the core region. In a placed grid, such gradients will be approached using discretization procedures, that are not suitable for such a high variation, as they usually involve a linear interpolation of values between the centers of the cells.

This situation resulted in several near-wall treatments. In general, two approaches can be distinguished (shown in Figure 4):

- Low Reynolds Number treatment (LRN)
- High Reynolds number treatment (HRN)

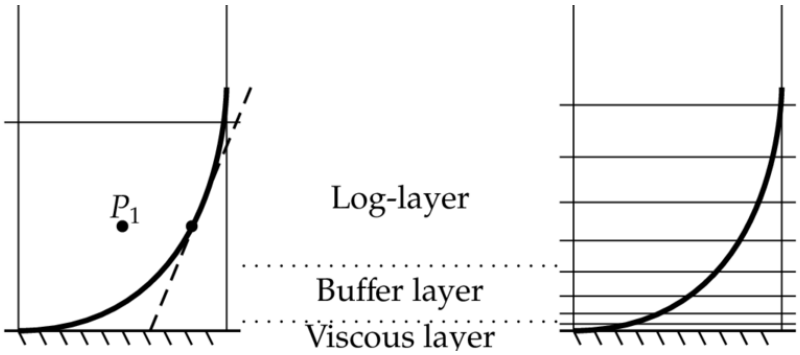

Figure 4: HRN (left) vs LRN(right) (Two equation turbulence models - CFD-Wiki n.d.)

The LRN integrates each equation up to the viscous sublayer and therefore the first calculation cell must have its centroid at $y^+ \approx 1$. Furthermore, some models require an additional treatment (damping functions) of the equations to ensure asymptotic consistency with the behavior of the turbulent boundary layer. This often makes the equations difficult to handle and increases the calculation time even further.

The HRN approach, also known as the wall function approach, is based on the velocity profile of the logarithmic law and therefore the first calculation cell must have its centroid in the logarithmic layer. The use of the HRN improves the convergence rate and often the numerical stability. That is why it will be used in this study.

3.2.2.1 Standard wall functions

Using the compact version of log-law:

$$\frac{U}{u_\tau} = \frac{1}{\kappa} \ln E y^+ \tag{14}$$

where $E = 9{,}8$.

Now using $\tau_\omega = \rho u_\tau^2$ it is obtained:

$$\tau_\omega = \frac{\rho u_\tau \kappa U}{\ln E y^+} \tag{15}$$

3.2.3 SST k-omega model

The SST turbulence model k-ω (Menter 1993) is a popular two-equation eddy viscosity model. The formulation of the shear stress transport (SST) combines the best of two fields. The use of a k-ω formulation on the inside of the boundary layer allows the model to be directly usable up to the wall through the viscous sublayer. The TSS formulation also changes to a k-ε behavior in free flow and therefore avoids the common k-ω problem that the model is too sensitive to the turbulence

properties of the incoming free flow. For this work the SST k-ω model has been selected for its good behaviour at large adverse pressure gradients and at flow separation.

The standard two-equation Menter SST model (written in conservation form) is provided by the following two equations, the first corresponding to the turbulence kinetic energy, k, and the second for the specific dissipation rate, ω:

$$\frac{\partial k}{\partial t} + U_j \frac{\partial k}{\partial x_j} = P_k - \beta^* k\omega + \frac{\partial}{\partial x_j}\left[(v + \sigma_k v_T)\frac{\partial k}{\partial x_j}\right] \tag{16}$$

$$\frac{\partial \omega}{\partial t} + U_j \frac{\partial \omega}{\partial x_j} = \alpha S^2 - \beta w^2 + \frac{\partial}{\partial x_j}\left[(v + \sigma_\omega v_T)\frac{\partial \omega}{\partial x_j}\right] + 2(1 - F_1)\sigma_{\omega^2}\frac{1}{\omega}\frac{\partial k}{\partial xi}\frac{\partial \omega}{\partial x_i} \tag{17}$$

where the kinematic eddy viscosity is computed from:

$$v_T = \frac{a_1 k}{\max(a_1\omega, \Omega F_2)} \tag{18}$$

More detailed information on constants and closure coefficients can be found at (Menter 1993).

3.2.3.1 Turbulence free-stream boundary conditions

Thus, with the chosen model, the turbulent flow would be defined through the turbulence kinetic energy, k, and the specific dissipation rate, ω:

$$k = \frac{3}{2}(UI)^2 \tag{19}$$

where U is the mean flow velocity and I is the turbulence intensity.

$$\omega = C_\mu^{-1/4}\frac{\sqrt{k}}{l} \tag{20}$$

where $C_\mu = 0{,}09$ is a turbulence model constant, and l is the turbulent length scale.

3.3 SimpleFoam solver

Now, once the equations governing the fluid and the turbulent model have been described, how they are to be solved will be explained.

For this work it has been believed that the most accurate OpenFOAM solver for the case is simpleFoam. A steady state solver for turbulent incompressible flows, using the SIMPLE algorithm. Being this stationary state has a much lower computational cost than transient solvers, and being the final goal of this research to evaluate the average reduction in the forces that a vehicle is subjected to by the action of wind thanks to wind barriers, therefore as these are average measures it is not necessary to use a transient solver. And obviously it is an incompressible fluid since it is subsonic flow.

This solver follows a segregated solution strategy. That means that the equations for each variable that characterizes the system (the speed u , the pressure p and the variables that characterize the turbulence) are sequentially solved and the solution of the precedent equation is inserted into the following equation. But when a steady state problem is solved iteratively, it is not necessary to completely solve the pressure-velocity linear coupling, since the changes between consecutive solutions would no longer be small. Therefore, simpleFoam can use the SIMPLE algorithm to solve the continuity equation (Eq. (9)) and the moment equation (Eq. (8)). Algorithm in which:

- A velocity field approximation is obtained by solving the momentum equation. The pressure gradient term is calculated using the pressure distribution of the previous iteration or an initial assumption.
- The pressure equation is formulated and solved to obtain the new pressure distribution.
- The velocities are corrected, and a new set of conservative flows is calculated.

3.3.1 SIMPLE algorithm

The sequence of each iteration of the SIMPLE (Semi-Implicit Method for Pressure-Linked Equations) can be summarized as follows:

1. Advance to the next iteration $t = t^{n+1}$.
2. Initialize u^{n+1} and p^{n+1} using latest available values of u and p.
3. Construct the momentum equations.
4. Under-relax the momentum matrix.
5. Solve the momentum equations to obtain a prediction for u^{n+1}.
6. Construct the pressure equation.
7. Solve the pressure equation for p^{n+1}.
8. Correct the flux for ϕ^{n+1}.
9. Update the pressure field: $p^{k+1} = p^k + urf \cdot p'$ where urf is the under-relaxation factor for pressure.
10. Correct the velocity for: $\vec{u}^{k+1} = \vec{u}^n - \frac{Vol\nabla p'}{\vec{a}_P^v}$ where $\nabla p'$ is the gradient of the pressure corrections, $\vec{a}_P^v$ is the vector of central coefficients for the discretized linear system representing the velocity equation and Vol is the cell volume.
11. If not converged, go back to step 2.

The discretized momentum equation and pressure correction equation are solved implicitly, where the velocity correction is solved explicitly. This is the reason why it is called "Semi-Implicit Method".

CHAPTER 4: Numerical setup

Throughout this chapter and the following one, the research work that has been carried out to reach the objectives already mentioned will be presented. Specifically, during this chapter the preparation of the CFD simulations and the geometries of the vehicles (truck, motorcycle and car) and the wind-break fences to be tested will be presented.

4.1 Geometries

In order to carry out the necessary simulations to achieve the goals of this thesis, various 3D geometries have been used, both self-made and provided by third parties, which will be shown below. The own designs have been made through the CAD software CREO Parametric by PTC.

4.1.1 Truck

For the design of the truck that has been used during this work we have tried to replicate the one used in (Cheli, Corradi, et al. 2011) and in the European projects (W.P.2.2.1 2005) and (W.P.2.3.2 2005), to be able to validate the numerical model with a contrasted source and thus give reliability to the data obtained later.

The model is inspired by the DAF LF commercial truck. At the time of the CAD design it has been tried to resemble as much as possible the main dimensions of the design to those used in (Cheli, Corradi, et al. 2011), but trying to make a simple design avoiding parts of the truck that would be a computational cost and would not vary the results of the aerodynamic studies of interest for this work, as are the parts of the engine, transmission and simplifying the design of the wheels and axles, also ,as in the designs of this truck in (Cheli, Corradi, et al. 2011), (W.P.2.2.1 2005) and (W.P.2.3.2 2005), have been omitted windows, air intakes, lights and other elements of little importance when studying the effects of side wind on the vehicle. In summary, the complex design of a real truck has been reduced to the maximum in all the details of designs that are irrelevant for this study, respecting the cab, the trailer and the chassis as their original design. The geometry of the truck used for this thesis, and its main dimensions, can be seen in the Figure 5.

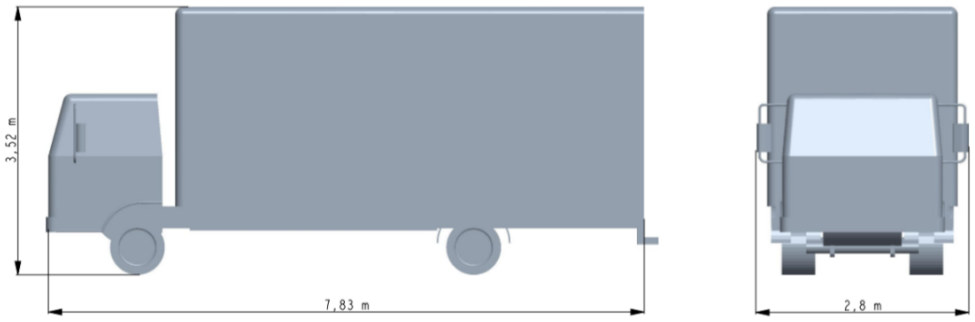

Figure 5: Main dimensions of the truck.

The truck just shown in Figure 5, being the largest vehicle to be tested, with a front area of 6,6 m^2 and a side area of 18,9 m^2, and therefore the most exposed to the action of the wind, will be the vehicle used to develop the most optimal barrier configuration to protect all road vehicles from the forces of the side wind. Therefore, it is assumed that for a fender to be able to protect all vehicles that could be on the road that it is desired to protect, it must be optimal to protect the most exposed vehicle and the one with the highest risk to the wind, which in the case of this thesis is the truck.

4.1.2 Motorbike

In the case of the motorbike to be tested, the design of this one has not been made like the one of the truck, instead it has been obtained through the geometry repository of OpenFOAM, because at the same time it is similar to the design of the motorbike used in (Fintelman, et al. 2015), therefore the validation of the numerical model of the simulations of this vehicle will be made comparing the results obtained with those presented in (Fintelman, et al. 2015).

To carry out this study, it was decided to give visibility to the risks faced by a motorcyclist in the face of a side wind, since almost all lines of research on this subject only take into consideration large and heavy vehicles such as trucks. Although motorbikes are not as exposed a road vehicle as a truck, these vehicles are extremely sensitive to wind variations and are the most unstable and vulnerable on the road, since for a motorcyclist almost any accident can be fatal.

The design to be used is the one of a sportive motorbike and its rider, more specifically the design is based on that of a Yamaha R1, one of the most sportive motorbikes in the market and therefore one of the commercial motorbikes with the best aerodynamic design, a design that has been improving since 1998.

The design of the motorbike used, and its main dimensions, can be seen in Figure 6, in addition the approximate front area of the motorbike together with the rider is 0,75 m^2.

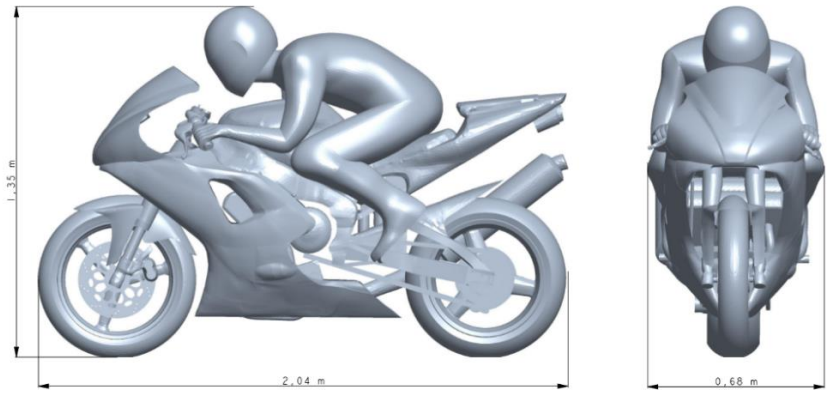

Figure 6: Main dimensions of the motorbike.

A design that, as can be seen, maintain a high level of detail, as far as all the elements of the bike are concerned, being able to appreciate in detail the engine, the brake group, the transmission and many other elements. But although having all this luxury of detail may seem like a privilege in reality it is not, because although having a design so adjusted to reality may provide results that are consequently more adjusted to reality this translates into a more complicated meshing geometry, which may give instabilities, and with it a higher computational cost. And what is sought in this project is to compare the forces to which the bike is subjected without defenses with those that are subjected with them and get the average reduction. Therefore, it is not necessary to have geometries identical to reality since the difference between the average results obtained with these geometries or with less detailed ones would barely change the results but would reduce the computational cost.

4.1.3 Car

To conclude, the last vehicle to be tested will be a car, as this is undoubtedly the most common vehicle on the roads, and therefore if you want to make a group of vehicles that include the most used, obviously could not miss the car.

In this case, like the motorbike, the design of the car has been obtained by a third party. In particular, the design of the DrivAer will be used for this work. The DrivAer is a generic car design made by the Technical University of Munich with the intention to fill the gap that existed when doing aerodynamic studies between too simple generic designs like the Ahmed Body and too complex designs, and thus create a generic car design that would be useful and similar to reality in aerodynamic studies without a big computational cost. There are also different configurations for the DrivAer, varying both its external and internal geometry. In this case the DrivAer design chosen is E_S_wM_wW, which means that the design consists of an estate back geometry, a smooth underbody, mirrors and wheels. This has been the choice because the estate back geometry makes the car more exposed to the side wind, the smooth underbody facilitates the meshing task

and reduces the computational cost with respect to a detailed underbodies, and finally it has been desired that the car has wheels and mirrors to resemble reality.

The design used and its main dimensions are shown in Figure 7:

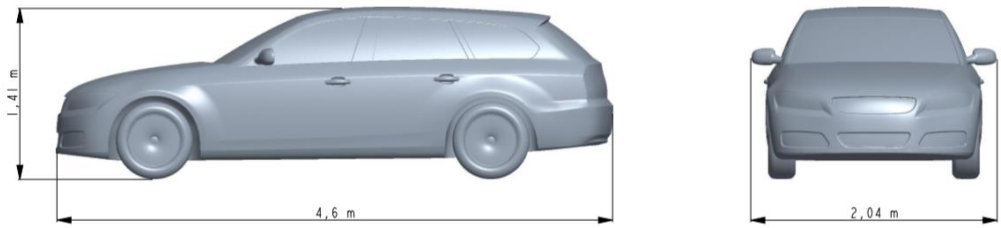

Figure 7: Main dimensions of the car.

The car, with a front area of 2.17 m^2, will not be as exposed to the side wind as the truck nor it is as unstable as the motorbike, but the action of the side wind on it is still very notorious and worthy of study.

4.1.4 Wind-break fences

The geometries of the wind barriers to be used for this work will now be presented. The fences have been designed in CAD, just like the truck, and are inspired by those used in (Alonso-Estébanez, et al. 2017). A simple design has been made, useful for checking their aerodynamic efficiency in computer software, so structural elements such as bases or pillars needed to support them have not been taken into account. As explained above for this type of study, adding elements to the geometries that are not important in their aerodynamic behaviour does not contribute to the results and does represent a computational cost.

Below, in Figure 8, can be seen the three types of barriers to be used and their position in relation to the vehicle:

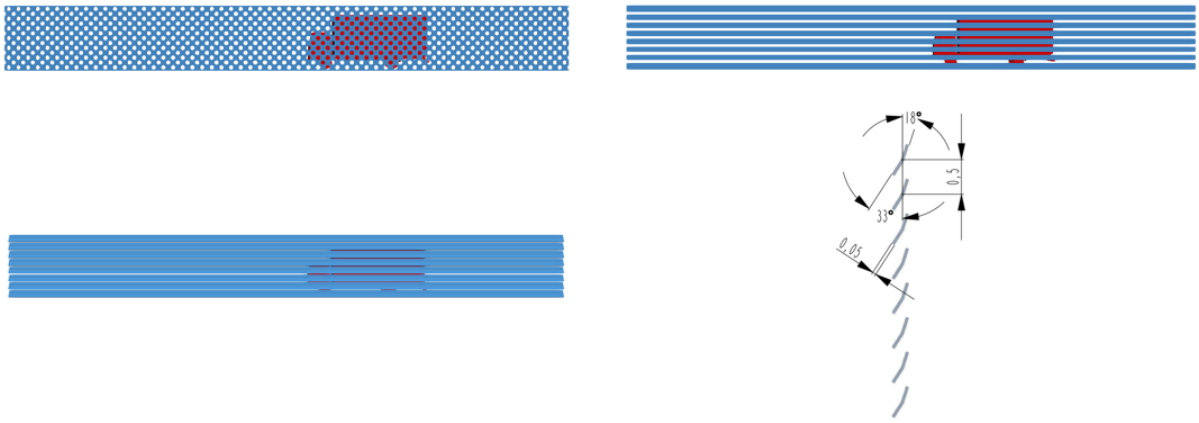

Figure 8:Wind fence models with a 30% porosity: (Top left)Wind fence model with circular holes; (Top right) Wind fence model with rectangular openings; (Bottom left) Wind fence model with plates; (Bottom right) Lateral view of the wind fence model with plates (wind direction from left to right).

The fences have a length of 35 m, from 19 m in front of the frontal face of the vehicle to 16 m behind. But in the case of wind yaw angle less than 20° the fence placed becomes 45 m long, from 29 m in front of the frontal face of the vehicle to 16 m behind. Since it is desired to simulate that the fence would be continued along the road. The concrete height of the fences that can be seen in Figure 8 is 4 m, but this height will be studied and analyzed to determine the optimal height, so fences with heights from 2 m to 4 m will be tested. In the same way the distance between the fence and the vehicle will also be studied between 2 m and 4 m, to find the optimal one. The fences are 5 cm thick

The fence with circular holes and the one with rectangular openings are typical in this type of studies, and inspired by those of Alonso, however the fence with plates is an original design inspired by that of Alonso, shown in Figure 1, but with a different arrangement of the plates. The design of the fence with plates of Alonso did not report good results, being its efficiency to protect from the wind worse than the fences with circular and rectangular holes. Therefore, the design was changed so that the plates deflected the wind upwards and thus the wind passed over the truck, contrary to the effect that this type of fence had with the configuration of Figure 1: Lungitudinal plates of a wind fence Figure 1, with which the wind was deflected downwards, a choice that did not produce good protection and produced an increase in the lift force with respect to the other fences.

With respect to porosity, the fences in Figure 8 have a porosity of 30%, with porosity defined as:

$$\beta = \frac{A_V}{A_T} \tag{21}$$

where A_V is the void area of the fence and A_T is the total area of this.

In this work the effect of porosity on the efficiency of a wind fence when protecting a vehicle from the action of the side wind will be studied. Therefore, fences with different degrees of porosity will be tested: 0% (which indicates an opaque fence and the same for the three types of geometries), 10%, 20% and 30%. The porosity in the fences will be varied by varying the open area of it, so for the fence with circular holes to vary the porosity will vary the diameter of the holes, in the case of the fence with rectangular openings will vary the width of these openings, and finally in the case of fences with plates its porosity will vary by varying the angles (shown in Figure 8 (bottom right)) of the plates, increasing or decreasing the distance between the plates through which the flow can pass.

4.2 Case setup

In this section the preparation that has been made for the realization of the subsequent simulations will be treated. The aerodynamic coefficients, the computational domain and the boundary conditions and the meshing of the geometries will be presented.

4.2.1 Aerodynamic coefficients and case velocities

As a result of the interaction between an airstream and a vehicle, forces and moments are imposed. These forces and moments, due to the complex distribution of pressures on a vehicle, can be summarized to those acting through the three main axis of the vehicle. The origin of the axis in a vehicle is defined in SAE J1594, where it says that, since the aerodynamic reactions of a vehicle are not related to the location of its center of gravity (position which is not always known), the center for the measurement of the forces and moments is found in the ground plane at the mid-wheelbase and the mid-track position.

The forces acting on the vehicle will be extracted once the pressure distribution has been resolved, as shown in CHAPTER 3:Numerical method. From this pressure distribution, by integrating it on the surface of the vehicle, the forces acting on the vehicle can be obtained. This operation will be carried out by the OpenFOAM functionality `forces`, which calculates the forces as follows:

Forces comprise normal pressure:

$$F_p = \sum_i \rho_i s_{f,i} (p_i - p_{ref}) \tag{22}$$

and tangential viscous contributions:

$$F_v = \sum_i s_{f,i} \cdot (\mu \boldsymbol{R_{dev}}) \tag{23}$$

where ρ is the density, $s_{f,i}$the face area vector, p the pressure μ the dynamic viscosity and $\boldsymbol{R_{dev}}$ the deviatoric stress tensor.

Moreover, the moments are the sum of the moments caused by the forces above the origin.

Once the forces and moments are calculated they become dimensionless by the aerodynamic coefficients:

$$C_D = \frac{F_D}{1/2\,\rho\, {V_R}^2 A} \tag{24}$$

$$C_S = \frac{F_S}{1/2\,\rho\, {V_R}^2 A} \tag{25}$$

$$C_L = \frac{F_L}{1/2\,\rho\, {V_R}^2 A} \tag{26}$$

And as for the moments, the coefficient that interests and will be used in this work will be the rolling moment coefficient:

$$C_M = \frac{M_R}{1/2\,\rho\, {V_R}^2 A\, h} \tag{27}$$

where F_D, F_S, F_L, are the drag force, the side force and the lift force respectively, M_R is the rolling moment, ρ is the density, V_R is the relative velocity, A the characteristic area (will be explained below) and h the characteristic height of the vehicle.

With regard to A, what has been called characteristic area, there is much confusion in the literature regarding what area to use to obtain the aerodynamic coefficients when studying cross wind. For the drag coefficient there is no doubt and the front area of the vehicle is always used, but for the other coefficients, lateral, lift and moment, in some cases the lateral area is used ((Cheli, Corradi, et al. 2011); (Alonso-Estébanez, et al. 2017)) and in others the frontal area ((Gillespie 1992); (Fintelman, et al. 2015)). Therefore, as the aerodynamic coefficients for this work are a way to compare the action of the wind on the vehicle in the different cases, being the area used to adimension the force, which is the real result of the simulation, it has been decided to use both the frontal and the side area to calculate the coefficients according to what has been used in the studies that will be utilized for the validation, in order to be able to compare the results with those of the validation directly. And as for the final results and conclusion of the investigation the reduction in the aerodynamic coefficient of each vehicle, for with or without fences, will be evaluated as a percentage, and thus the use of the side or front area will not come into play in the final results.

Speaking now about the relative speed, (Kramer, Grundmann and Gerhardt 1991) described the parameters that influence the aerodynamic loads of a vehicle under cross-wind conditions, and derived the relationship between cross-wind, V_W, speed and vehicle speed, V_V:

$$V_R = \sqrt{{V_W}^2 + {V_V}^2 + 2V_W V_V \cos\alpha} \tag{28}$$

where is $V_R$is the relative velocity and α the angle between vehicle speed and wind speed (as shown in Figure 9).

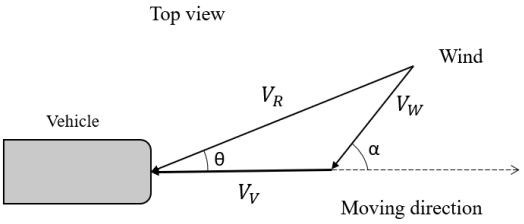

Figure 9: Speed scheme seen from the top.

In this work it will be assumed for all cases that the wind speed is always perpendicular to that of the vehicle, because this would be the most unfavourable case for the resistance of a vehicle to the cross wind, since as has been seen in Eq. (8) for an $\alpha = 90°$ the highest relative speed is obtained, and furthermore in this study we wish to study the maximum number of yaw angles, but always from a real point of view (Table 1), and the larger α is, the larger θ is.

During the research it is desired to check the efficiency of the wind fences in situations of real wind speed and vehicle speed, so different cases with plausible speeds have been prepared to study the barriers in five different yawing angles, from 10° to 50°, shown in the following table:

Yaw angle (θ)	V_V		V_W		V_R	
[°]	[km/h]	[m/s]	[km/h]	[m/s]	[km/h]	[m/s]
10	120	33.333	21.159	5.8776	121.8512	33.848
20	120	33.333	43.676	12.132	127.7013	35.473
30	120	33.333	69.282	19.245	138.5641	38.490
40	90	25	75.519	20.977	117.4867	32.635
50	70	19.444	83.423	23.173	108.9007	30.250

Table 1: Velocities of the cases according to their yaw angle.

where the relative velocity is calculated as shown in the Eq. (28), but as already mentioned an $\alpha = 90°$ angle will be considered so the equation is reduced to:

$$V_R = \sqrt{{V_W}^2 + {V_V}^2} \tag{29}$$

as $\cos 90 = 0$.

In planning the speeds for the cases in Table 1, as already mentioned, the intention was to use plausible speeds, so for the speed of the vehicle typical European road speeds were taken, such as 120 km/h, 90 km/h and 70 km/h. When choosing the wind velocities to make driving at these wind speeds plausible, the Beaufort scale has been taken as a reference, shown in Table 2, so according to this scale the wind speed at which it is credible to drive has been limited to around 80 km/h, which corresponds to the last case of 50°.

For more than 50 years, no more yawing angles have been considered, since to obtain these, the vehicle speed should be reduced to an urban speed, a situation that does not interest to consider in the study of wind fences, since these are designed to be placed on the roads, outside the cities. Or the wind speed should be very high, wind intensity for which it would be difficult to think about driving, and with hurricane gusts of wind with random directions for which protection cannot be guaranteed with wind fences.

Level	V_W [km/h]	Description
Light	0-20	Calm; smoke rises vertically - Leaves and smaller twigs in constant motion.
Moderate	21-40	Dust and loose paper raised; small branches begin to move - Branches of a moderate size move; small trees begin to sway.
Strong	41-74	Large branches in motion; umbrella use becomes difficult; empty plastic garbage cans tip over - Twigs broken from trees; cars veer on road.
Very strong	75-117	Larger branches break off trees, and some small trees blow over; construction/temporary signs and barricades blow over - Widespread vegetation damage; more damage to most roofing surfaces; asphalt tiles that have curled up and/or fractured due to age may break away completely.
Hurricane	≥118	Considerable and widespread damage to vegetation, a few windows broken, structural damage to mobile homes and poorly constructed sheds and barns; debris may be hurled about.

Table 2: Beaufort scale.

4.2.2 Grid, boundary conditions and simulation settings

4.2.2.1 Main settings

As already mentioned, the aerodynamic study of the different vehicles and the effect of the wind fences on them will be tested through CFD simulations using the open source OpenFOAM, specifically using the snappyHexMesh preprocessor, the simpleFoam solver (explained in the section 3.3 SimpleFoam solver) and the paraView postprocessor. The preparation and features of these CFD simulations will be shown below.

In order to solve the incompressible steady state equations RANS, it has been chosen to use the two equations of the k-omega SST turbulent model (section 3.2.3 SST k-omega model), for which it will first be necessary to calculate the values of these turbulence parameters, turbulence kinetic energy, k, with the Eq. (19), and the specific dissipation rate, ω, with the Eq. (20).

To initialize the simulation, the basic potentialFoam solver is used. This solver initializes internal fields away from the walls for viscosity computations. PotentialFoam is a potential flow solver which solves for the velocity potential (i.e. Phi) to calculate the volumetric face-flux field (i.e. phi) from which the velocity field (i.e. U) is obtained by reconstructing the flux (OpenFOAM: User Guide: potentialFoam n.d.).

For incompressible steady-state potential flows, the governing equation of the velocity potential satisfies the Laplace's equation:

$$\nabla^2 \phi = 0 \tag{30}$$

where ϕ is the velocity potential.

Velocity field (i.e. u) can then be computed from the velocity potential as follows:

$$u = \nabla \phi \tag{31}$$

where the velocity field is solenoidal:

$$\nabla \cdot u = 0 \tag{32}$$

The numerical schemes of the simulation are defined in the `fvSchemes` dictionary. The fvSchemes dictionary in the system directory sets the numerical schemes for terms, such as derivatives in equations, that are calculated during a simulation. The terms that must typically be assigned a numerical scheme in fvSchemes range from derivatives, e.g. gradient∇, to interpolations of values from one set of points to another. The aim in OpenFOAM is to offer an unrestricted choice to the user, starting with the choice of discretisation practice which is generally standard Gaussian finite volume integration. Gaussian integration is based on summing values on cell faces, which must be interpolated from cell centres. The user has a wide range of options for interpolation scheme, with certain schemes being specifically designed for particular derivative terms, especially the advection divergence ∇ • terms (OpenFOAM User Guide 2011).

For this work the selected numerical schemes are as follows:

- The first time derivative $\left(\frac{\partial}{\partial t}\right)$ terms: `steadyState`: sets time derivatives to zero.
- Gradient schemes (∇):
    - default: `Gauss linear`: The Gauss entry specifies the standard finite volume discretisation of Gaussian integration which requires the interpolation of values from cell centres to face centres. The interpolation scheme is then given by the linear entry, meaning linear interpolation or central differencing.
    - grad(U): `cellLimited Gauss linear 1`: The cellLimited scheme limits the gradient such that when cell values are extrapolated to faces using the calculated gradient, the face values do not fall outside the bounds of values in surrounding cells. 1 guarantees boundedness.
- Divergence schemes ($\nabla \cdot$):
    - div(phi,U): `bounded Gauss linearUpwindV grad(U)`: Second order, upwind-biased, unbounded.
    - div(phi,k): `bounded Gauss limitedLinear 1`: linear scheme that limits towards upwind in regions of rapidly changing gradient, 1 is strongest limiting.
    - div(phi,omega): `bounded Gauss limitedLinear 1`
    - div((nuEff*dev2(T(grad(U))))): `Gauss linear`: Second order, unbounded.

- Surface normal gradient schemes:
  - default: `limited 0.333`: Non-orthogonal correction.
- Laplacian schemes (∇^2):
  - default: `Gauss linear limited 0.333`
- Interpolation schemes:
  - default: `linear`

All the choices that have been made regarding the choice of numerical schemes are based on seeking maximum precision without making the case unbounded. For more information on the definition of these parameters (OpenFOAM User Guide 2011).

One last numerical parameter to comment on the preparation of the simulation are the relaxation factors. These parameters that come into play in the SIMPLE algorithm, limit what a solution can vary from the previous iteration, as seen in section 3.3.1 SIMPLE algorithm, being a simulation that will require more time for low relaxation factors and a simulation with risk of becoming unlimited for high relaxation factors. Being those chosen for this case equal to 0.7 for velocity, kinetic energy and specific dissipation rate, and 0,3 for pressure.

Once all these parameters are adjusted, the simulation becomes solved by iterating until low residual values are obtained and the convergence of the aerodynamic forces acting on the vehicle is reached.

4.2.2.2 Computational domain and boundary conditions

The size of the computational domain has been chosen according to the literature so that it is large enough to fully develop the wake created by the vehicle and the wind fences, minimize the blockage of the domain and minimize the influence of boundary conditions on the numerical results, but not larger than necessary, which would lead to unnecessary computational cost, as can be seen in Figure 10:

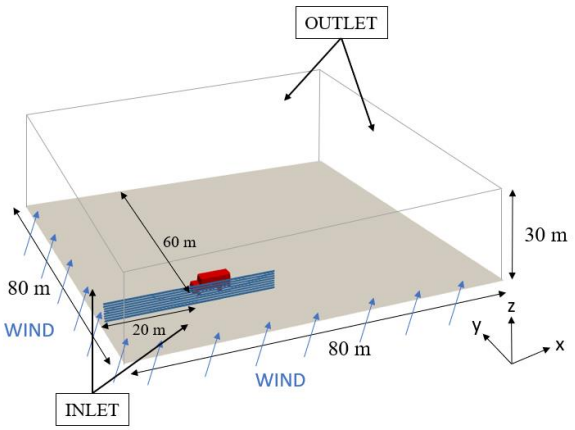

Figure 10: Computational domain.

The domain has been prepared for the simulation of the largest vehicle, which in this case is the truck, which has approximate dimensions of length L=8 m and height H=4 m (Figure 5), so the dimensions of the domain have been set at 10L=80 m in length and width (Salati, et al. 2018) and 8H=32 m in height (rounded to 30 m).

The domain has two inlets, through which the flow will enter the domain and two outlets, through which the flow will leave the domain. The flow in the domain will be composed by the supposed wind speed and the vehicle speed, thus entering the domain by the inlets as the relative speed between both speeds and the yaw angle, values shown in Table 1. The domain has an upper wall and a lower wall, on which the vehicle and the fence will be supported, simulating the ground.

The vehicle will be placed on the ground (lower wall) closer to the inlets, 20 m from the middle of the front of the vehicle to each one, than to the outlets, 60 m from the middle of the front of the vehicle to each one, since it is a stationary state simulation and with the initialization the flow in the domain will be completely developed upstream, so the necessary space between the vehicle and the inlets is not for the flow to develop but to have space for a sufficient mesh to calculate this flow, and thus more space is left downstream for the correct interpretation of the wake produced by the fences, which is assumed to be large. But, as already mentioned (4.1.4 Wind-break fences), for angles less than 20 meters the fence will be 29 meters ahead of the vehicle so for these cases the vehicle will be placed 30 m from each inlet and 50 m from each outlet.

The boundary conditions used in the simulations are as follows:

- INLET: Fixed flow velocity and yaw angle with the above turbulence conditions and a zero gradient pressure boundary condition.
- OUTLET: An inlet-outlet boundary condition has been imposed for velocity, which means that the outflow is treated as a zero gradient and allows for upstream flow (a condition that will not occur in this study), while for pressure the average relative pressure has been set at 0 Pa.
- TRUCK: A no-slip condition has been imposed (U_x, U_y, U_z =0) and standard wall functions are applied.
- FENCE and LOWER WALL: To simulate the vehicle's movement, a fixed speed equal to the assumed vehicle velocity in the x-direction has been imposed, and like the truck, standard wall functions.
- UPPER WALL: As this wall is simulated as the sky, a slip condition has been imposed on it, so that it does not influence the numerical results.

4.2.2.3 The mesh

In CFD simulations the meshing is one of the most important points since the quality of the mesh will condition the numerical results obtained, which could be wrong or, with a poor-quality mesh, the case could become unstable. Although on the other hand it is not possible to make a super fine mesh to assure the accuracy of the simulation since this would suppose an enormous computational cost, reason why at the time of the meshing , the greater challenge is the one to obtain a good and

optimized mesh, that is to say that it allows to obtain correct numerical results with the smaller possible computational cost.

The OpenFOAM pre-processing utility snappyHexMesh will be used to perform the meshing. The snappyHexMesh utility generates 3-dimensional meshes containing hexahedra and split-hexahedra automatically from triangulated surface geometries, or tri-surfaces, in Stereolithography (STL) or Wavefront Object (OBJ) format (OpenFOAM User Guide 2011).

Summarized snappyHexMesh works like this (OpenFOAM User Guide 2011):

1. The user must create a background mesh of hexahedral cells that fills the entire region within by the external boundary.
2. Cell splitting at feature edges and surfaces.
3. Removal of the cells inside the surfaces.
4. Cell splitting in specified regions, like refinement boxes.
5. Snapping to surfaces: Moving cell vertex points onto surface geometry to remove the jagged castellated surface from the mesh.
6. Mesh layers.

The strategy followed when creating the mesh of the domain and of each of the vehicles for the different cases has been to take the truck as a reference as it is the largest vehicle and the one that will create a more extensive wake due to the action of the wind on it, and as it is the only vehicle for which there is a good reference of experimental data for the different yawing angles with which to carry out the validation. Therefore, the strategy will be to optimize a mesh for each yaw angle in the case of the truck and validate it and use these meshes for the rest of the vehicles (car and motorbike), that is, with the same dimensions of the refinement boxes, since it has been assumed that if this level of fineness is capable of extracting correct numerical results on a large wake, it should be able to extract good numerical results from smaller wakes in the same way. In this way, although it is not an optimized mesh and goes against what is expressed in the previous paragraph, it ensures the correctness of the results of the bike and the car, for which there is no experimental source for validation as in the case of the truck.

In the same way also for each meshing process there will be an attempt to optimize in number of cells trying with different levels of refining until arriving at the point in which the results become constant, since as a mesh is refined it gets closer to the correct result until it is reached and no matter how much more the mesh is refined the result remains the same. This process will be carried out more carefully in the case of the truck and then for the rest of the vehicle it will only be as a check that the level of refinement required is the same.

4.2.2.3.1 Truck

Like it has already been said, the truck will be the geometry with which the characteristics of each mesh (of each yaw angle) will be developed and then applied to the rest of the vehicles.

As specified in the steps that follows the snappyHexMesh utility the first step is to create a background of hexahedral cells that covers the whole domain. This background will be the first level (level 0) of refinement in the mesh, background that for this work has been fixed in cells of one meter, the domain has been divided in 80x80x30 cells, which come to be 192000 cells.

The second level (which for snappyHexMesh this will be level 3, for each level of refinement each cell is divided into four, so level 3 means that each cell on the background will be divided into 64) of refinement in the mesh will be a large refinement box that will wrap around the entire wake created by the truck and the pressure gradient created upstream. A second smaller refining box around the truck will be the third level (level 4) of refinement that will be in the mesh. The cells surrounding the truck will be divided into two other levels (level 5 and 6), a higher level for those surfaces of the truck with steeper angles, and around the truck six layers will be applied to satisfy the y-plus needed to correctly solve the wall functions (3.2.2 Near-wall treatments). All this can be seen more clearly in the following figures:

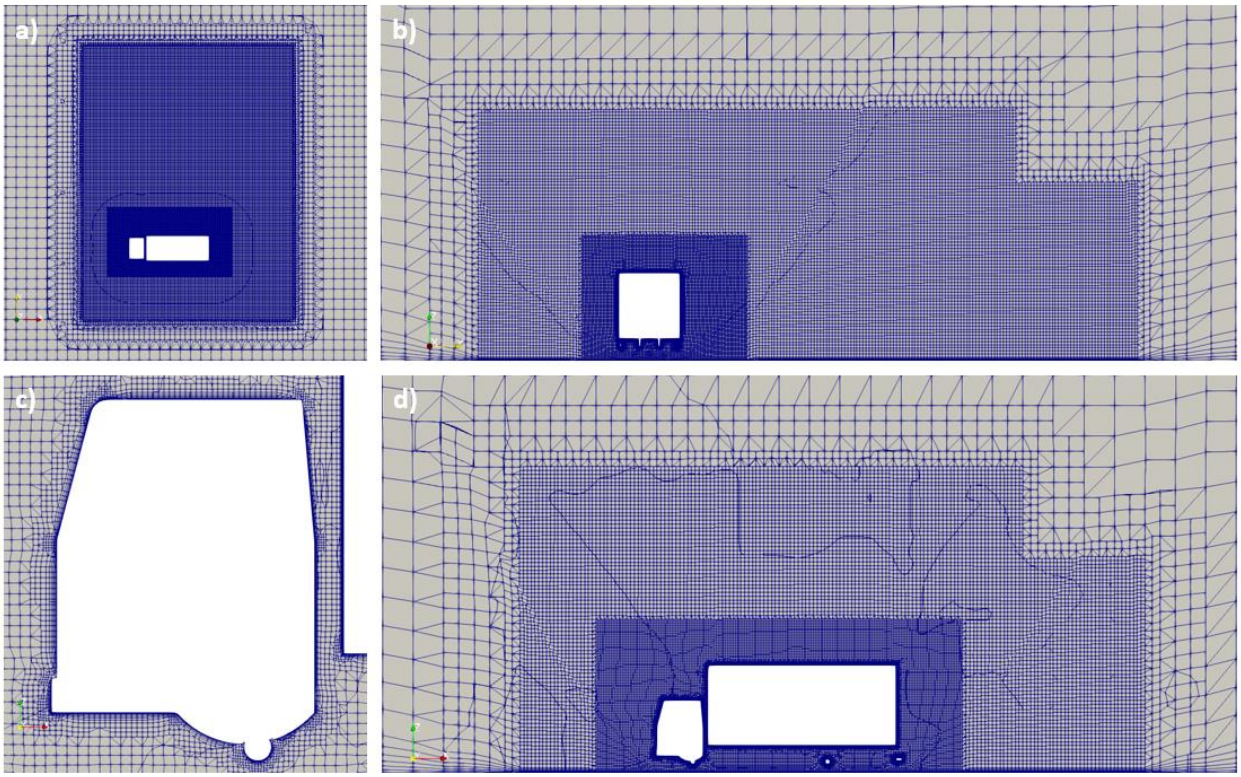

Figure 11: Truck mesh for a 50° yaw angle: a) View of the refinement boxes on the x-y plane for z=2; b) View of the refinement boxes on the y-z plane for x=4; c) View of the layers on the truck cabin; d) View of the refinement boxes on the x-z plane for y=0.

The strange lines seen in Figure 11 between the cells of the mesh appear when the postprocessor triangulates the cells contained in the plane of the slice, in reality these lines do not exist in the mesh.

It is recalled that the origin of coordinates is located on the ground in the middle of the front of the vehicle

The mesh shown in Figure 11 is the definitive mesh for performing the truck simulations for a wind yaw angle of 50, this specific mesh consists of 6.7 million cells and an average y+ of 77, which guarantees the good functionality of the HRN wall functions (y+ which according to the literature for this type of study must be below 300).

Reaching this mesh optimized for this simulation is a long and laborious job. To reach the level of refinement necessary to achieve good numerical results, the behaviour of the truck at a yaw angle of 90° has been simulated for different levels of refinement and total number of cells, since this is the case in which, although it is not realistic, the truck is more stressed by the wind and it will be the starting point for the subsequent validation with the experimental results of (Cheli, Corradi, et al. 2011).

The figure below shows how the values of the lateral and momentum aerodynamic coefficient, as they are the most significant in this case, grow (in absolute value) as the number of cells increases until they reach a point where they remain constant.

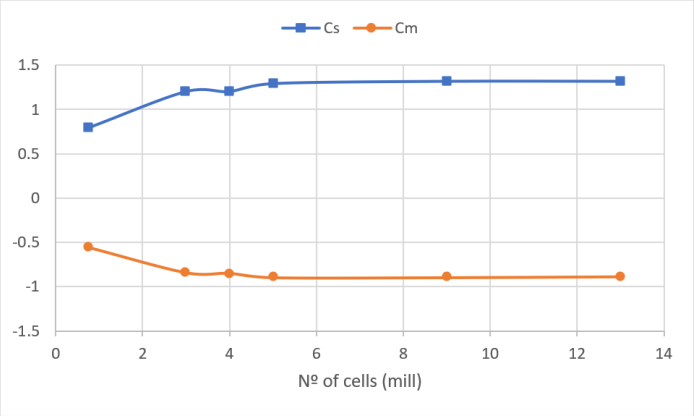

Figure 12: The effect of the number of cells on the truck's aerodynamic coefficients for a 90° yaw angle.

In Figure 12 it can be seen how from approximately 6 million cells the aerodynamic coefficients remain constant.

The strategy followed to arrive at the definitive and optimized meshes of the truck was to carry out the validation, which will be shown later, with a mesh that is represented by the penultimate point in Figure 12 with about 9 million cells. Once the numerical model was validated, the number of cells was moved backwards while maintaining the results of the aerodynamic coefficients

constant until arriving to meshes with a number of cells of about 6.5 million as that shown in Figure 11.

A mesh that would report correct results for all yaw-angle cases could have been created but solving the cases with this mesh would have a higher computational cost, so a different mesh has been created for each yaw-angle case. The difference between each of these meshes results in having longer refinement boxes in the x-direction at lower yaw angles and longer refinement boxes in the y-direction at higher yaw angles (Appendix A: Meshes for each yaw angle)

4.2.2.3.2 Motorbike

The procedure for the mesh of the motorbike, as already mentioned, will be to introduce the geometry of the bike in the refinement boxes of the truck's mesh and maintain its parameters, since it is assumed that if the mesh is fine enough to report good results for the truck, it is for the cases of the bike.

The resulting mesh used for the cases of the bike with a yaw angle of 40 is shown below:

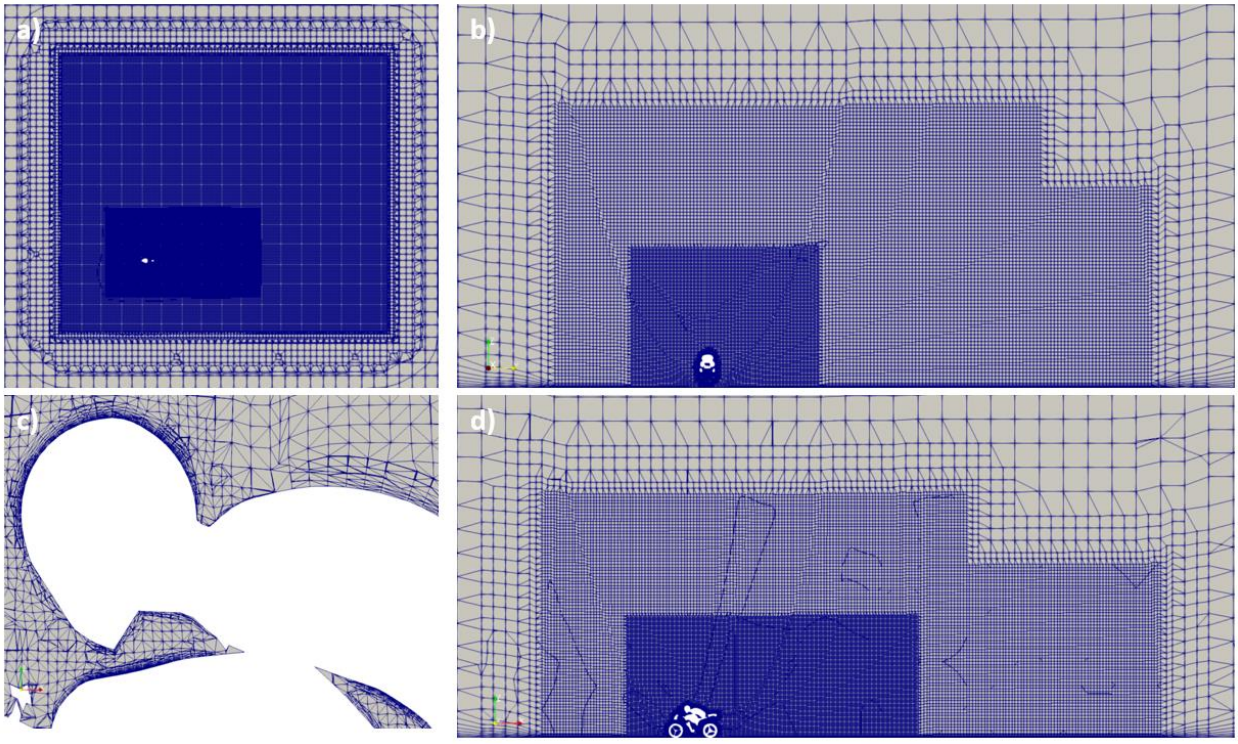

Figure 13: Motorbike mesh for a 40° yaw angle: a) View of the refinement boxes on the x-y plane for z=1; b) View of the refinement boxes on the y-z plane for x=1; c) View of the layers on the rider; d) View of the refinement boxes on the x-z plane for y=0.

Figure 13 shows the mesh used in for the motorcycle in the cases for a 40° yaw angle, mesh that is equal in terms of the refinement boxes to that mesh that will be used for the cases of the truck with a 40° yaw angle. This particular mesh of the motorbike has 5 million cells and an average y+

of 90. Given the complexity of the geometry of the bike, explained previously (4.1.2 Motorbike), it has been necessary to increase the number of layers on the surface of the motorbike from 6 to 8 because of its hard geometry it is more complicated to apply the layers on these.

As with the truck, by way of assurance it has been verified that the number of cells is the optimum by simulating a specific case, in this case for a yaw angle of 30, because this is the only angle in common between the validation references and the cases that are desired in this work, for different levels of refinement and number of cells:

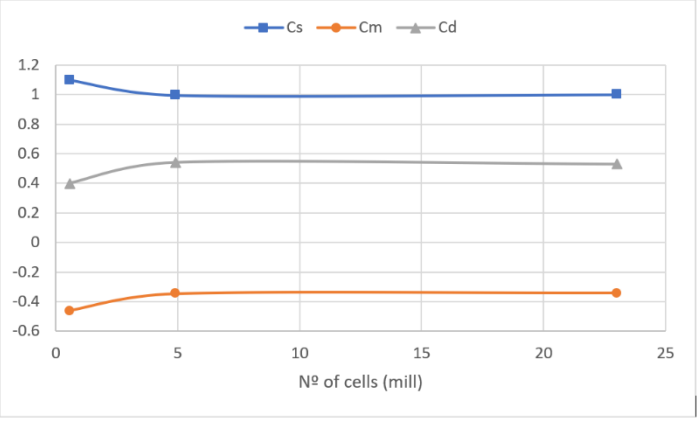

Figure 14: The effect of the number of cells on the motorbike's aerodynamic coefficients for a 30° yaw angle.

As seen previously with the truck, the aerodynamic coefficients vary from the poorest meshes to the optimum point where the coefficients become constant. Therefore, as shown in Figure 13, although it cannot be concluded that the optimum point is for 5 million cells, since more cases would be needed to be simulated for lower cell numbers, it can be concluded that the results for a 5 million cell mesh are correct since they are the same as those for an over-refined 23 million cell mesh.

4.2.2.3.3 Car

For the meshing of the car, the same procedure will be followed as for the motorcycle. The refinement boxes of the truck and its parameters will be copied and the geometry of the car will be introduced, thus obtaining a mesh that ensures the correctness of the numerical results during the simulations.

The figure below shows the mesh used for the car in the case of a wind yaw angle of 30°, again this mesh is the same as the one used for the truck with a yaw angle of 30°, but with the geometry of the truck inside instead of the car:

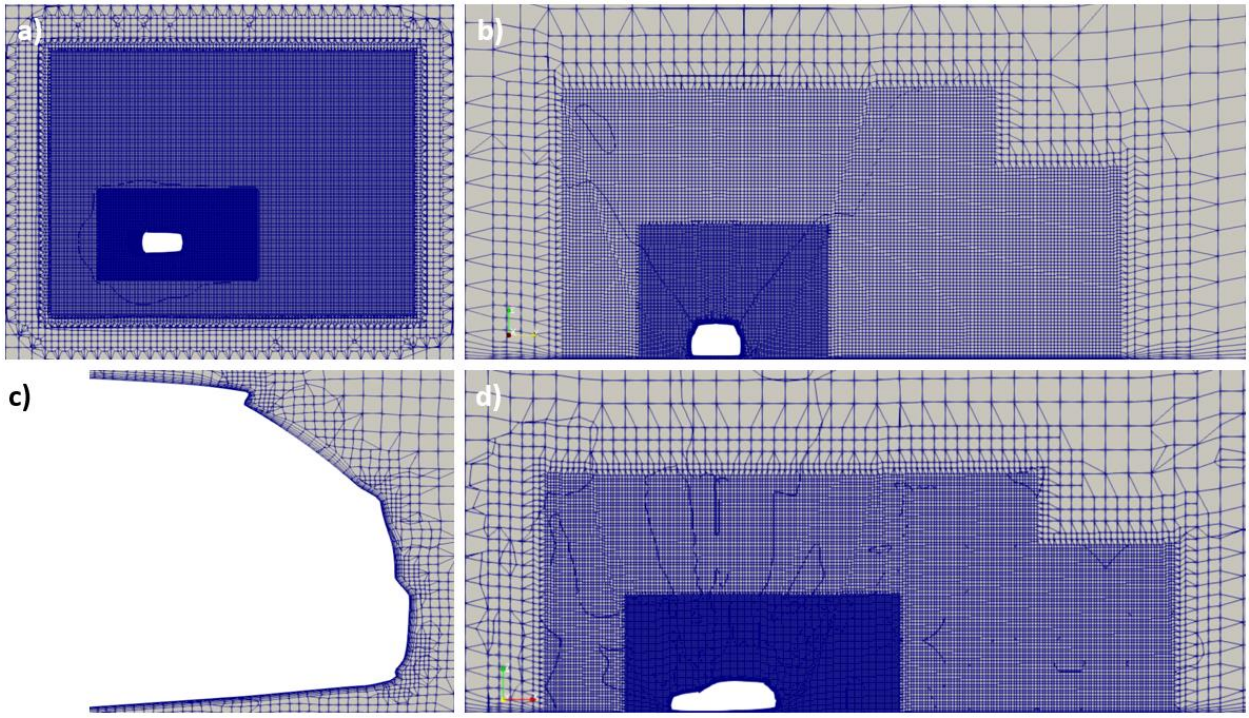

Figure 15: Car mesh for a 40° yaw angle: a) View of the refinement boxes on the x-y plane for z=1; b) View of the refinement boxes on the y-z plane for x=2; c) View of the layers on the rear of the car; d) View of the refinement boxes on the x-z plane for y=0.

The mesh shown in figure 15 consists of 5.14 million cells, and in the case of the car the average y+ is 106 with 6 layers, like the truck, which is still below the y+ of 300 indicated as the limit according to the literature for wall functions.

As it has been done with the motorbike, a slight validation of the correctness of the mesh and its optimization will be carried out. For the case of the car, different simulations will be made for different levels of refinement and number of cells for the case with a yaw angle of 0, since these are the only results available from the literature for the subsequent validation.

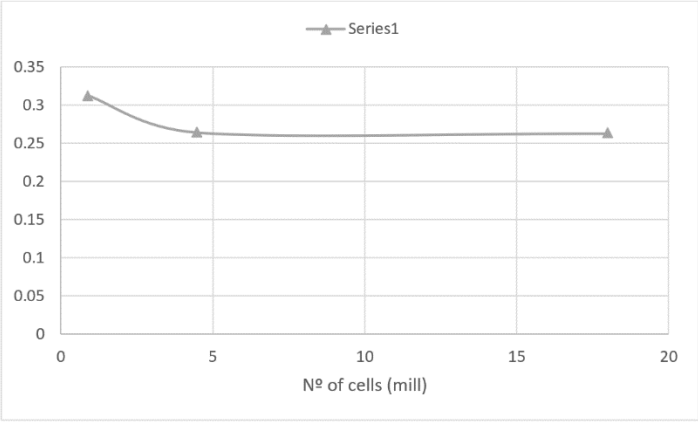

Figure 16: The effect of the number of cells on the car's aerodynamic coefficients for a 0° yaw angle.

Again, with the results obtained shown in figure 16, where the car drag coefficient obtained for different number of cells is compared, it can be concluded that a mesh for the car of about 5 million cells satisfies the required refinement and the results are the same as for a mesh of 18 million cells.

4.2.2.3.4 Wind-break fences

At the time of meshing the fences, since there is no data with which to validate the mesh, several simulations have been made with different configurations of levels of refinement, additional layers and number of cells. Specifically, the case to be used for validation is that of a fence with circular holes with a 10% porosity, as the same mesh is supposed to be suitable for all types of fences to be tested, and a wind with a yaw angle of 50°. The result of the aerodynamic coefficients of these simulations is shown in the following graph:

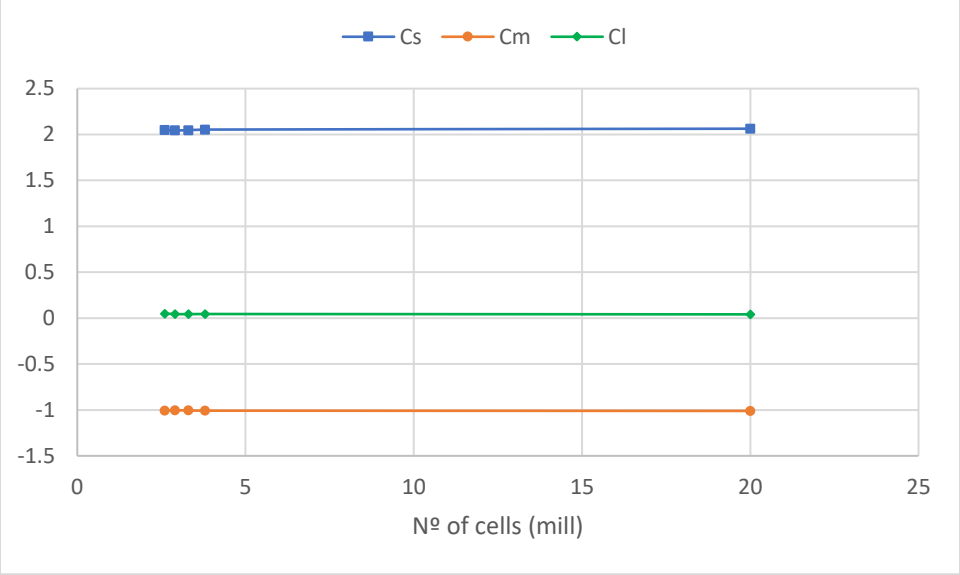

Figure 17: The effect of the number of cells on the fence's aerodynamic coefficients for a 50° yaw angle.

As can be seen from the first attempt it was already at the point with the same results as a mesh with 20 million cells. Specifically, the mesh that will be used is the second point of the graph, mesh which contains 2.9 million cells and an average y+ of 200, remember that the limit is 300.

The mesh of the fences will be composed of two refinement boxes, a larger one that will collect most of the wake (level 2) and a smaller one around the fence (level 3). In addition, the cells surrounding the fence surface will have two upper levels, as in the mesh of the vehicles, (level 4 and 5) and finally the fence surface will have two layers to obtain a y+ below 300.

Once the fences have been meshed, this mesh will be fused with those of the vehicles in each case in order to test the vehicle together with the fences and see how these affect the behaviour of the vehicle against the wind.

The following shows what the mesh of the truck and the rectangular holes fence with 10% porosity and a yaw angle of 10 would look like:

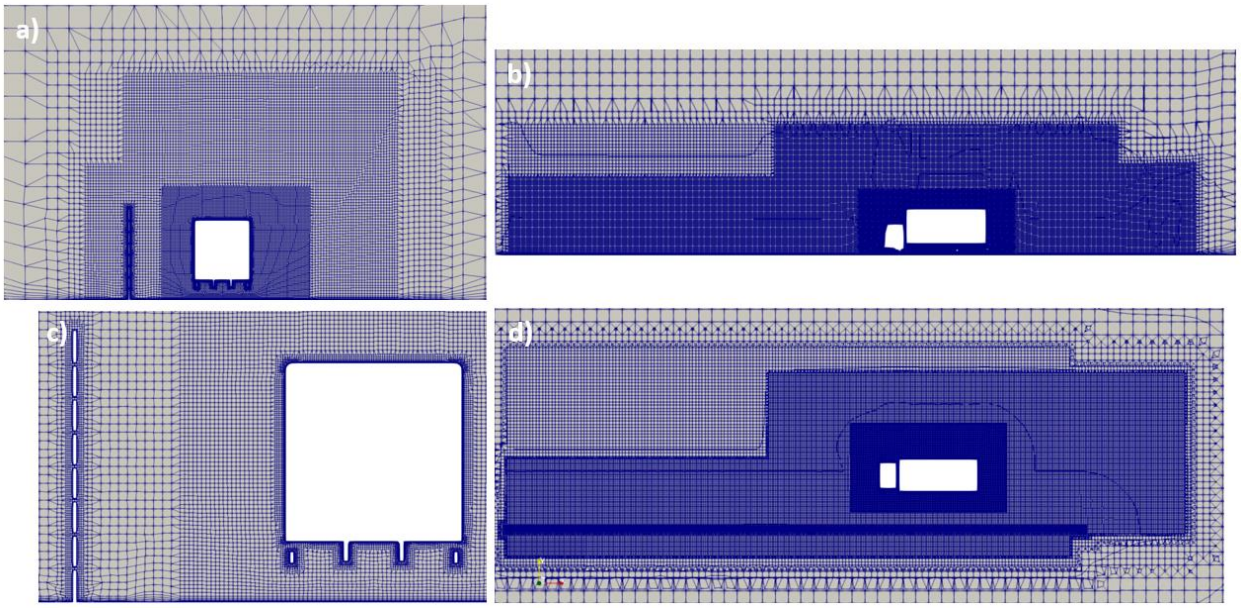

Figure 18: Truck and rectangular fence with 10% porosity mesh for a 10° yaw angle: a) View of the refinement boxes on the y-z plane for x=4; b) View of the refinement boxes on the x-z plane for y=0; c) View of the layers on the fence and trailer; d) View of the refinement boxes on the x-y plane for z=2.

It should be remembered that since the mesh shown in Figure 18 is the one in which the wind would have a yaw angle of 10, the fence shown has a total length of 45 m, with 29 m of fence in front of the front of the truck, which in this case is placed 30 m from the inlets. For all other cases the fence will be 35 m long and the truck will be positioned 20 m from the inlets.

As can be seen in Figure 18, there are four refinement boxes, two from the original truck mesh and two from the one from the fence, and there are three different levels in the refinement boxes, the least fine box is the big one from the fence mesh, the smallest box from the fence and the biggest one from the truck are the same level and are joined together and finally the finest box is the one surrounding the truck.

Finally, this mesh that joins the fence and the truck consists of 9 million cells.

4.2.3 The validation

During this section, the numerical model of each of the vehicles will be validated with external references, comparing the results obtained by the model just explained and those obtained by other studies, either experimentally or numerically.

4.2.3.1 Truck validation

For the validation of the numerical model of the truck, the results obtained by the own model will be compared with those obtained in (Cheli, Corradi, et al. 2011) in an experimental way.

In (Cheli, Corradi, et al. 2011) the aerodynamic behaviour of a truck is studied, which has been tried to replicate, in a wind tunnel. For the validation as it is wanted to imitate the conditions of the wind tunnel the speed of the wind will be fixed of 20 m/s and the yaw angle of the wind will vary from an angle of 0° to one of 90° in intervals of 15°.

The aerodynamic coefficients shall be calculated with the equations (24), (25), (26) and (27), for which V_R=20 m/s, A=6.6 m^2 , wich is the frontal area, for the drag coefficient of equation (24) and A=18.9 m^2, which is de lateral area, for equations (25), (26) and (27), in equation (27) h=2.62 m. These parameters will be used for all the studies carried out with the truck, and are the same as those used in (Cheli, Corradi, et al. 2011). It should be remembered that, as has already been said, these parameters have no influence on the final result, since the percentage difference will be studied; the important aspect is to know how to interpret them and always use the same ones throughout the work for the same geometry.

The results of the aerodynamic coefficients obtained experimentally in (Cheli, Corradi, et al. 2011) and those obtained with our numerical model will be shown below:

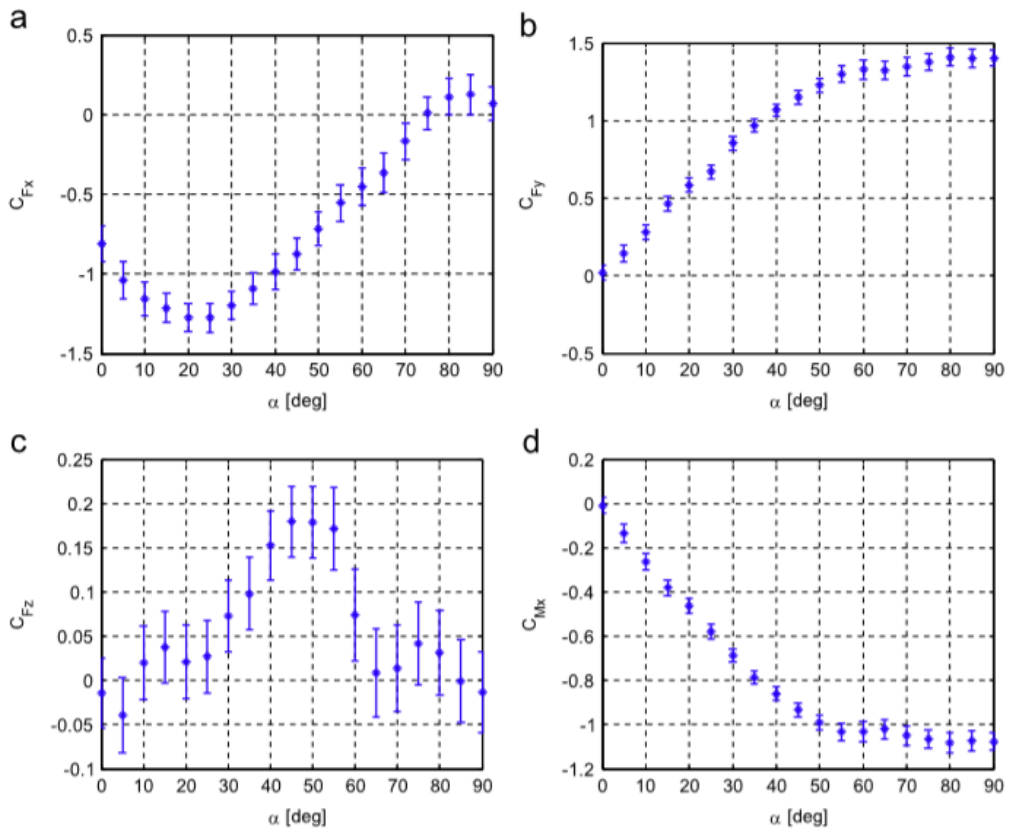

Figure 19: VAN, flat ground, low turbulence: longitudinal C_{Fx} (a), lateral C_{Fy} (b), vertical C_{Fz} (c) force coefficients and roll C_{Mx} (d), moment coefficients (Cheli, Corradi, et al. 2011).

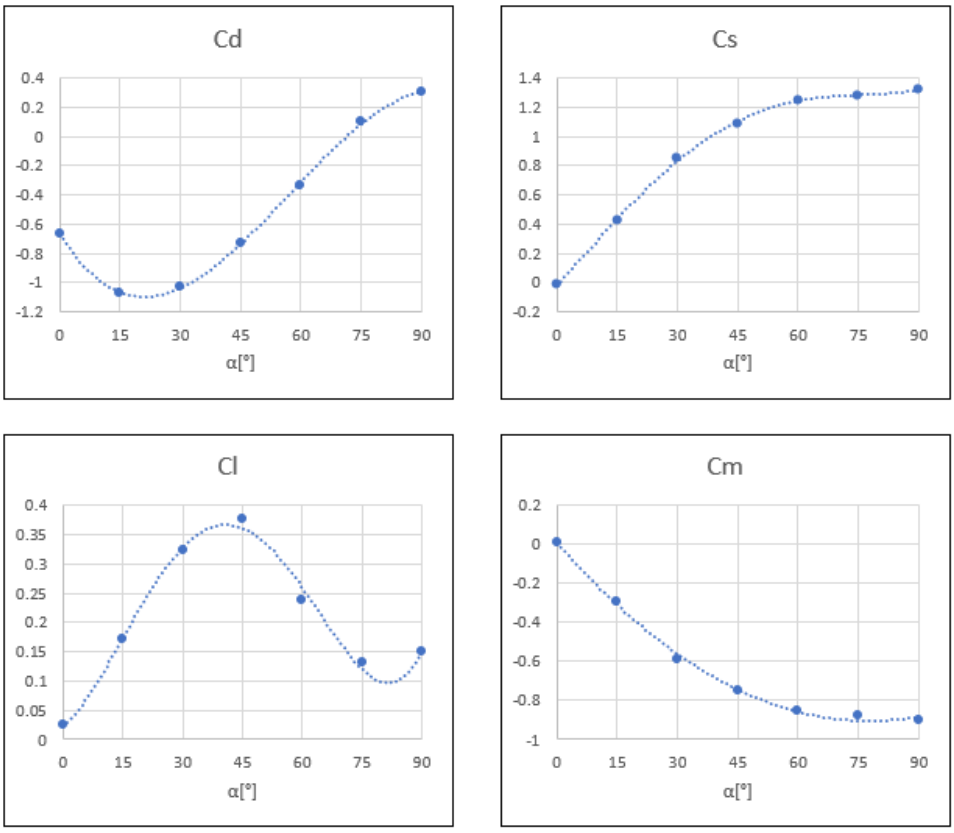

Figure 20: Aerodynamic coefficients obtained with the numerical model of a truck on a flat floor for different yaw angles and polynomial trendlines: Cd drag coefficient (top left); Cs side coefficient (top right); Cl lift coefficient (bottom left); Cm roll moment coefficient (bottom right).

The first thing that can be seen when comparing the graphs of the aerodynamic coefficients in Figure 19 and Figure 20 is the similarity in the shape of the curves that form the results, which suggests that the evolution that has been seen in the truck's aerodynamic coefficients obtained with the numerical model by changing the yawing angle of the wind is correct and represents the behavior of these coefficients for a real case, since it behaves like those obtained experimentally in (Cheli, Corradi, et al. 2011).

On the other hand, when comparing the numerical values of the coefficients in Figure 19 with those in Figure 20, differences can be seen. In the first place, as regards the drag coefficient, the values obtained with the numerical model during almost the whole curve have an absolute value lower than those mean values of Figure 19, although taking into account the bars of the deviation error it could be said that the values of Figure 20 correspond almost closely to those of Figure 19. Talking now about the side force coefficient and the roll moment coefficient, since the moment coefficient depends directly on the side force coefficient, it can be seen again how the absolute value of the numerical model results is slightly lower than the results obtained in the wind tunnel. Finally, the lift coefficient shows a greater difference in the numerical values, since even though both curves have the same shape, the values obtained with the numerical model in Figure 20 are always greater than those in Figure 19.

Therefore, taking into account what has been mentioned above, and having carried out all the checks and tests possible, such as seeing that with finer meshes the result would still be the same (Figure 12), it has been concluded that the numerical model is correct and faithfully represents reality as the graphs in Figure 20 show the same curve shape as those in Figure 19 and the numerical values, despite the differences already mentioned, are comparable. Therefore, it has also been concluded that the deviation in the absolute value of the aerodynamic coefficients is due to the fact that it has not been possible to replicate exactly the geometry of the truck used in (Cheli, Corradi, et al. 2011), what was foreseeable since the detailed plans of the vehicle were not available, and it can also be attributed to the fact that it has not been tried to imitate a wind tunnel with the boundary conditions but a road in an open space. Thus, the numerical model to simulate the truck is validated.

The data presented from the validation of the truck can be used to briefly comment on notable aspects of a vehicle's behaviour when faced with yaw-angle variation. For example, in the previous graphs, as far as the drag coefficient is concerned, it can be seen that, contrary to what may be initially thought, this coefficient does not have its maximum for a yaw angle of 0°, rather it increases until it finds its maximum at an angle of approximately 20° and then it decreases until it crosses the horizontal axis as the yaw angle increases. As for the lateral coefficient and the roll moment coefficient, it can be seen that they are directly related and what should be highlighted is that these coefficients increase their absolute value in a linear way up to an angle of 45° where the curve begins to grow with a much smaller slope and between 75° and 90° it hardly varies and its maximum is found. The lift coefficient has a more complicated curve to visualize than the previous ones, but what is important to highlight is that it increases up to 45 linearly in the same way that the side and momentum coefficients do, and when they stop growing in such a notorious way the lift coefficient falls drastically.

Finally it is necessary to make a clarification, during the thesis the drag coefficient will be taken as positive when it refers to a force that goes in the positive of our x string, that is against the vehicle, for this validation the sign of this coefficient has been changed so that it is easier to compare visually with Figure 19 when appearing in this the drag coefficient with the opposite sign criterion.

4.2.3.2 Motorbike validation

For the validation of the numerical model of the motorbike, the results obtained in (Fintelman, et al. 2015) will be used to compare them with those obtained with the current model. In (Fintelman, et al. 2015) is studied the behavior of a Yamaha R1 motorbike, a geometry similar to the motorbike of the current work, under the effects of cross wind for different yaw angles.

The aerodynamic coefficients shall be calculated with the equations (24), (25), (26) and (27), for which V_R=25 m/s, A=0.75 m^2 which is the frontal area and will be used for all coefficients, in equation (27) h=1.5 m. These parameters will be used for all the studies carried out with the motorbike, and are the same as those used in (Fintelman, et al. 2015).

The graphs below show the results for the aerodynamic coefficients obtained in (Fintelman, et al. 2015) and the current model:

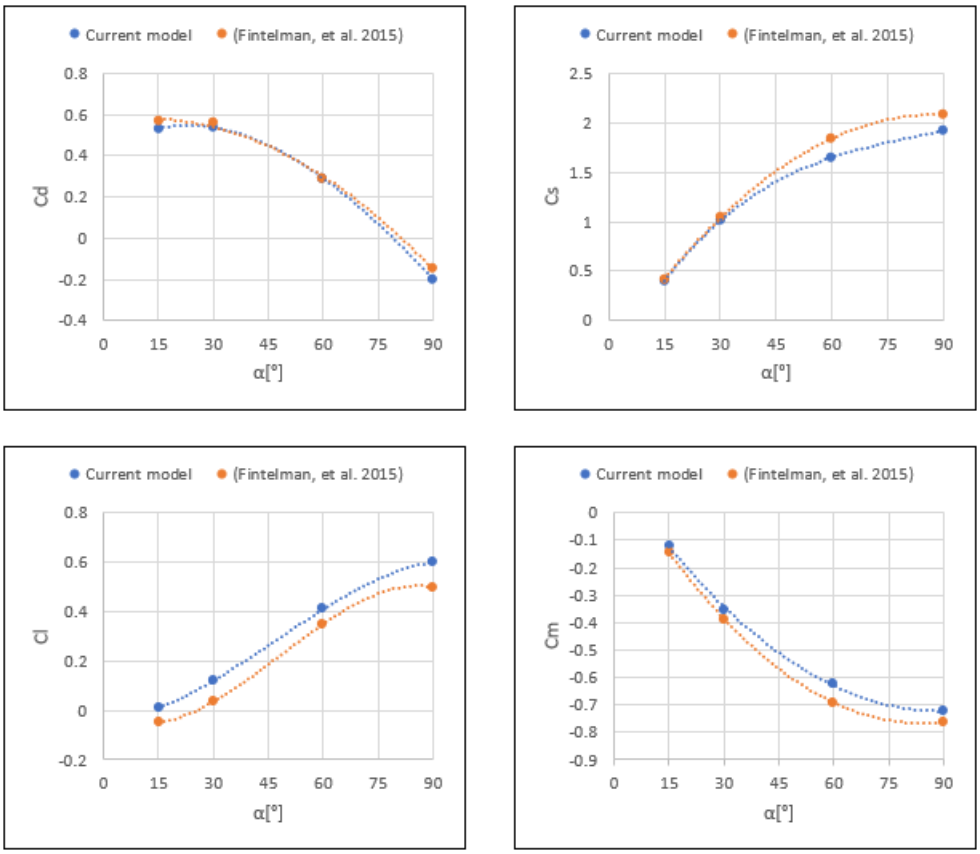

Figure 21: Comparation of aerodynamic coefficients obtained with the numerical model and in (Fintelman, et al. 2015) of a motorbike for different yaw angles and polynomial trendlines: Cd drag coefficient (top left); Cs side coefficient (top right); Cl lift coefficient (bottom left); Cm roll moment (bottom right).

Figure 21 shows how the results obtained are largely in line with those of (Fintelman, et al. 2015), with the lift coefficient being the only one that varies slightly. Variations that can be due to the difference between the two models and the boundary conditions, being the current model a stationary state RANS simulation and the one of (Fintelman, et al. 2015) a transient DDES simulation. In addition, one of the biggest differences between the two simulations is that in (Fintelman, et al. 2015) simulation the wheels of the motorbike have angular velocity according to the supposed movement of the motorbike, while in the current work these remain static, a difference that can explain the light difference in the values of the lift coefficient. The numerical model of the motorbike is validated by this verification.

Regarding the behaviour of the motorbike in relation to the different yaw angles of the cross wind shown in figure 21, if we compare it with the behaviour of the truck in figure 20 we can see how, while the tendency of the aerodynamic coefficients in relation to the increase of the yaw angle is the same, in the behaviour of the motorbike one can see curves that vary in a smoother way than those that describe the behaviour of the truck. This is due to the lower exposure to wind that a

motorbike has in front of a truck due to its softer shapes in front of the rough geometry of the truck that does not favour the flow of the side wind.

4.2.3.3 Car validation

Finally, the last validation to be carried out is that of the car, validation for which the results of three different works will be used, one carried out experimentally (Heft, Indinger and Adams 2012, a) and another two carried out numerically (Heft, Indinger and Adams 2012, b); (Peters, et al. 2015). Unlike the other two vehicles for the car, no previous work has been found in which their aerodynamic coefficients were studied in cross wind, so the validation of the car will be only for front wind.

The aerodynamic coefficients shall be calculated with the equations (24), (25), (26) and (27), for which V_R=40 m/s, A=2.17 m^2 which is the frontal area and will be used for all coefficients, in equation (27) h=1.41 m. These parameters will be used for all the studies carried out with the car.

The results of the cited work and of the current model for the DrivAer drag coefficient with a yaw angle of 0° are presented below:

Work	Drag coefficient (Cd)	Difference [%]
Current study	0.263	-
Experimental (Heft, Indinger and Adams 2012, a)	0.243	8.2
RANS (Heft, Indinger and Adams 2012, b)	0.241	9.1
RANS (Peters, et al. 2015)	0.256	2.7

Table 3: Drag coefficient obtained with the current numerical model compared to others obtained experimentally and numerically for 0° yaw angle.

As can be seen in Table 3, the drag coefficient obtained with the current model is always greater than that obtained with the rest of the works, but it should be noted before commenting on these results that the other works are carried out with the DrivAer with the geometry of the top fastback. Geometry shown below:

Figure 22: DrivAer fastback (DrivAer n.d.).

Therefore this difference in the rear of the car causes the differences in the results of Table 3, since the fastback has a more aerodynamic geometry, compared to the configuration selected for this work, which creates a smaller wake and therefore a lower pressure gradient between the front and

rear of the vehicle, which justifies the higher drag coefficient of the car used in this work. The model can therefore be considered to have produced good results.

Despite not being able to perform a validation of the car model for cross wind with different yaw angles, the positive validation against the front wind together with the satisfactory validation of the truck and motorbike models, which as already mentioned on several occasions the meshing, the boundary conditions and the settings of the simulation are the same for all three vehicles, leads to the assumption that the numerical model of the car will also report correct results against the cross wind.

CHAPTER 5: Results

During this chapter the most efficient prototype of a wind-break fence will be developed. To do this, first it will be studied the different effect that each proposed fence geometry has and its porosity on the protection of a vehicle against the wind, then it will be studied the effect that the height and the distance at which the fence is placed from the vehicle has on this protection and finally it will be considered the advantages that can bring to place a deflector on top of the fence and how this should be.

To facilitate this work, not all of these simulations will be carried out on each vehicle, but rather the most suitable fence configuration will be found to protect the vehicle most exposed to the cross wind, and therefore the one that is most at risk, which in the case of the vehicles that have been presented the most exposed is the truck, and then check the efficiency of the final fence configuration reached over the other two vehicles, the motorbike and the car, as it has been assumed that if a fence is capable of protecting the largest vehicle from the wind it will also be capable of protecting less bulky vehicles.

In the same way, in order to speed up the research, the simulations in search of the most suitable fence to protect the truck from the cross wind will not be carried out on all the cases indicated in the Table 1, but they will be carried out for the yaw angles of 10°, 30° and 50°, and finally, once the development of the fence has been completed, the two remaining cases of yaw angle (20° and 40°) will be added to check that for these angles the fence is also effective.

5.1 Development of the wind-break fence

During this section, the effect on the protection of the vehicle of the various parameters to be chosen in the configuration of the final windbreak fence shall be studied, being these parameters the geometry of the fence, its porosity, its height, the distance between the fence and the vehicle and the angle of the deflector.

When choosing between the different configurations, the two most important parameters to be reduced for this work are the side force coefficient and the roll moment coefficient, since the main objective of these wind breakers is to ensure the safety of the vehicles against cross wind. However, the drag coefficient will not be overlooked, which, although with a lower priority, will be tried to reduce in order to take advantage of the fences to reduce vehicle fuel consumption.

As already mentioned, this study will be carried out on the geometry of the truck for yaw angles of 10°, 30° and 50°, taking as a reference the aerodynamic coefficients of the truck as a simplification of the behaviour that the truck is having against the fence. Therefore, the

aerodynamic coefficients of the truck for the three yaw angle cases to be considered in this section are shown below:

Yaw angle	Cm	Cd	Cs	Cl
[°]	[-]	[-]	[-]	[-]
10	-0.1896828	0.9679464	0.2818404	0.09958932
30	-0.5341295	0.9797852	0.7885149	0.2773088
50	-0.7951284	0.5898147	1.166686	0.3646858

Table 4: Truck aerodynamic coefficients for yaw angles of 10°, 30° and 50°.

5.1.1 Influence of geometry and porosity

Firstly, the influence of the geometry of the open space of the fence and its porosity on the behaviour of the vehicle will be studied.

For each type of geometry three levels of porosity will be studied, 10%, 20% and 30%, as well as a fence with 0% porosity, meaning opaque, which will be the same for all three types of geometry. Assuming that the effect of the porosity in the fence has a relatively linear behavior and therefore that with these four porosities can be interpolated between them.

What is expected from this comparative study that will be carried out is to discover if one of the geometries is clearly more feasible, or less feasible, to protect the vehicle, and for this which is the ideal porosity, since it is expected that for small porosities the effect on the vehicle is to turn the lateral force in the opposite direction to the wind, and that for large porosities the effect of the fence on the vehicle is not sufficient and there remains a lateral force that pushes the vehicle in the direction of the wind.

In conclusion, what must be sought is the geometry for which to the porosity for which the side force coefficient and the roll moment coefficient are cancelled for the lowest drag coefficient

The distance and height of the fences to which the porosity is to be varied must be fixed and for this case a height of 4 m and a distance of 3 m between vehicle and fence have been chosen, trusting that this height and distance are sufficient to protect the vehicle from the wind and that these parameters do not influence the study of the porosity and geometry.

Below are the graphs of how the aerodynamic coefficients vary for each open space geometry in the fence (circular holes, rectangular and plates) according to its porosity (0%, 10%, 20% and 30%) for yaw angles of 10°, 30° and 50°.

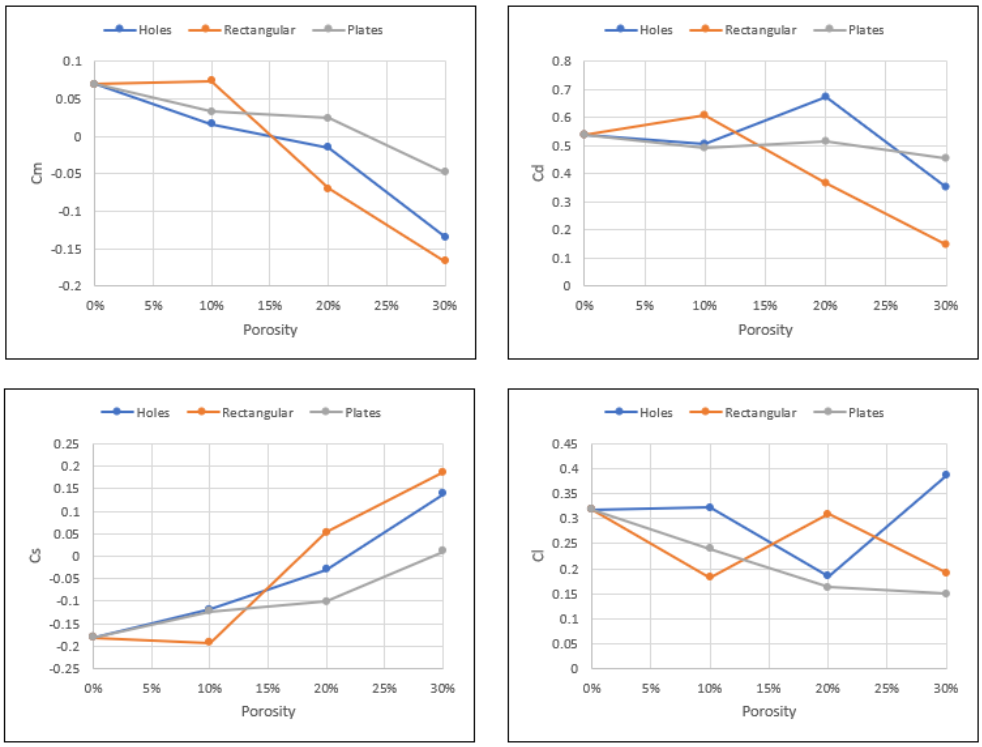

Figure 23: Aerodynamic coefficients of the truck with fence for each geometry and porosity for a yaw angle of 50°.

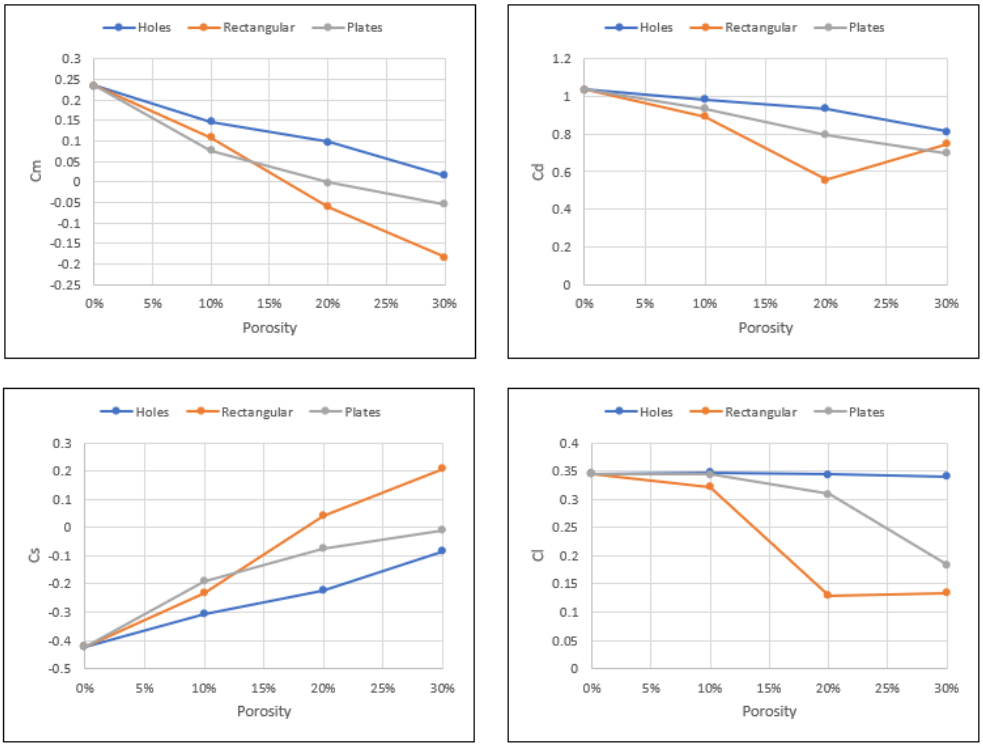

Figure 24: Aerodynamic coefficients of the truck with fence for each geometry and porosity for a yaw angle of 30°.

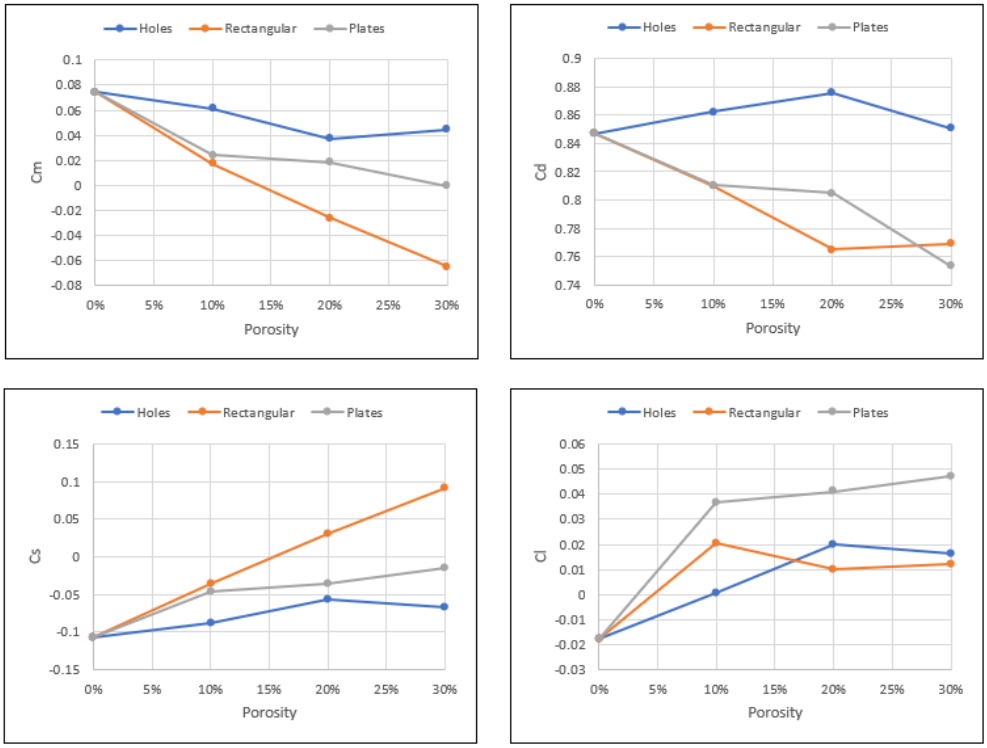

Figure 25: Aerodynamic coefficients of the truck with fence for each geometry and porosity for a yaw angle of 10°.

A quick glance at the graphs just presented shows that, contrary to what was believed, there is no geometry that is more favorable than the others, instead all three have a similar behaviour with some peculiarities. What has been fulfilled in comparison to what was expected is that for low porosities there is a negative side force coefficient, which means that the truck is experiencing an attraction force towards the fence, and a positive roll moment coefficient, which means that the truck would roll over towards the fence. On the other hand for higher porosity there is a positive side force coefficient, which means the side force pushes the truck with the wind direction, and a negative roll moment coefficient, which means the truck would roll over to the side opposite to the fence.

Furthermore, it can be seen, as expected, that the side force coefficient and the roll moment coefficient vary in the same way (with an opposite sign due to the criterion of signs adopted).

In view of the complexity of the data in the graphs, each figure will be analyzed separately, meaning that each yaw angle will be analyzed separately.

Starting from Figure 23,regarding the comparison of the aerodynamic coefficients of the truck with the opaque fence with those of the truck without fence in Table 4, it can be quickly seen how there is a significant improvement in terms of side force and roll moment coefficients. On the other hand, the drag coefficient and the lift coefficient do not show any improvement.

Discussing now the behavior of each fence regarding the variation of its porosity, in the moment coefficient it can be seen how the fence with rectangular openings and the one with circular holes

cross the horizontal axis at the same point and before than the fence with plates, behavior that can be seen similar in the side force coefficient but with the fence with rectangular openings crossing the axis before than the one with circular holes. Regarding the drag coefficient the only fence that reduces it considerably with the increase of the porosity is the one with rectangular openings while for the fence with plates this coefficient hardly varies and with the fence with circular holes it fluctuates up and down from the value of an opaque fence. In the lift coefficient the only curve that decreases uniformly is that of the plate fence while the other two do not have a clear behaviour.

Then, the only conclusions that can be drawn from the behavior of these three types of fences and the influence of their porosity for a yaw angle of 50°, is that the fence that seems to have a softer behavior against the variation of its porosity is the fence with plates. On the other hand the fence with rectangular openings has a much more pronounced response to the variation of its porosity in terms of protection from side force, and therefore the same for the roll moment, and as its porosity increases the drag coefficient decreases. Finally, with regard to the fence with circular holes, it can be said that, as with rectangular openings, it has a rapid response to the variation in its porosity, but with regard to the support and drag coefficients, it cannot be determined whether this porous fence has any advantage over an opaque one.

Moving on now to the case with a yaw angle of 30 from Figure 24, with respect to the aerodynamic coefficients of the truck with an opaque fence there has been a sharp drop in the coefficient of lateral force with respect to that of the truck without a fence, which although in absolute value has decreased by nearly a half continues to be a significant lateral force, but in this case of attraction to the fence, which continues to be a danger, the same can be seen with the moment coefficient. The drag coefficient has even increased slightly, and the lift coefficient has decreased a little. So, for a yaw angle of 30 an opaque fence will never be recommended.

With regard to the variation of the aerodynamic coefficients with the increase of the porosity, the fence with rectangular openings is again the first curve to cross the horizontal axis for the moment coefficient for a porosity of around 15%, while this time the fence with plates crosses the horizontal axis before the one with circular holes, which does not cross it and would need a porosity greater than 30% to cancel out the moment experienced by the truck. For the lateral coefficient there is a similar behaviour but with the peculiarity that for this coefficient the fence with plates, despite having annulled the moment coefficient for a 20% porosity, does not cross the horizontal axis. For the drag coefficient the fence with plates decreases smoothly linearly, while the fence with circular holes also decreases but to a lesser extent and the fence with rectangular openings is again the one that decreases the drag coefficient the most but with a rise for porosity of 30%. Regarding the lift coefficient, the curve that decreases the most is the one of the fence with rectangular openings, followed by the fence with plates, while the fence with circular holes remains basically constant.

The conclusions of this case are that the fence with rectangular openings is again the one with a greater slope, being the one that most decreases the value of the drag and lift coefficient with the increase in porosity. On the other hand in this case the curve of the fence with circular holes is the

one that has been kept more constant, and the fence with plates has had an intermediate behaviour between the other two fences

Finally the case of the truck with fence and a yaw angle of 10° shown in Figure 25. The aerodynamic coefficients of the truck with an opaque fence with respect to those of the truck without fence do not vary notably, decreasing the coefficients of side force and roll moment until changing sign, the drag coefficient decreases slightly but the most remarkable thing is that the lift coefficient becomes negative, thus pushing the truck down to the asphalt.

In this case the variation of the aerodynamic coefficients with respect to the variation of the porosity of the fence does not vary strongly. With regard to the roll moment and side force coefficients, the curve with a clearly greater slope is again the one with rectangular openings, being the only one that crosses the horizontal axis but varying its value only by two tenths. In the drag coefficient the curves of fences with rectangular openings and with plates decrease by one tenth, while the fence with circular holes increases the drag coefficient as the porosity increases. In the lift coefficient the three curves grow.

The conclusion regarding the behaviour of the curves of the previous case may be similar, but the conclusion to be drawn from this case is that the aerodynamic coefficients for a yaw angle of 10 do not vary strongly, so the decision on the geometry and porosity of a fence to protect a truck from wind must be taken based on the results for higher yaw angles.

Finally, after this analysis of the results presented, several conclusions can be drawn. With regard to the behaviour of the truck when faced with a wind fence, it can be concluded that for any type of fence and yawing angle the truck will receive protection on the side forces and roll moment, but this protection for opaque or low porosity fences can produce a force of attraction of the vehicle towards the fence, but this is always less than the force to which it was initially subjected. Regarding the drag coefficient for opaque or low porosity fences the truck will not receive a considerable protection for this coefficient, but for higher porosities it can be achieved to reduce the drag force to which the truck is subjected. Finally, it cannot be concluded that wind barriers, except for specific configurations, are capable of significantly reducing the lift coefficient of the truck.

The conclusions that can be drawn from each fence are that the fence with plates behaves more smoothly when faced with variations in its porosity than the other two, which means that it would be easier to adjust its porosity to achieve the desired benefits in terms of wind protection. The circular hole fence presents different behaviours when varying the yaw angle, being for high angles sensitive to the variation of its porosity and for low angles very little sensitive to this variation and presenting for high porosities an excessive protection from the wind for the lateral forces, making these contrary to the wind direction, and also it does not seem to be able to diminish the drag and lift coefficient of the truck, so together with its different behaviour for different yaw angles make it the worst choice. Finally, the fence with rectangular openings is very sensitive to the variation of its porosity, so it would be more difficult to configure it correctly than the fence with plates, but

of the three fences it seems to be the most capable of protecting the vehicle from the drag force and the lift force, as well as having the same behaviour for all yaw angles.

Once the conclusions have been drawn for each fence, a preliminary choice will be made in terms of geometry and porosity. One of the aspects that have been seen is that any type of fence is capable of canceling the lateral forces for a certain porosity, porosity for which it usually also cancels the roll moment, so on this basis we must look for other benefits that can be extracted from a wind barrier, such as reducing the drag and lift coefficient, finally an important requirement is that the fence selected must be capable of protecting the truck for any angle of yaw. Taking all this into account, it has been chosen as a preliminary choice, since there are still many variables to study such as height, distance and deflector, the best option is considered to be the fence with rectangular openings, since it is the only one that cancels out the side forces and the roll moment around the same porosity for all yaw angles, being this porosity around 20%, moreover for this porosity it presents great advantages for the drag coefficient, always decreasing it in a notorious way.

The next step will be to understand how the airflow reacts to the wind fences in the ParaView post processor to visually understand the difference between the porosities of the rectangular openings fence.

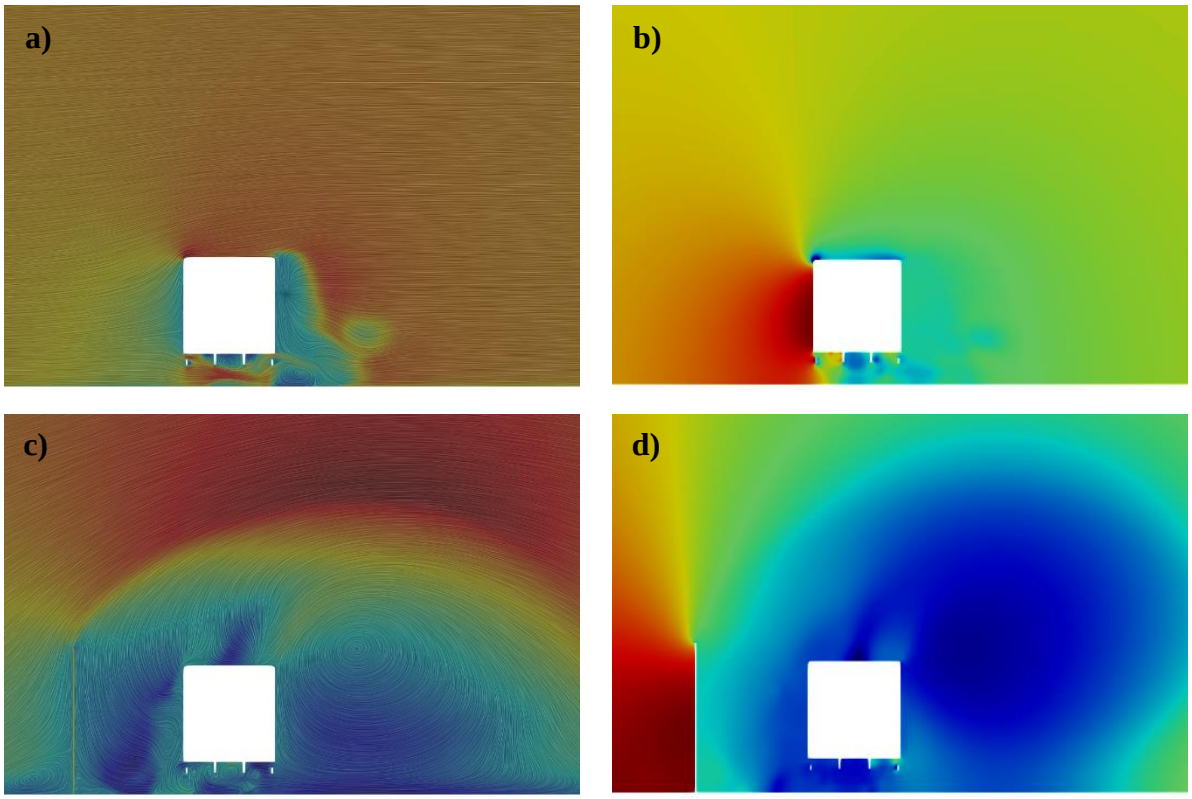

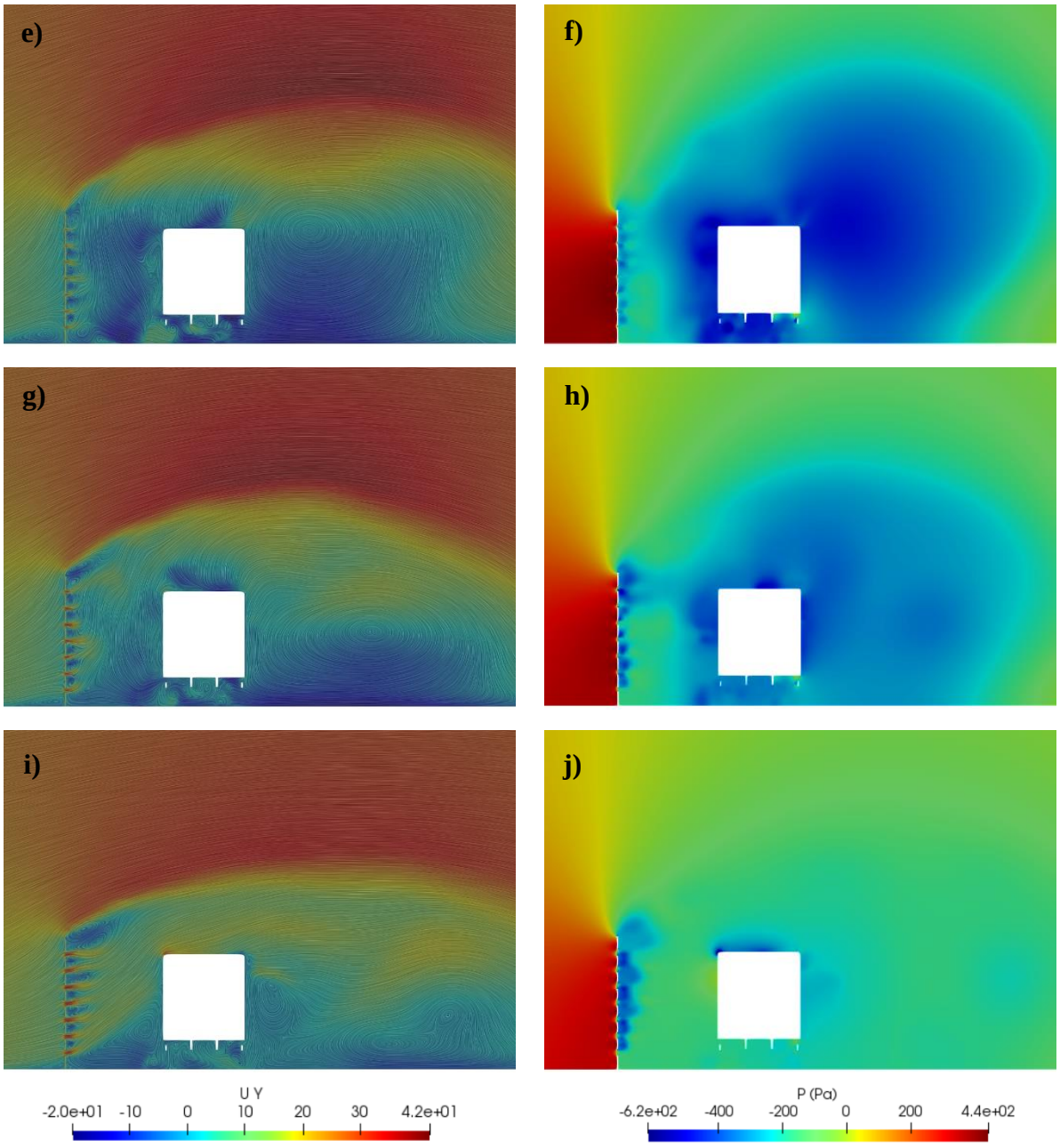

Figure 26: Velocity in the y-coordinate and pressure contours in the y-z plane for x=2m calculated with the results of the numerical models for the following cases for a 50° yaw angle: truck without fence a) and b); truck with opaque fence c) and d); truck with fence with rectangular openings 10% porosity e) and f); truck with fence with rectangular openings 20% porosity g) and h); truck with fence with rectangular openings 30% porosity i) and j).

Analyzing the images shown it can be seen firstly how in the case of the truck without fence the flow decelerates with respect to the speed of the free flow before impacting on the side of the truck, where a strong pressure gradient can be seen while on the other side of the truck a slight depression can be seen where the flow ascends and the speed on the y-axis is almost 0. This gradient and the

subsequent depression on the sides of the truck explain the lateral force to which a vehicle is subjected in the cross wind.

For the cases of the truck with fence one can see how this pressure gradient that in the previous case was on the left side of the truck is now on the left side of the fence, thus protecting the fence to the truck from the impact of the air flow, and this air can be seen to pass over the fence, accelerating its speed and passing this flow at a higher speed over the truck, which indicates that for a fence that is not high enough this accelerated flow would impact the top of the truck, providing a large roll moment with the danger of overturning that this entails.

Now looking specifically at the cases of the truck with a fence for which the coefficient of side force is negative, such as the cases of the opaque fence and the fence with a porosity of 10%, it can be seen how a depression is produced behind the fence, leaving a stagnant flow between the truck and the fence that sucks in the air and rises vertically, and although another strong depression can also be seen behind the truck, this is produced by a vortex that impacts laterally on the truck, all this produces the side force that pushes the truck to the fence. This vortex should be considered in further studies because of the instability in the vehicles that it can cause.

Finally analyzing the last two cases, the truck with a fence of rectangular openings with a porosity of 20% and 30%, cases for which the lateral force is positive in the y-axis, and for the case of the fence with a porosity of 20% almost 0, it can be seen how the depression between the truck and the fence is lower due to the greater amount of air flow that is able to cross the fence through the openings. The higher porosity also causes that the airflow over the fence and the truck is less accelerated, making the vortex behind the truck less noticeable for the case with 20% porosity and almost imperceptible for 30% porosity. In the case of the fence with a 20% porosity, the pressures on both sides of the truck are almost equal, so the lateral force suffered by the truck is almost 0. On the other hand, in the case of a 30% porosity, a considerable mass of air already passes through the openings at a certain speed, so this flow causes a small gradient on the upper left side of the truck and a depression on the other side of it, which causes an increase in the lateral force, This fact that a gradient is produced by the impact of the air flow on the upper half of the truck may justify why the moment coefficient changes sign before the side force does.

5.1.2 Influence of height and distance

After having analyzed the most complex part of the wind fence design, such as the influence of geometry and porosity on its efficiency, proceed to study the influence of height and distance between the truck and the fence on the efficiency of protecting a vehicle from the action of cross winds.

To carry out this study three heights will be considered, 2 m, 3 m and 4 m, and each of them at three different distances from the truck, 2 m, 3 m and 4 m. Given the impossibility of carrying out these tests for each of the proposed geometries and their different porosities, due to the time that this would require, an assumption will be made that will have to be subsequently validated. Since

the three types of geometries have a common point, for a porosity of 0%, this study of height and distance is going to be carried out using the opaque fence, assuming that the behaviour seen in the previous section on the variation of the effectiveness of the fence according to its porosity is the same regardless of the height of the fence and its distance from the vehicle. Assuming this hypothesis it would only be necessary to carry out this study on the opaque fence and then with its results move vertically on the ordinate axis the graphs of Figure 23, Figure 24 and Figure 25.

The aim of this study is to understand how varying the height of the fence and its distance from the vehicle varies the aerodynamic coefficients of the vehicle in order to bring together this knowledge with that obtained in the previous section, on the influence that different fence geometries and their porosity have on these aerodynamic coefficients, in order to be able to get the maximum performance out of a windbreak fence by choosing the best configuration to cancel out the side force coefficient, the roll moment coefficient and reduce the drag coefficient as much as possible.

Again, as in the previous section, the simulations to be carried out to complete this study will be done on the truck with a yaw angle of 10°, 30° and 50°, and as just indicated with an opaque fence.

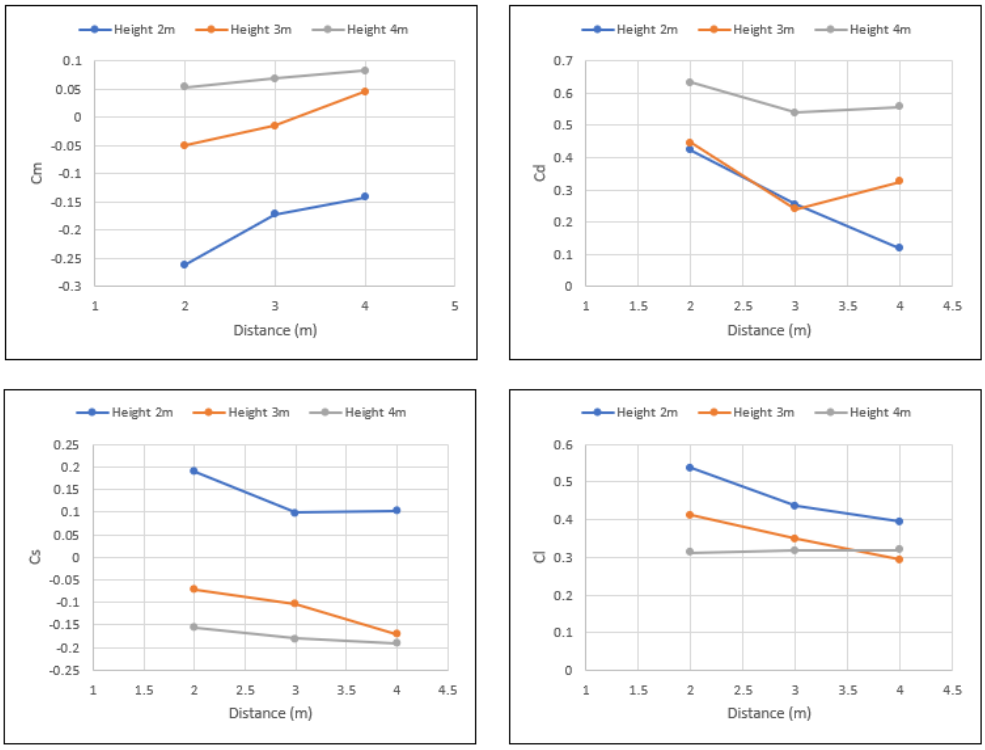

Figure 27: Aerodynamic coefficients of the truck with fence for each height and distance for a yaw angle of 50°.

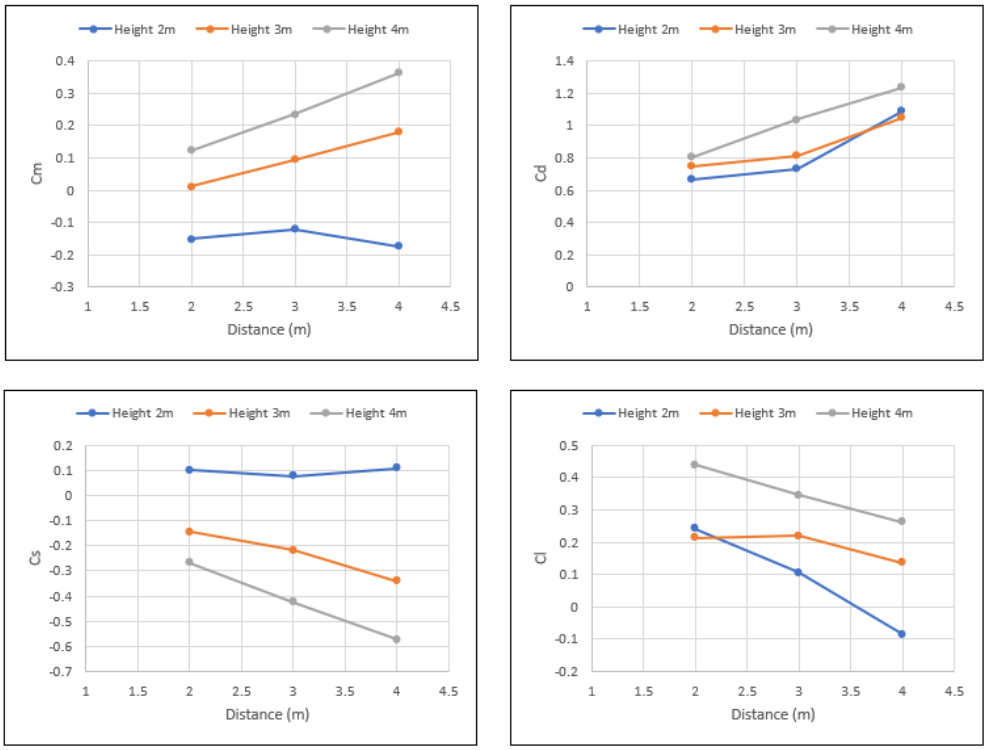

Figure 28: Aerodynamic coefficients of the truck with fence for each height and distance for a yaw angle of 30°.

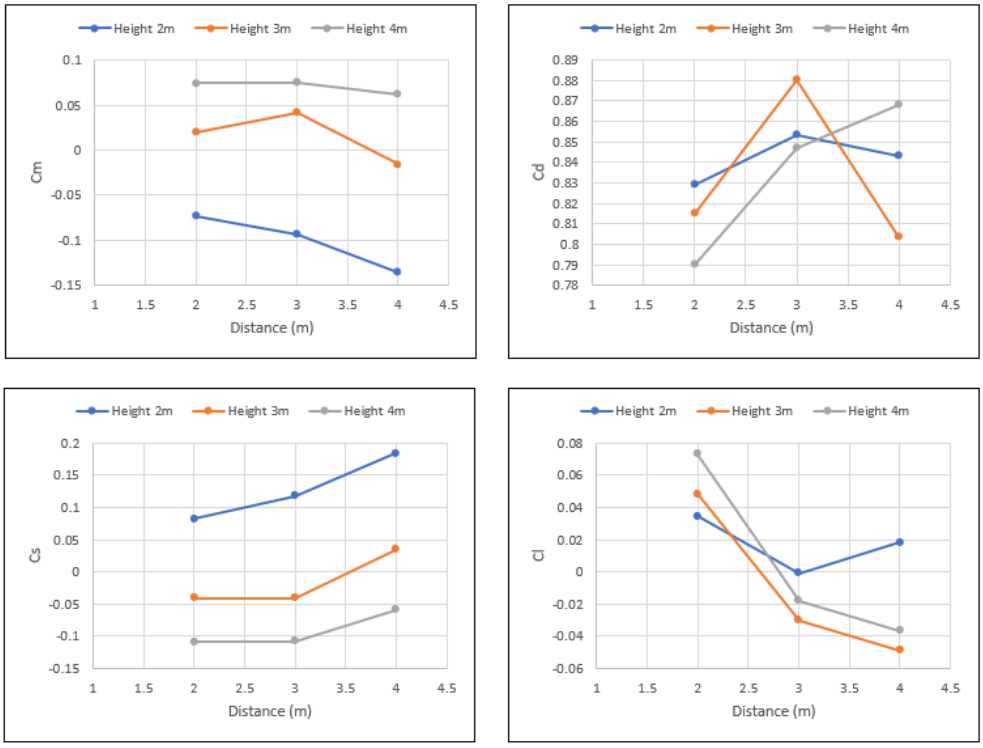

Figure 29: Aerodynamic coefficients of the truck with fence for each height and distance for a yaw angle of 10°.

The graphs just presented show the results of the simulations that have been carried out for different heights and distances between fence and vehicle, analyzing these results will draw the relevant conclusions on the influence of these two parameters on the ability of a windbreak fence to protect a vehicle from the action of crosswind.

To analyze the results, given the difficulty of understanding the data by analyzing all the graphs at once, the same strategy will be followed as when analyzing the results in the previous section. The results for each yaw angle will be analyzed separately and for each one of them the behavior of each curve will be extracted. Once this analysis is done, the common behaviors for the three yaw angles will be recognized and general conclusions on the influence of height and distance will be drawn in order to determine the most successful configuration.

The analysis will start with the results obtained for a yaw angle of 50°. In Figure 27 it can be seen again how the roll moment coefficient and the side force coefficient follow the same trend (for opposite sign). In the graphs of these two coefficients it can be seen how increasing the distance between the fence and the vehicle provides greater protection against side wind, but for the fence with a height of 2 meters this protection is much lower than for the heights of 3 m and 4 m, for a height of two metres at a yaw angle of 50, it would be impossible to cancel out the lateral force and roll moment suffered by the truck, since it is recalled that these cases are with opaque fences, which as seen in the previous section are the choice of porosity that offer maximum protection. On the other hand, for the other two heights, 3 m and 4 m, protection is achieved as expected, which changes the sign of the lateral force, changing the sign of the moment coefficient as well in the case of the 4 m high fence for all distances and in the case of the 3 m high fence for distances over 3 m. Talking now about the drag coefficient, the fences with a height of 2 m and 3 m reduce this coefficient very significantly compared to a truck without a windbreak fence for this yaw angle (Table 4), especially for the 2 m fence as its distance increases. On the other hand, the 4 m high fence increases this coefficient for a distance of 2 m and keeps it almost constant to that of the truck without fence for the distances of 3 m and 4 m. Finally the lift coefficient remains constant slightly below the value without fence for the 4 m high fence for all distances, while the other two fence heights reduce the coefficient as their distance increases, this being higher than that of the truck without fence for the 2 m fence and starting from above to end up reducing it slightly for the 3 m fence.

To summarize, the fence with a height of 2 m is not able to cancel the side force and roll moment coefficients, and increases the lift coefficient considerably, despite the fact that the drag coefficient is reduced to a greater extent the greater the distance. The 4 m high fence offers excessive protection for all the distances tested (an event which, as we have seen, is solved by increasing the porosity) and has no influence on the lift coefficient, but increases the drag coefficient when it is close to the vehicle and does not improve it for higher distances. Finally, the fence with a height of 3 m achieves good protection against cross wind for the moment and lateral force coefficients, slightly lower than that of the 4 m fence, and is able to reduce the drag coefficient and slightly the lift coefficient for distances greater than 3 m.

Turning now to the results for a yaw angle of 30°, Figure 28, the behaviour that can be found for the side force and roll moment coefficients is the same as for the previous case, the greater the distance the greater the protection, with the 2 m high fence continuing without being sufficient to protect the truck from the cross wind and with the other two fences again changing the sign of these two coefficients, again providing the fence with a height of 4 m a more exaggerated protection than the 3 m fence. As for the drag coefficient, the behaviour when increasing the distance is the opposite to the previous case, the greater the distance the drag coefficient increases, being again the 4 m fence the one that reports worse results for this coefficient, increasing it by the truck without fence for a distance higher than 3 m. On the other hand, the 2 m and 3 m high fences have a similar efficiency in this aspect, but exceeding the value of this coefficient for the truck without fence for a distance of 4 m. Finally, the lift coefficient behaves in the opposite way to the previous case with regard to the height of the fence, the higher the height, the lower the efficiency, and this coefficient is reduced again with the increase of the distance.

The conclusions that can be drawn from the analysis in the previous paragraph are that again the fence with a height of 2 m is not sufficient to cancel out the lateral forces despite being the one with the best results for the drag and lift coefficients. The 4 m fence can protect the truck from lateral forces but performs less well on the other two coefficients. Finally, the 3 m high fence is able to protect from lateral forces and presents a good intermediate efficiency between the 2 m and 4 m fences for the other two coefficients.

To finish in the results for a yaw angle of 10° of the Figure 29 it can be seen, as already commented in this study of the geometry and porosity, that the aerodynamic coefficients do not vary as for the rest of yaw angles when varying the configuration of the wind fence. In the lateral force and roll moment coefficients there is a behaviour opposite to the other two cases, as the distance increases the protection decreases, and with regard to the heights the height of 2 m is again insufficient and the other two heights are capable of cancelling the lateral forces. Regarding the drag coefficient, the best results are given for the 4 m fence at a distance of 2 m, which increases this coefficient as the distance increases. On the other hand, the worst results for the 3 m and 2 m heights are unexpectedly for the intermediate distance of 3 m. Finally, the lift coefficient decreases as the distance increases, and can become negative for heights of 3 m and 4 m, but this coefficient was already small for the truck without a fence, so its variation is less important.

The conclusions for this yaw angle regarding the lateral force and roll moment coefficients are the same as for the previous cases, a 2 m high fence is not sufficient. With regard to the drag coefficient no conclusive conclusions can be drawn about the influence of height and distance on this coefficient since for each distance a different height is less effective. Finally, the lift coefficient does not deserve to be taken into consideration due to its low value.

Once this critical analysis has been carried out on the results obtained, it is desired to determine which fence height and distance are optimal to protect the truck from the cross wind.

Firstly, despite its efficiency in terms of drag and lift coefficients for almost all yawing angles at any distance, the 2 m high fence must be discarded as the priority of this work is to achieve a windbreak fence capable of cancelling out the lateral force coefficient and the tilting moment coefficient. Already considering only the fences with height of 3 m and 4 m, both adjusting their porosity are able to cancel the lateral force coefficient and overturning moment coefficient. Talking about the optimal distance this should be 3 m because the fence should offer good results for all yaw angles, and for an angle of 50° the worst result of the drag coefficient is with a distance of 2 m and for an angle of 30° the worst result is for a distance of 4 m (the angle of 10° is not taken into consideration because its variation is small), so the distance that brings a higher overall efficiency is 3 m. For the sustenance coefficient at a greater distance it is less, but with a distance of 3 m it does not vary much with respect to that of 4 m and this coefficient is the least relevant for this study.

Therefore the decision should be between a 4 m high fence or a 3 m high fence, both at 3 m distance from the vehicle, as a preliminary choice, pending confirmation of the hypothesis presented for this study, that the behaviour of the porosity is independent of the height and distance of the fence, the 3 m high fence has been chosen due to its much better efficiency in the drag coefficient than the 4 m high fence, despite the fact that for the 3 m high fence it does not reach to annul the moment coefficient for a yaw angle of 50°, although its value is very small, so it remains to be seen how the porosity behaves in a 3 m high fence and a 3 m distance.

5.1.2.1 Verification of the hypothesis

To carry out the study of the height of the fence and distance between fence and vehicle a hypothesis was formulated for which the behaviour of the variation of the porosity seen in point 5.1.1 Influence of geometry and porosity would be the same for any height and distance, so that we would only have to carry out the height and distance simulations for an opaque fence and then move vertically on the ordinate axis the graphs in Figure 23, Figure 24 and Figure 25. This hypothesis must be now validated in order to conclude the most effective configuration of geometry, porosity, height and distance between fence and vehicle.

To validate the hypothesis, the graph of the fence with rectangular openings for the different yaw angles will be translated by moving the initial point of these curves, which is the result of an opaque fence, for the results obtained for this fence with a height of 3 m and a distance of 3 m, and the result obtained for a fence with rectangular openings and a porosity of 20%, configuration that has been indicated as optimal in point 5.1.1 for its effective behaviour for all yaw angles, shall be compared with the real result of this configuration obtained numerically by the simulation of the model. In turn, this result will be compared with the result of the fence with rectangular openings with a height of 4 m obtained previously to confirm whether there is indeed an improvement in the results of the truck's aerodynamic coefficients obtained.

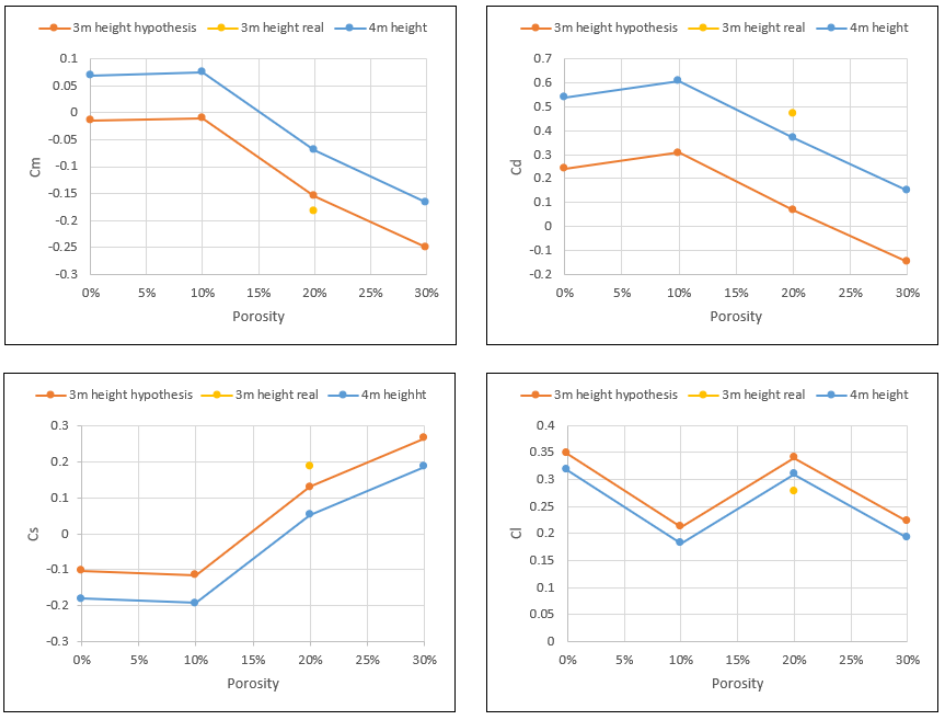

Figure 30: Aerodynamic coefficients of the truck for a 50° yaw angle with a fence with rectangular openings for a height of 4 m, 3 m according to the hypothesis and 3 m with 20% porosity according to the numerical model.

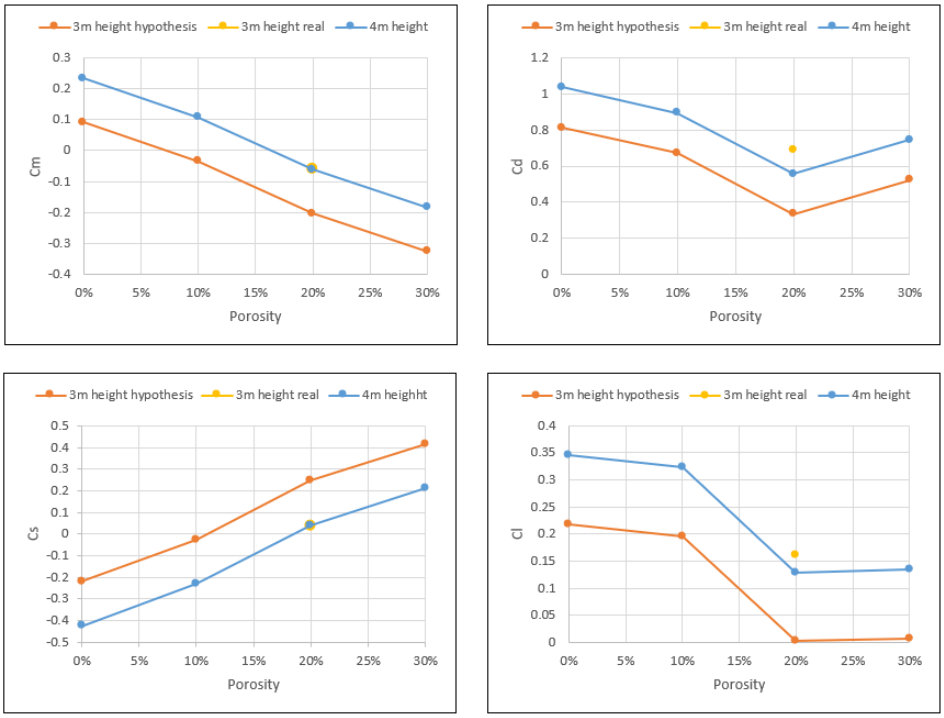

Figure 31: Aerodynamic coefficients of the truck for a 30° yaw angle with a fence with rectangular openings for a height of 4 m, 3 m according to the hypothesis and 3 m with 20% porosity according to the numerical model.

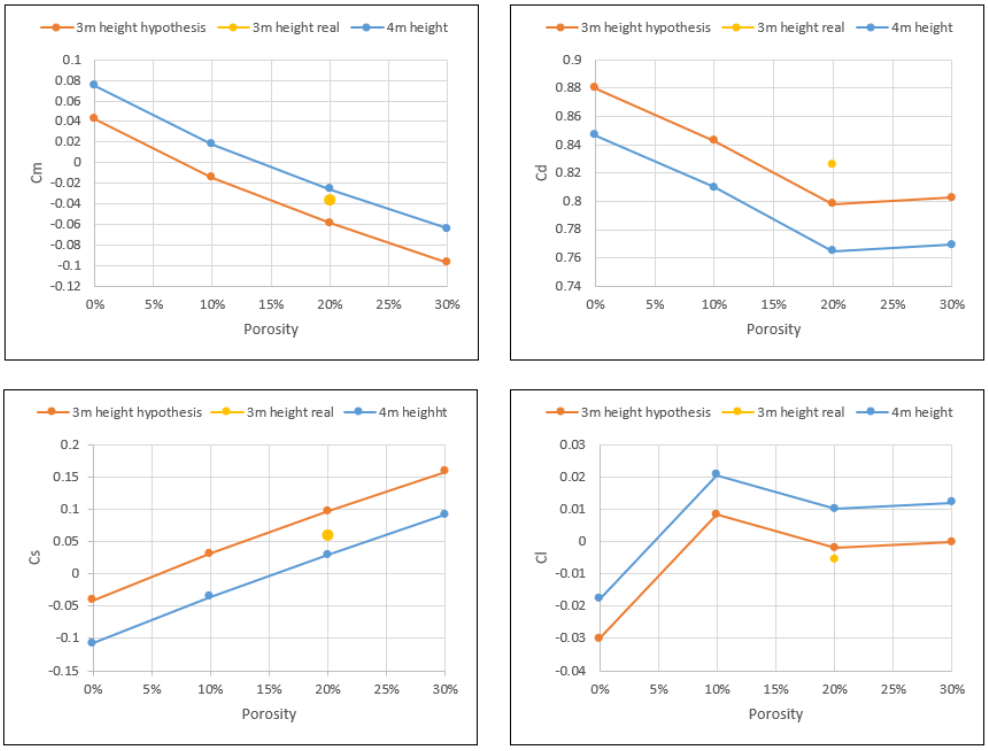

Figure 32: Aerodynamic coefficients of the truck for a 10° yaw angle with a fence with rectangular openings for a height of 4 m, 3 m according to the hypothesis and 3 m with 20% porosity according to the numerical model.

The analysis of the results just shown will be followed by a discussion of the correctness of the hypothesis and the efficiency of a fence with rectangular openings and a 20% porosity of 3 m high and a distance to the vehicle of 3 m with respect to the same fence with the same distance to the vehicle and a height of 4 m.

Firstly in Figure 30, results for a yaw angle of 50°, it can be seen how the real results for the 3 m fence with rectangular openings and 20% porosity are close to the results achieved with the hypothesis for the side force and roll moment coefficients, although with a slightly lower protection. For the case of the drag coefficient it can be clearly seen that the hypothesis is not correct and the fence with a height of 3 m would have a lower efficiency in this coefficient than the 4 m fence. In the lift coefficient the real result is close to that of the hypothesis but having a value closer to that of the 4 m fence, the real value providing better protection in this coefficient but being this value similar for all cases.

In Figure 31 the real value of the 3 m fence in the side force and roll moment coefficients is practically the same as that of the 4 m fence with a porosity of 20%, thus providing greater protection in this case than initially expected by applying the hypothesis. For the drag coefficient the real value of the 3 m fence is again worse than that of the 4 m fence, moving considerably away from the value expected by the hypothesis. Finally, for the lift coefficient the real value of the 3 m fence is again closer to the value of the 4 m fence than to that of the hypothesis, giving this value less protection.

To finish the real results for the 3 m fence for a yaw angle of 10° (Figure 32) show a higher protection for the side force and roll moment coefficients, but approaching the values obtained by means of the hypothesis. In the drag coefficient the real value, as in the previous cases, is again worse than expected by the hypothesis and worse than that of the 4 m fence. In the lift coefficient this real value is close to that obtained through the hypothesis and is also close to that of the 4 m fence.

As a conclusion on the correctness of the hypothesis, it should be separated according to the coefficient to be studied. For the side force coefficient and the roll moment coefficient the hypothesis is close to reality, also because the results for these coefficients of the 3 m and 4 m high fence are similar, so the hypothesis in these coefficients could be considered correct for an initial approximation, not for obtaining an exact value. For the lift coefficient the hypothesis is not close to the real value for a yaw angle of 30°, being relatively accurate for the other two angles, but these results do not allow to validate the hypothesis for this coefficient. Finally for the drag coefficient the hypothesis has been clearly erroneous, reporting at all times the real value for a 3 m fence a worse effectiveness than the 4 m fence, it is reminded that the main advantage for choosing the 3 m fence was that it had a higher efficiency in reducing the drag coefficient. Therefore, once this analysis has been carried out, it is considered that the hypothesis previously presented has not been validated, being able only to bring the real result closer to the side force and roll moment coefficients.

This study has shown the variation of the aerodynamic coefficients by varying the porosity of the fence according to its height. The conclusion is that this behaviour is not independent of the variation in height. It can be concluded that for the side force and roll moment coefficients the variation of height makes the variation of results more pronounced when varying the porosity for large yaw angles, such as 50°, and makes this variation smoother with respect to the opaque fence for intermediate and small angles, such as 30° and 10°. On the other hand, for the drag coefficient for large yaw angles this coefficient when decreasing the height increases its value when increasing the porosity, and decreases it smoothly for smaller angles. In the lift coefficient, it has been possible to verify that the lower the height of the fence, the smoother the variation of this coefficient is in relation to the variation of the porosity. All these preliminary conclusions should be confirmed by performing more simulations for more porosities and fence heights.

Seeing these results it seems that the option of the 3 m windbreak fence is not the best option when it is desired that this fence has rectangular openings and a porosity of 20%, since for the values of the side force and roll moment coefficients this value is farther from being cancelled or with the same value as the 4 m fence, being the cancellation of these coefficients the objective of this work, and for the drag coefficient the 3 m fence has a value always greater than that of the 4 m fence. But as these fences must be realistic and be able to be placed on the sides of the road, the lower the fence is, the less impact it will have on the ecosystem and it will mean a saving of material. Therefore, a study will be carried out to see if adding a deflector at the top of the fence can reduce

the side force, roll moment and drag coefficients of the 3 m fence before taking a final decision on the final configuration of the fence.

5.1.3 Influence of a deflector and its angle

In this section it will be studied the benefits in the aerodynamic coefficients of the truck of adding a deflector at the top of the fence, and the optimal angle of this one to protect a vehicle from the action of the crosswind will be studied. Below is presented the geometry of the deflector that has been incorporated into the fence and the reference that will be taken for its angle, which will be the angle formed by the deflector with the horizontal. The effect of the variation of the deflector angle will be studied for angles of 20°, 40°, 60° and 80°.

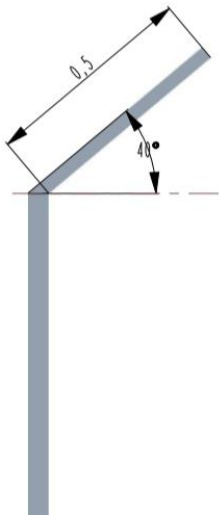

Figure 33: Geometry of the deflector that extends along the fence with an angle of 40°.

For this study, the truck geometry will be used as in the previous ones and the fence in which the deflector will be incorporated to study its benefits will be the opaque fence, since, as has been said, it is the starting point for all the fence geometries and the trend of the truck's aerodynamic coefficients when varying the angle of the deflector is independent of the porosity since what the deflector does is change the direction that the flow takes when it passes over the fence, as will be demonstrated later. It is emphasized that in this case it is being affirmed that the tendency of the variation of the coefficients when varying the angle of the deflector is independent to the porosity of the fence, hypothesis different to the already denied one of the previous section in which the difference between the coefficients of the different opaque fences was equal to the differences in the coefficients for a certain porosity.

As mentioned at the end of the previous section, it is desired to reduce by means of the deflector the aerodynamic coefficients produced by the 3 m fence so as to make it as effective as the 4 m fence. Therefore, the opaque fence to which the deflector will be incorporated will have a height of 3 m, and as it has already been shown that the optimum distance for our case is 3 m, this will be the distance between the fence and the vehicle.

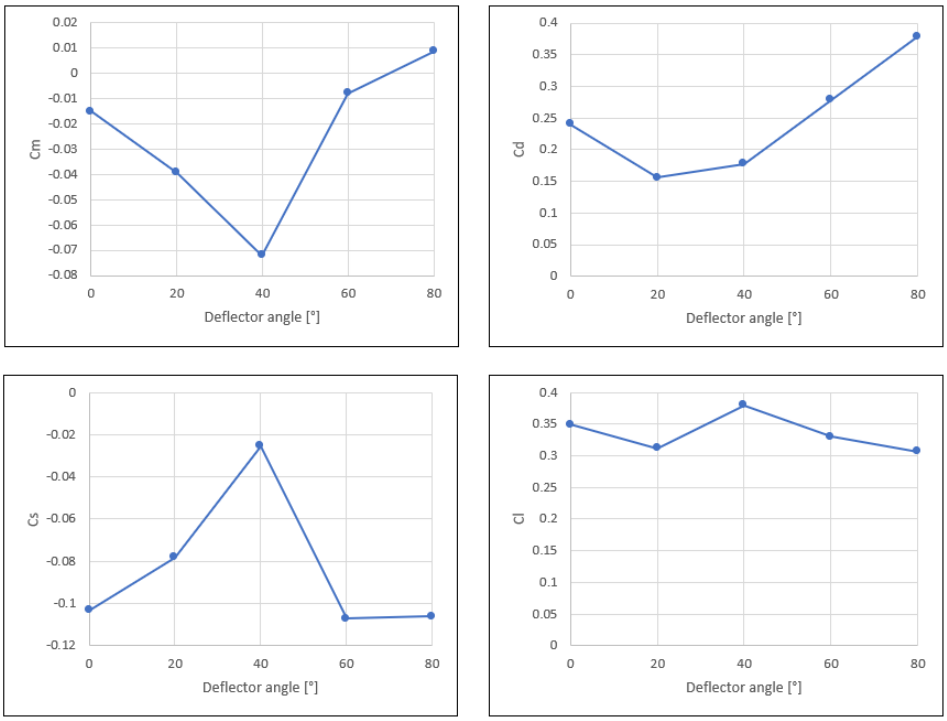

Figure 34: Aerodynamic coefficients of the truck with opaque fence 3 m height and distance for different deflector angles for a yaw angle of 50°.

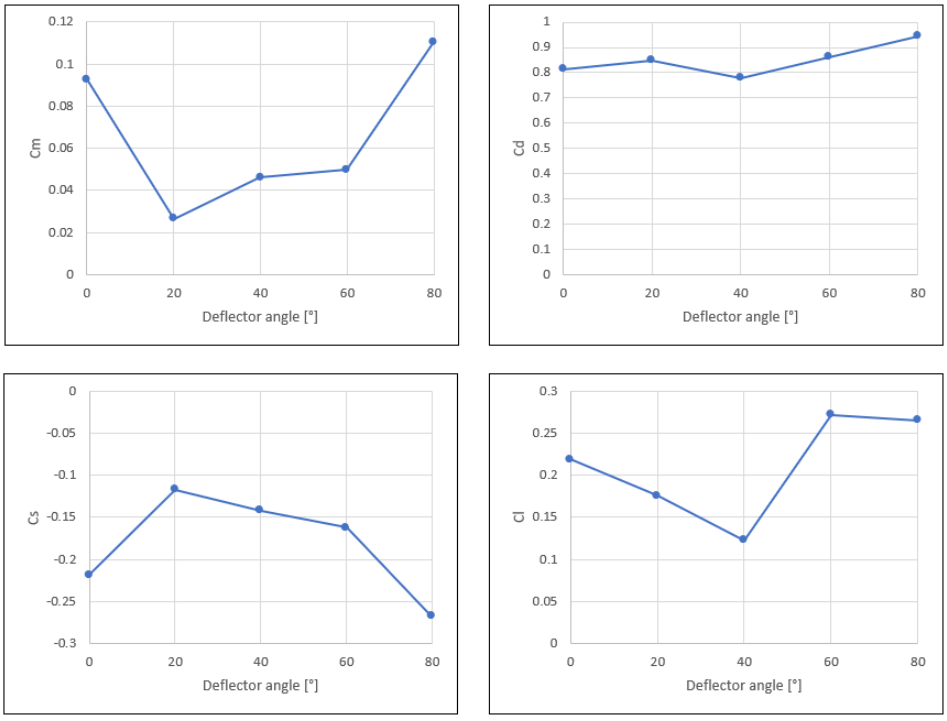

Figure 35: Aerodynamic coefficients of the truck with opaque fence 3 m height and distance for different deflector angles for a yaw angle of 30°.

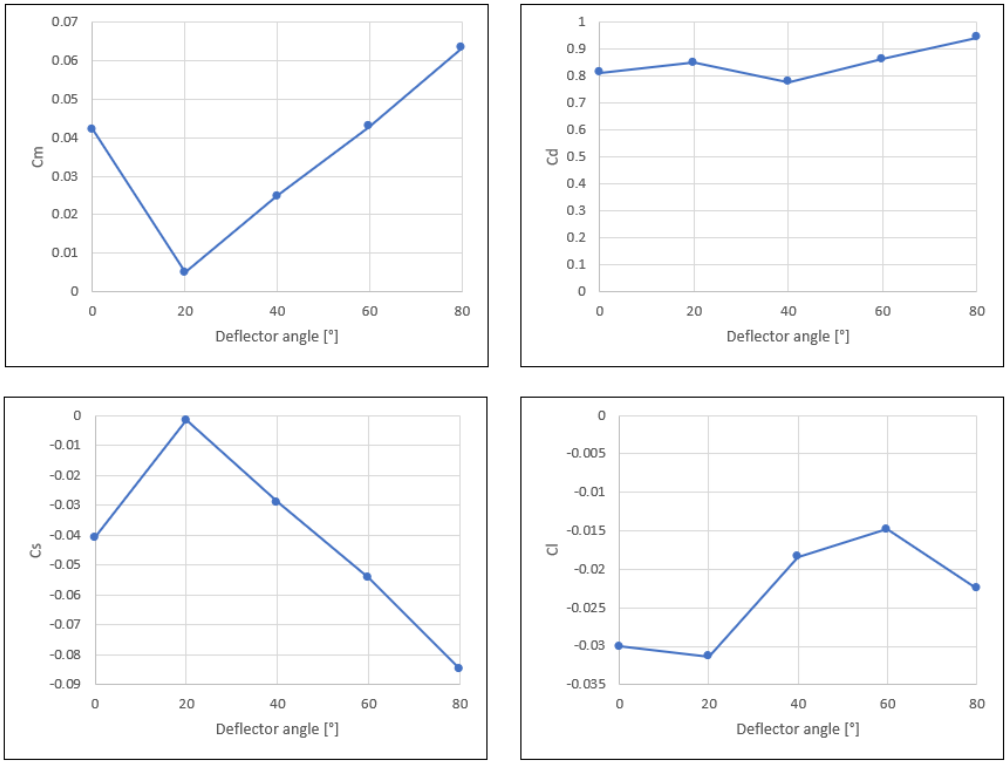

Figure 36: Aerodynamic coefficients of the truck with opaque fence 3 m height and distance for different deflector angles for a yaw angle of 10°.

Figure 34, Figure 35 and Figure 36 show the aerodynamic coefficients of the truck for a 3 m high opaque fence at a distance of 3 m for different deflector angles. It should be clarified that in these graphics the deflector angle of 0° does not indicate a horizontal deflector but rather shows the results for a 3 m fence without a deflector.

In Figure 34, case for a yaw angle of 50°, it can be seen that with the incorporation of the deflector the protection for the side force and roll moment coefficients decreases until the angle of 40° where the protection rises again exceeding the initial value for angles greater than 60. Approximately for a deflector of 70° the opaque fence would annul the roll moment coefficient. For the drag coefficient its value decreases with the deflector angle of 20° but from this point on this value begins to increase passing the initial value for angles of 60° and 80°. The lift coefficient seems to decrease with increasing deflector angle, but this reduction is almost negligible.

In the case of a yaw angle of 30° (Figure 35) there is a similar trend to the previous one. For the side force and roll moment coefficients, the deflector with 20° reduces the protection of these coefficients of the truck by the action of the wind and when increasing this angle, the protection increases until passing the value of the fence without deflector for the angle of 80°. In the drag coefficient when increasing the angle, the value of this coefficient increases slightly. The lift coefficient is reduced for small angles, such as 20° and 40°, and is increased for larger angles, such as 60° and 80°.

For the case in which the yaw angle is 10° shown in Figure 36 the behavior to the variation of the deflector angle is the same as for the previous case. The protection for the lateral forces and moment decreases for the angle of 20° and increases when this angle increases, obtaining a greater protection than the initial one for the angles of 60° and 80°. The drag coefficient is slightly increased when the deflector angle is increased. And finally, the effect of the deflector on the lift coefficient is almost imperceptible due to the low value that was already present for the fence without deflector.

Now drawing the general conclusions of the optimal angle of the deflector, it cannot be concluded that there is a perfect angle for which the deflector is most optimal in all coefficients and yaw angles, and it can be concluded that for large deflector angles it is possible to increase the protection of the lateral forces that one had with the fence without deflector but at the cost of an increase in the drag coefficient. The deflector does not manage to vary very significantly the aerodynamic coefficients of the vehicle that were already available for the fence without deflector, but the deflector can be understood as a tool to be added to the selected windbreak fence to vary in a small way the coefficients obtained according to the needs of this fence, as it has been seen for low porosity the protection of the lateral force is excessive changing its sign, so with the deflector it would be wanted to lower that protection, in order to make the fence as efficient as possible.

Looking now at the design of the specific windbreak fence being developed in this work, in order to use a height of 3 m it was desired to be able to increase the protection of the lateral forces that it exerted on the truck by decreasing the side force and roll moment coefficients through the incorporation of a deflector, and also that the deflector would be capable of decreasing the drag coefficient to make this fence competitive with the 4 m height fence. But once studied the effect of the deflector on the aerodynamic coefficients it can be concluded that this effect cannot be achieved since the extra protection that can be obtained from the deflector for the lateral forces is not very significant and it would not be enough to cancel the lateral force and roll moment coefficients when using a 3 m high fence with rectangular openings and 20% porosity. In addition, to achieve this extra protection the deflector should be designed with a great angle to the horizontal, such as one of 80°, which causes an increase in the drag coefficient, so for the configuration of geometry and porosity that is desired to make the 3 m high fence is not the best option.

In this way, the fence with rectangular openings and a porosity of 20% of 4 m high at a distance of 3 m from the vehicle is considered again and it will be tried by incorporating a deflector to make it as effective as possible, cancelling out the side force and roll moment coefficients, and at the same time trying to reduce the drag coefficient. Because, as shown in Figure 30, Figure 31 and Figure 32, it offers greater protection against lateral forces than the 3 m high fence, and with it, a lower drag coefficient is obtained for the truck.

5.1.4 Development of the final windbreak fence model

In this last section of the study of the influence of the different parameters to be chosen when designing a windbreak fence, the final model will be made by adding a deflector to the fence with rectangular openings of 20% porosity with a height of 4 m and a distance from the truck of 3 m.

Below are shown the aerodynamic coefficients that have been obtained for the truck with this fence, to know what needs to be met by the deflector and thus be able to choose its angle:

Yaw angle	Cm	Cd	Cs	Cl
[°]	[-]	[-]	[-]	[-]
10	-0.02595	0.764926	0.029667	0.010128
30	-0.06084	0.556179	0.0413	0.12931
50	-0.06954	0.367147	0.053033	0.309384

Table 5: Aerodynamic coefficients of the truck with a fence of rectangular openings with a porosity of 20%, a height of 4 m and a distance of 3 m.

As can be seen in Table 5, the coefficients of lateral force and tilting moment are only in the order of hundredths, so they are very close to being cancelled. What the deflector must provide is an increase in the protection of these coefficients, which has been seen in the previous section to be achieved with large deflector angles, which in turn can lead to an increase in the drag coefficient but it is hoped that this may not be very significant.

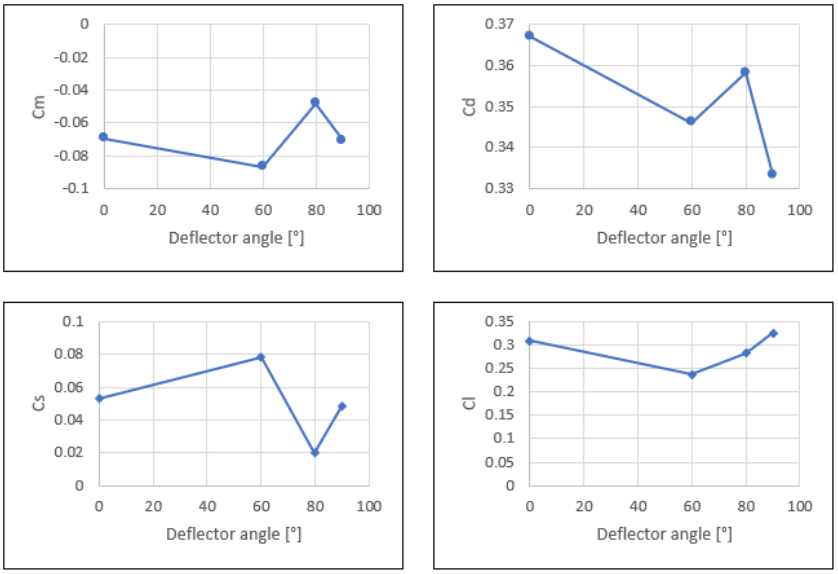

Figure 37: Aerodynamic coefficients of the truck with fence with rectangular openings of 20% porosity with a height of 4 m and a distance of 3 m for different deflector angles for a yaw angle of 50°.

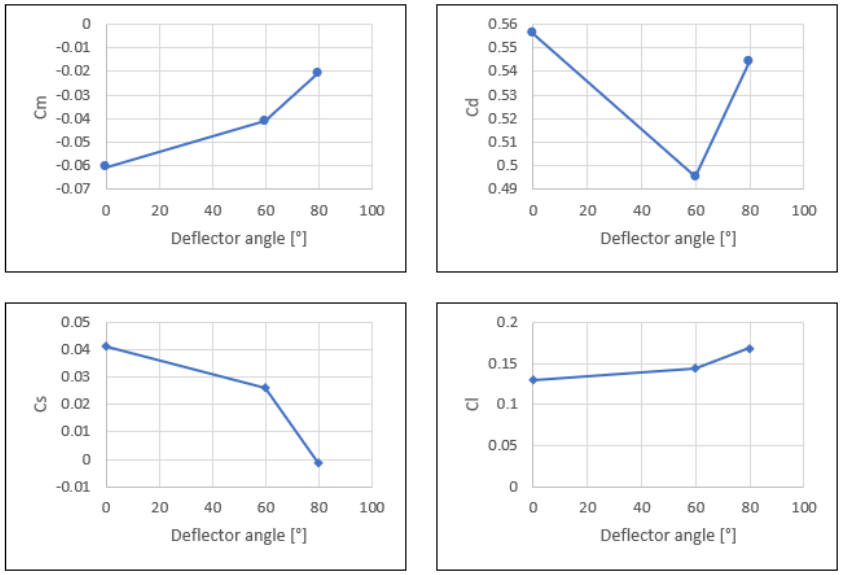

Figure 38: Aerodynamic coefficients of the truck with fence with rectangular openings of 20% porosity with a height of 4 m and a distance of 3 m for different deflector angles for a yaw angle of 30°.

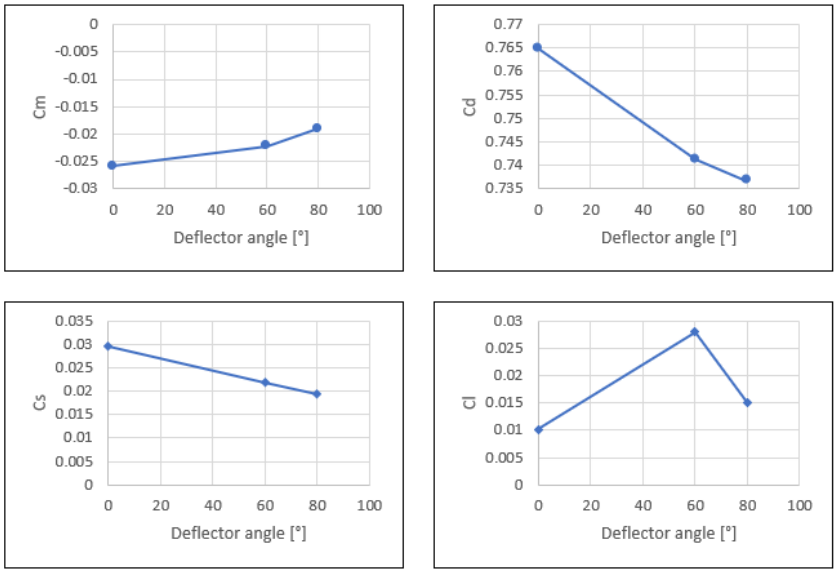

Figure 39: Aerodynamic coefficients of the truck with fence with rectangular openings of 20% porosity with a height of 4 m and a distance of 3 m for different deflector angles for a yaw angle of 10°.

In the graphs just shown there are the aerodynamic coefficients of the truck for the fence in question with a deflector of 60° and 80°, it should be noted that as in the previous section the deflector of 0 indicates the fence without deflector.

These graphs also confirm the hypothesis made in the previous section that the tendency of the deflector angle to influence the aerodynamic coefficients is independent of the porosity of the fence, since as can be seen again the greater the deflector angle, the greater the protection against

lateral forces (in the graphs in Figure 37 the angle of 90° is not considered a deflector since it is completely vertical).

In order to achieve the objective of reducing the side force and roll moment coefficients, the 60° and 80° deflector angles have been tested on the fence, as it is already known that the greater the angle, the greater the protection, and in the case of the 50° yaw angle in Figure 37, it has been tried to introduce the 90 angle, a vertical wall, to check whether the tendency to increase the protection continued, which has been found not to be the case. As can be seen in the graphs, the deflection angle of 80° was the one that achieved the maximum reduction of the side force and roll moment coefficients, which, although they were not cancelled out, were considered to have been reduced to a negligible level, and therefore the main objective of the windbreak fence was achieved. With respect to the drag coefficient, this has remained almost constant with respect to that obtained without the deflector, so the second objective of the windbreak fence has also been met, namely, to be able to reduce the drag coefficient.

The numerical values of the graphs and the truck without fence will also be shown below:

Deflector angle [°]	Cm	Cd	Cs	Cl
No fence	-0.79513	0.589815	1.166686	0.364686
No deflector	-0.06954	0.367147	0.053033	0.309384
60	-0.08661	0.346079	0.078523	0.237967
80	-0.0481	0.35818	0.019937	0.283055
90	-0.07044	0.333178	0.048499	0.325725

Table 6: Aerodynamic coefficients of the truck without fence with a fence with rectangular openings of 20% porosity with a height of 4 m and a distance of 3 m for different deflector angles for a yaw angle of 50°.

Deflector angle [°]	Cm	Cd	Cs	Cl
No fence	-0.53413	0.9797852	0.788515	0.277309
No deflector	-0.06084	0.5561789	0.0413	0.12931
60	-0.04102	0.49511364	0.025968	0.143569
80	-0.02068	0.54433909	-0.00125	0.168683

Table 7: Aerodynamic coefficients of the truck without fence with a fence with rectangular openings of 20% porosity with a height of 4 m and a distance of 3 m for different deflector angles for a yaw angle of 30°.

Deflector angle [°]	Cm	Cd	Cs	Cl
No fence	-0.18968	0.967946	0.28184	0.099589
No deflector	-0.02595	0.764926	0.029667	0.010128
60	-0.02224	0.74125	0.022003	0.028006
80	-0.01907	0.736658	0.019528	0.015131

Table 8: Aerodynamic coefficients of the truck without fence with a fence with rectangular openings of 20% porosity with a height of 4 m and a distance of 3 m for different deflector angles for a yaw angle of 10°.

In the tables just shown can be seen the numerical values obtained with the fence with rectangular openings with a porosity of 20%, a height of 4 m, a distance of 3 m and a deflector of 80°, numbers in which it is clear the great effectiveness that has been achieved of the wind breaker fence.

The appearance of the final fence is shown below:

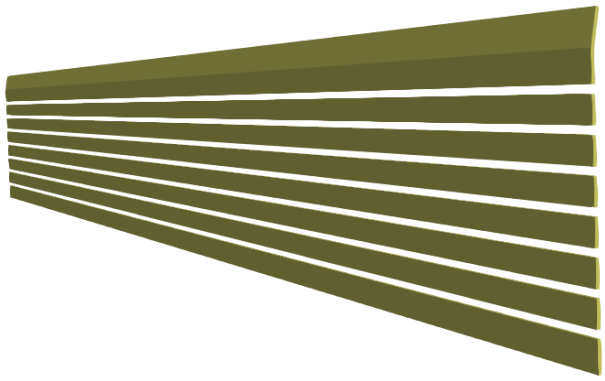

Figure 40: Windbreak fence with rectangular openings with a porosity of 20%, a height of 4 m, a distance of 3 m to the truck and a deflector of 80°.

Once the development of the wind barrier has been completed and the parameters studied, its effectiveness can be checked for the three geometries, truck, car and motorbike, in the five cases shown in Table 1.

5.2 Efficiency of the wind-break fence for the truck

This section will show the results of the aerodynamic coefficients obtained for the truck without windbreak fence and with the definitive wind fence configuration developed in the previous section that can be seen in Figure 40.

Yaw angle	Cm	Cd	Cs	Cl
[°]	[-]	[-]	[-]	[-]
10	-0.1896828	0.9679464	0.2818404	0.09958932
20	-0.3741334	1.072582	0.5736986	0.1778144
30	-0.5341295	0.9797852	0.7885149	0.2773088
40	-0.6875822	0.7866296	0.9965915	0.3950466
50	-0.7951284	0.5898147	1.166686	0.3646858

Table 9: Truck aerodynamic coefficients for the five cases of yaw angle proposed.

Table 9 shows the aerodynamic coefficients of the truck for the five yaw angle cases proposed in Table 1. As can be seen, and is to be expected, the roll moment coefficient and the side force coefficient increase as the yaw angle does, but contrary to what can be believed the drag coefficient

has its maximum for a yaw angle of 20 and from this it starts to decrease. The lift coefficient has its maximum for a yaw angle of 40 and decreases from there. All these phenomenon were already observed in the validation of the model in 4.2.3.1 Truck validation. This in turn validates the results obtained in the Table 9.

Below are the results of aerodynamic coefficients for each case of yaw angle of the truck with and without fence and the percentage reduction to check the efficiency of the selected fence.

10° Yaw angle	Cm	Cd	Cs	Cl
Without fence	-0.18968	0.967946	0.28184	0.099589
With fence	-0.01907	0.736658	0.019528	0.015131
Reduction [%]	89.94711	23.89472	93.07134	84.80707

20° Yaw angle	Cm	Cd	Cs	Cl
Without fence	-0.37413	1.072582	0.573699	0.177814
With fence	0.062729	0.799411	-0.09132	0.157813
Reduction [%]	116.7665	25.46853	115.917	11.24841

30° Yaw angle	Cm	Cd	Cs	Cl
Without fence	-0.53413	0.9797852	0.788515	0.277309
With fence	-0.02068	0.54433909	-0.00125	0.168683
Reduction [%]	96.12887	44.4430175	100.1584	39.17131

40° Yaw angle	Cm	Cd	Cs	Cl
Without fence	-0.68758	0.7866296	0.996592	0.395047
With fence	-0.07246	0.3284619	0.064715	0.245583
Reduction [%]	89.46118	58.2444014	93.5064	37.83452

50° Yaw angle	Cm	Cd	Cs	Cl
Without fence	-0.79513	0.589815	1.166686	0.364686
With fence	-0.0481	0.35818	0.019937	0.283055
Reduction [%]	93.95096	39.27242	98.29114	22.38398

Table 10: Final results of the aerodynamic coefficients of the truck with and without fence and their percentage reduction.

In the same way, for a better understanding of the reduction that has been obtained, graphs of the percentage reduction of each case of yaw angle for each aerodynamic coefficient of the truck will be shown.

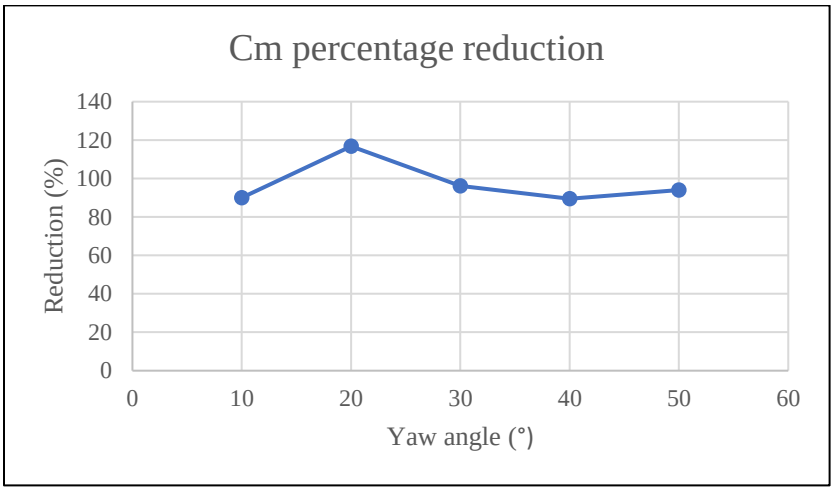
Cm percentage reduction
Reduction (%)
140
120
100
80
60
40
20
0
0
10
20
30
40
50
60
Yaw angle (°)

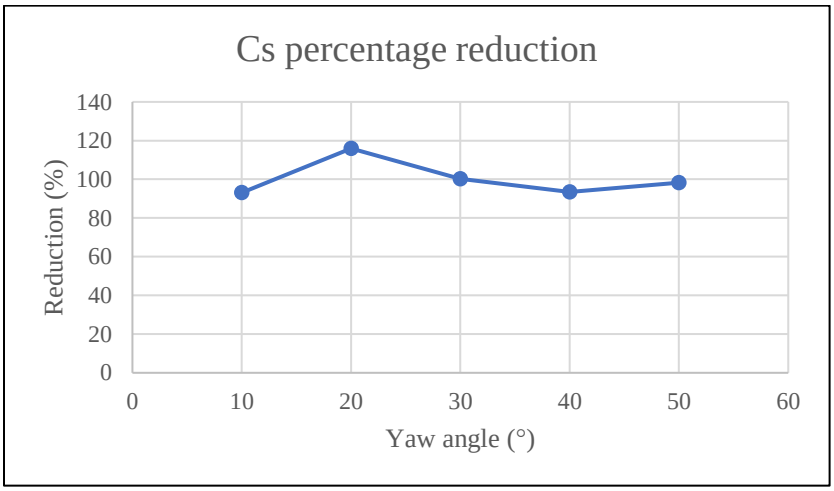
Cs percentage reduction
Reduction (%)
140
120
100
80
60
40
20
0
0
10
20
30
40
50
60
Yaw angle (°)

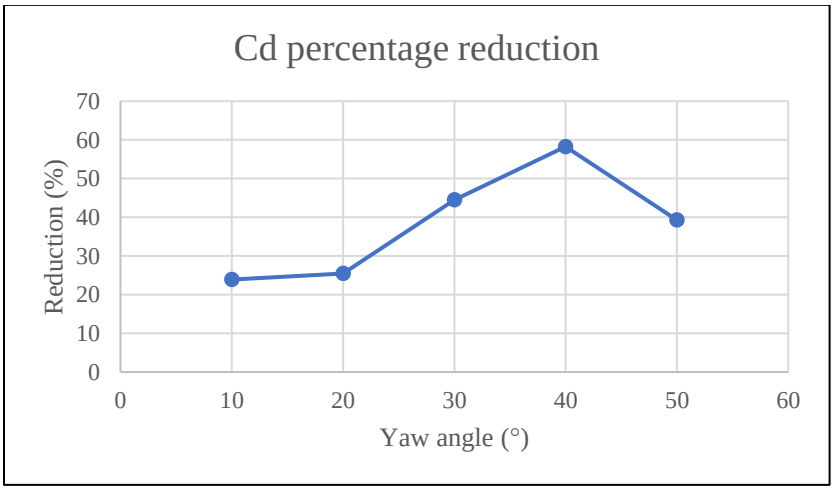
Cd percentage reduction
Reduction (%)
70
60
50
40
30
20
10
0
0
10
20
30
40
50
60
Yaw angle (°)

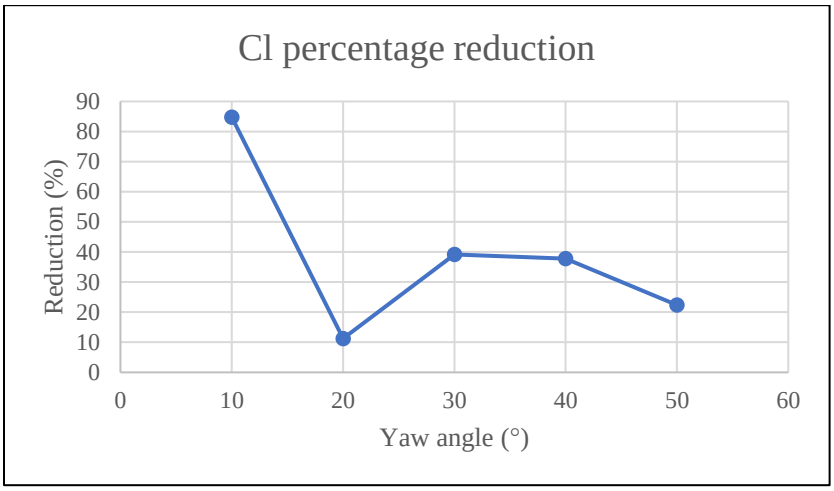

Figure 41: Final percentage reduction of the aerodynamic coefficients of the truck when incorporating the fence.

As can be seen in figure 41, according to the first objective that had been set for the wind fence, to cancel the roll moment and side force coefficients, for all yaw angles the reduction of these coefficients is almost 100%, the angles for which the reduction is further away from 100% are the yaw angle of 10 and 20, cases in which these coefficients were already low so they can also be considered cancelled. The second objective was to be able to reduce the drag coefficient of the truck, an objective that has also been successfully achieved, with a greater reduction for the higher yaw angles.

The lift coefficient has also been reduced in different ways for the different cases, but as this is not one of the initial objectives it will not be taken into consideration in the final conclusions.

Therefore, finally, with an average reduction in the roll moment coefficient of 90.5%, an average reduction in the side force coefficient of 93.8% and an average reduction in the drag coefficient of 38.3%, the objectives for this wind fence can be considered to have been successfully met, and its study in the case of the truck has been completed (these average reductions have been made with the reductions in the absolute value so as not to have reductions above 100% that alter this average).

5.3 Efficiency of the wind-break fence for the motorbike

Throughout this project, a windbreak fence has been developed to reduce the side force and roll moment coefficients of a truck as much as possible, which means that the fence has been optimized for the geometry of the truck. At the beginning of this work a hypothesis was formulated that a wind fence must be optimized to be able to protect the largest vehicle, in this case the truck, since, if it is able to protect this vehicle, it will be able to protect less bulky vehicles from the action of the cross wind on them.

So now that it has been proven that the wind fence meets the objectives of reducing the coefficients of the truck, and therefore has been optimized for this geometry, it should be checked the efficiency

that the fence has for the rest of the vehicles. Specifically in this section there will be a study of the behaviour of the motorbike, geometry presented in Figure 6,in cross wind when incorporating the fence in Figure 40.

Yaw angle	Cm	Cd	Cs	Cl
[°]	[-]	[-]	[-]	[-]
10	-0.06011	0.4936956	0.228572	0.03101
20	-0.19067	0.5593668	0.602111	0.008956
30	-0.34761	0.5416205	0.99572	0.102999
40	-0.46852	0.4795531	1.291104	0.218602
50	-0.56435	0.4061231	1.530704	0.358269

Table 11: Motorbike aerodynamic coefficients for the five cases of yaw angle proposed.

The results in Table 11 show the aerodynamic coefficients of the motorbike without the windbreak fence for the five yaw-angle cases presented in Table 1. In the behavior of the motorbike against the action of the cross wind, one can see, as expected, a behavior similar to that of the truck. The roll moment and side force coefficients increase (in absolute value) as the yaw angle increases, since the greater the angle, the greater the air flow impact on the side of the vehicle, causing this increase. As for the drag coefficient, again its maximum is found for a yaw angle of 20° and from this it decreases, but it can be seen that even if it decreases its difference between the maximum and minimum value is not very large. On the other hand, the sustaining coefficient falls slightly from 10° to 20° and then increases its value notably.

Below are the results obtained for the aerodynamic coefficients of the motorbike when incorporating the windbreak fence.

10° Yaw angle	Cm	Cd	Cs	Cl
Without fence	-0.06011	0.493696	0.228572	0.03101
With fence	-0.00446	0.377351	0.016379	0.072578
Reduction [%]	92.58034	23.56612	92.83437	-134.05

20° Yaw angle	Cm	Cd	Cs	Cl
Without fence	-0.19067	0.559367	0.602111	0.008956
With fence	0.043876	0.398625	-0.10669	0.02599
Reduction [%]	123.012	28.73642	117.7194	-190.201

30° Yaw angle	Cm	Cd	Cs	Cl
Without fence	-0.34761	0.541621	0.99572	0.102999
With fence	0.090389	0.501022	-0.32378	0.088119

Reduction [%]	126.0032	7.495673	132.5174	14.44671

40° Yaw angle	Cm	Cd	Cs	Cl
Without fence	-0.46852	0.479553	1.291104	0.218602
With fence	0.189308	0.481277	-0.60741	0.171546
Reduction [%]	140.4056	-0.35944	147.0459	21.52596

50° Yaw angle	Cm	Cd	Cs	Cl
Without fence	-0.56435	0.406123	1.530704	0.358269
With fence	0.299335	0.498213	-0.97029	0.289489
Reduction [%]	153.0407	-22.6754	163.3883	19.19801

Table 12: Final results of the aerodynamic coefficients of the motorbike with and without fence and their percentage reduction.

And as in the previous section for the truck, below are the graphs of the percentage reduction of each aerodynamic coefficient of the bike for each yaw angle, to facilitate the understanding of the results obtained from Table 12.

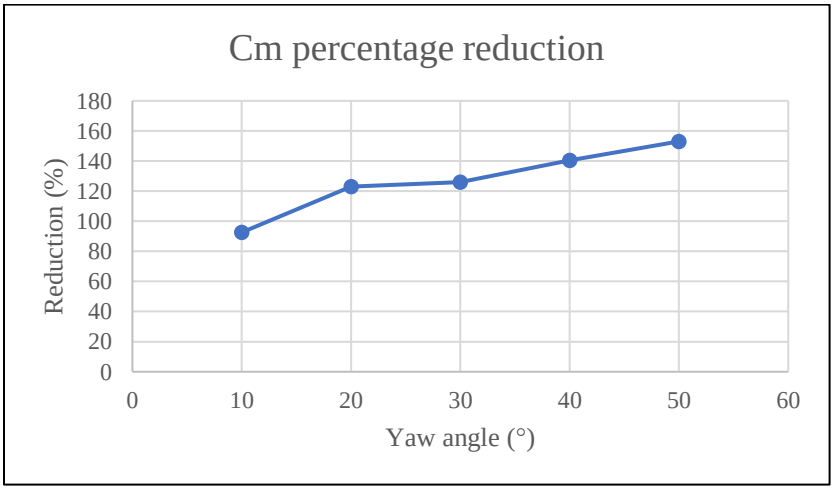

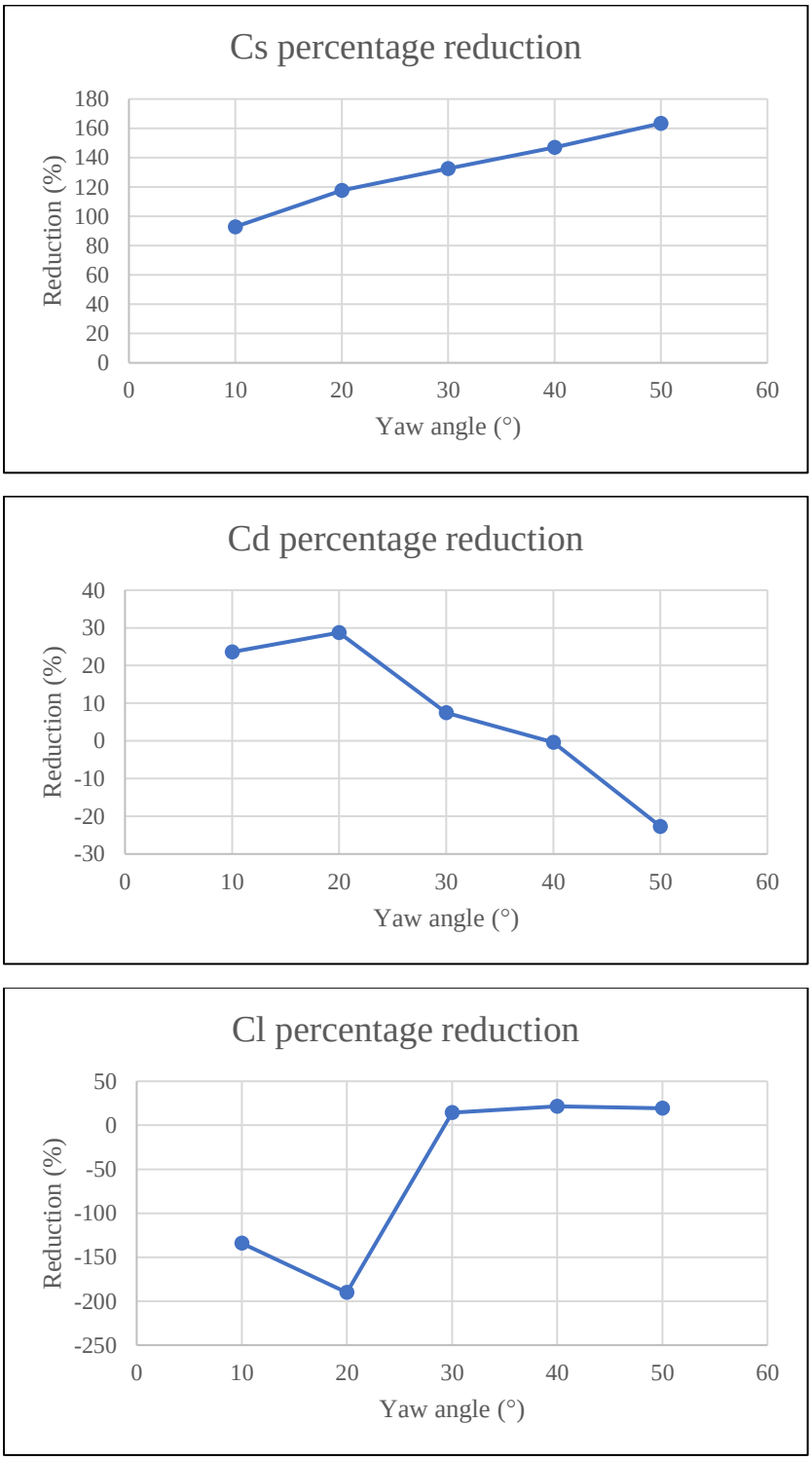

Figure 42: Final percentage reduction of the aerodynamic coefficients of the motorbike when incorporating the fence.

In Figure 42 it can be seen how in the case of the motorcycle the fence provides excessive protection in reducing the side force and roll moment coefficients, making this force and moment contrary to its initial direction and with a considerable value for the highest yawing angles.

It should be noted that the fence has been configured 3 m from the side of the truck which means that it is approximately 4 m from the motorbike, and furthermore the relative height of the fence to the motorbike is much higher than the relative height of the fence to the truck. Once these peculiarities have been considered, the results obtained can be analyzed.

As studied in point 5.1.2 Influence of height and distance, by increasing the height of a fence the protection of the fence for the side force and the roll moment coefficients is increased for all yaw angles, and by increasing the distance for the yaw angles of 50° and 30° (Figure 27 and Figure 28) this protection is also increased, while for the yaw angle of 10° (Figure 29) by increasing the distance between the fence and the vehicle this protection is lowered. This reasoning explains why there is such an exaggerated protection for these coefficients of the bike for all yaw angles except for the angle of 10° where the protection is optimal.

In the drag coefficient a poor reduction is seen that becomes even negative for the yaw angle of 50°. This could be explained by the behaviour shown in Figure 27 and Figure 28 where the higher the fence height the higher the drag coefficient, but this behaviour of the influence of the fence height on the drag coefficient was not confirmed in point 5.1.2.1 Verification of the hypothesis. So this behaviour of increasing the drag coefficient by increasing the yawing angle could be due to the geometry of the motorcycle, the interaction of the motorcycle fairing shapes with the flow that is created between the fence and the motorcycle could be responsible for the increase of the drag force, this reasoning is just an idea that would have to be studied.

The lift coefficient significantly increases its value with the addition of the fence for low angles and is reduced slightly for large and intermediate angles.

Therefore, with average reductions of 70% in the roll moment coefficient, 66.4% in the side force coefficient and 7.4% in the drag coefficient, it is considered that in the case of the motorbike the efficiency of the selected wind fence is considerably lower than in the case of the truck, which is reasonable since the fence has been designed to optimize it for the truck case, but that the objective of reducing the effect of the lateral forces caused by the wind on the motorbike has been achieved, although on the other hand it is not considered that the objective of reducing the drag coefficient has been achieved, because even though an average reduction has been achieved it is very low and its value has been increased for the yaw angle of 50°.

5.4 Efficiency of the wind-break fence for the car

The last section of this work will be to check the efficiency of the proposed wind fence prototype in the geometry of the car, presented in Figure 7. It is expected that the fence efficiency for the car will be intermediate between the fence efficiency for the truck and for the motorbike, since as explained in the previous section the fence efficiency for the motorbike is reduced due to the fact

that the distance between the fence and the vehicle is greater than for the truck and that the relative height is also greater, so that as the distance between the fence and the car is closer to the distance between the truck and the fence, its efficiency is expected to be better than for the motorbike.

Yaw angle	Cm	Cd	Cs	Cl
[°]	[-]	[-]	[-]	[-]
10	-0.13787	0.3517189	0.394682	0.136913
20	-0.23923	0.4126233	0.686862	0.284006
30	-0.32541	0.3874694	1.007253	0.410337
40	-0.45082	0.2342738	1.334845	0.921125
50	-0.53355	0.2043267	1.403321	0.781078

Table 13: Car aerodynamic coefficients for the five cases of yaw angle proposed.

Table 13 shows the aerodynamic coefficients of the car for the five different yaw angles proposed. In the variation of these coefficients with the variation of the yaw angle the same behaviour is seen as for the rest of the vehicles, which gives confidence that the results are correct. The roll moment and side force coefficients increase their absolute value as the angle increases. The drag coefficient has its maximum as in the previous cases for a yaw angle of 20° and from this angle the drag coefficient decreases with the increase of the yaw angle. The lift coefficient has its maximum as in the case of the truck for a yaw angle of 40°, a maximum that is likely to be found for a yaw angle of 45°.

The following table will show the results obtained for the aerodynamic coefficients of the car when including the wind fence and its percentage reduction with respect to the values of Table 13.

10° Yaw angle	Cm	Cd	Cs	Cl
Without fence	-0.13787	0.351719	0.394682	0.136913
With fence	-0.02198	0.253652	0.034547	-0.07095
Reduction [%]	84.05891	27.88218	91.24689	151.8223

20° Yaw angle	Cm	Cd	Cs	Cl
Without fence	-0.23923	0.412623	0.686862	0.284006
With fence	0.115946	0.339088	-0.27701	0.114649
Reduction [%]	148.4663	17.82141	140.3301	59.63138

30° Yaw angle	Cm	Cd	Cs	Cl
Without fence	-0.32541	0.387469	1.007253	0.410337
With fence	0.112126	0.318348	-0.31433	0.40387
Reduction [%]	134.4573	17.83914	131.2065	1.576119

40° Yaw angle	Cm	Cd	Cs	Cl
Without fence	-0.45082	0.234274	1.334845	0.921125
With fence	0.112717	0.216026	-0.18908	0.685411
Reduction [%]	125.0025	7.788971	114.1651	25.58984

50° Yaw angle	Cm	Cd	Cs	Cl
Without fence	-0.53355	0.204327	1.403321	0.781078
With fence	0.164385	0.008623	-0.2463072	1.250296
Reduction [%]	130.8093	95.77991	117.5517	-60.0731

Table 14: Final results of the aerodynamic coefficients of the car with and without fence and their percentage reduction.

Again as in the previous cases the percentage reductions of each aerodynamic coefficient of the car for each yaw angle shown in Table 14 will be presented graphically to facilitate the analysis of the final results.

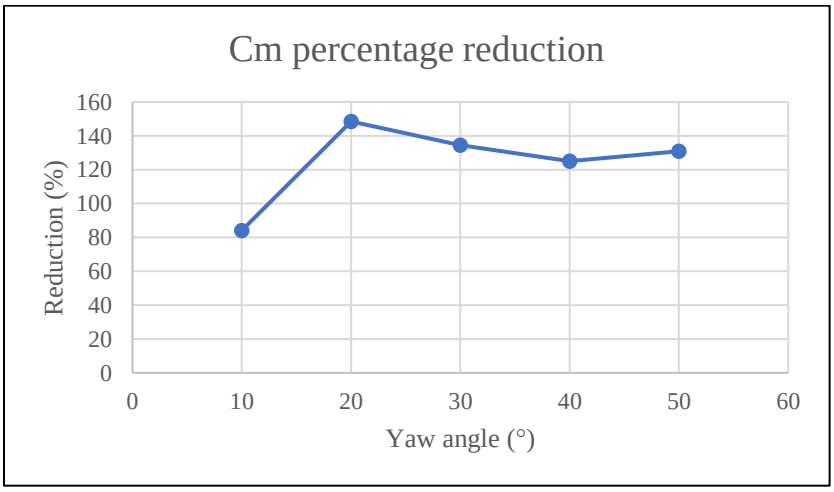

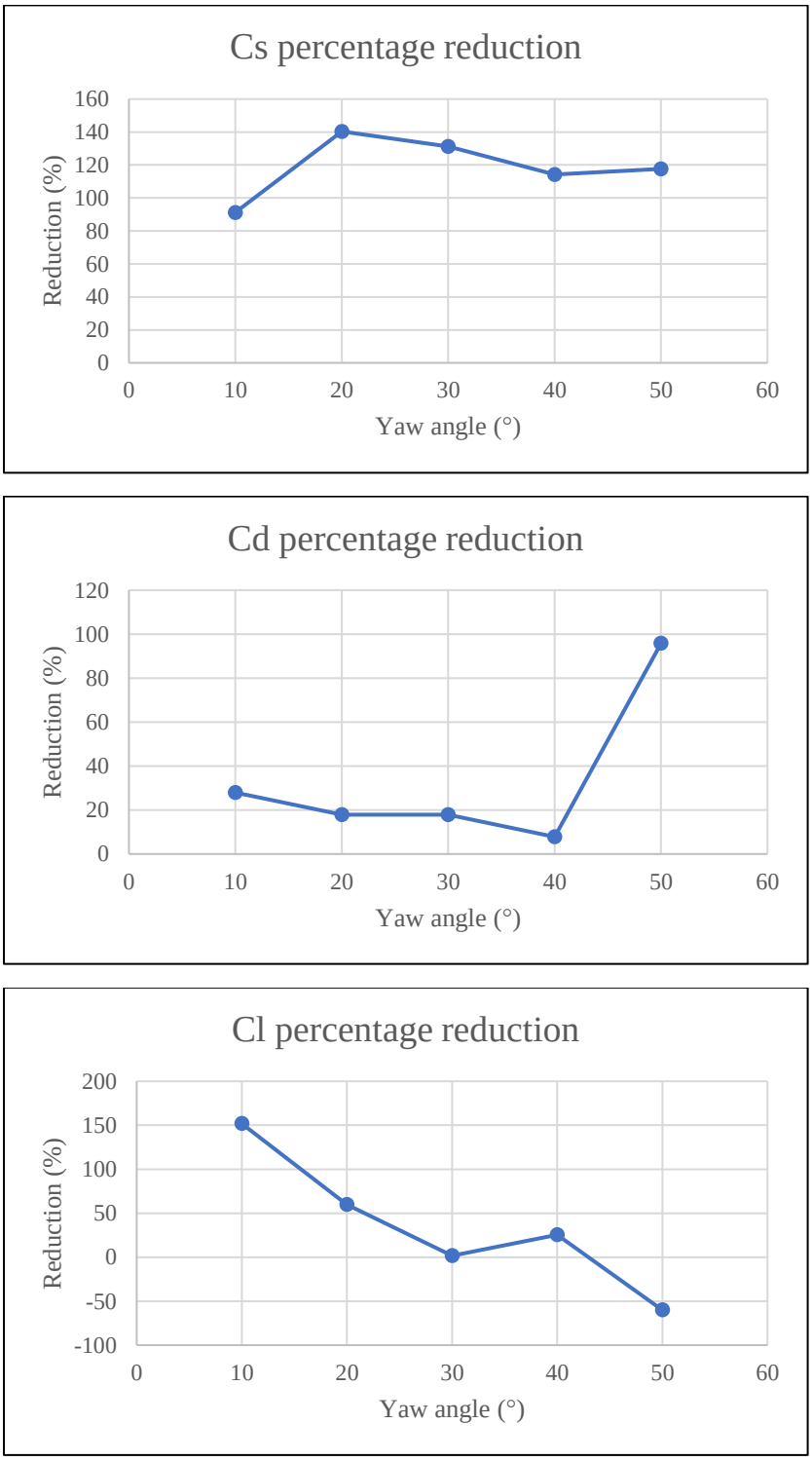

Figure 43: Final percentage reduction of the aerodynamic coefficients of the car when incorporating the fence.

Before analyzing the results in figure 43 it should be mentioned that the distance between the car and the truck is approximately 3.4 m and that its height is slightly higher than that of the motorbike together with the rider.

Starting with the reduction of the roll moment and side force coefficients, it can be seen how, as in the case of the motorbike, the reduction of these coefficients has been excessive. In the previous case this excessive protection grew as the yaw angle increased reaching its maximum for a 50° angle, while in the case of the car the maximum is reached for a 20° yaw angle and from this angle when the yaw angle increases the protection remains constant between 120% and 140%. Again, as in the previous case, the angle of 10° offers the least protection. The reasoning for these facts is the same as for the case of the motorbike, by increasing the distance between the vehicle and the fence and increasing the relative height between the fence and the vehicle the protection increases, thus giving an excess that causes the lateral forces to change direction and attract the vehicle towards the fence for yaw angles greater than 10°.

Talking now about the drag coefficient its reduction is normal and acceptable for yaw angles between 10° and 40° decreasing this reduction as the yaw angle increases, but for the case in which the yaw angle is 50° a strange phenomenon has occurred by which the drag coefficient has been reduced by 96% almost cancelling it out. This result at first sight could be seen as an error so the simulation of this case has been revised and repeated achieving the same result, so as there are no indications that this result is wrong it must be considered correct. This phenomenon that has occurred for the case of the car with a 50° yawing angle is considered a casual phenomenon by which the conditions of the simulation together with the geometry of the car have made the drag coefficient to be almost annulled punctually for the case of a 50° yawing angle. This event deserves to be studied more in depth to find out what the causes have been, understanding that it could be useful to reduce the drag coefficients of the vehicles with the use of the windbreaks.

The lift coefficient has had a very considerable reduction for the yaw angle of 10°, where the lift coefficient has come to change sign producing an improvement in the adherence to the asphalt of the car. For the angles of 20° and 40° this reduction has been acceptable, while for the angle of 30° the reduction is almost imperceptible and for the angle of 50° the value of this coefficient has been increased.

Finally, the efficiency of the windbreak chosen in the case of the car can be summarized in average reductions in the absolute value of the coefficients of 69% for the roll moment coefficient, 77.6% for the side force coefficient and 33.4% for the drag coefficient, counting the case of the yaw angle of 50°, and 17.8% excluding it.

Taking into account the average percentage reductions presented in the previous paragraph, it can be concluded that the objective of reducing the lateral forces acting on the car by the action of the cross wind has been achieved, to a lower extent than for the truck but with a significant reduction, and as for the objective of reducing the drag coefficient it can be considered that it has also been achieved, not with great success but with a significant reduction taking into account that the reduction of this coefficient was not the priority.

CHAPTER 6: Conclusions

6.1 Conclusions on methodology

This chapter of conclusions will begin with a critical analysis of the steps that have been taken to reach the final results, to determine what could have been done better, and to guide future studies that can be made from this work.

Starting with the preparation that has been made for the simulations set out in CHAPTER 4: Numerical setup, this setup was correct for the results to be obtained, which was to extract from the simulations the average forces in each direction to which the truck was subjected by the action of the cross wind. The adjustments and methodology followed to create the numerical model have been successfully validated (4.2.3 The validation), so the choice of solver (SimpleFoam) and turbulent model (SST k-omega) has been the right one. The turbulent model chosen to solve the RANS equations has met its performance characteristics for low Reynolds numbers, adverse pressure gradients and separate flow regions, what has led to good and reliable results. As well as the chosen boundary conditions have proven to be correct

The meshing performed with the SnappyHexMesh utility has proven to be correct and has been optimized to achieve the lowest possible computational cost with different tests for different levels of mesh refinement. The meshing and the validation of the truck were the most complicated and laborious parts of this work but it paid off, since there were no sources as complete for the validation of the motorbike and the car as for the validation of the truck, the meshes created and validated for the truck were used for the other two geometries, and therefore these meshes compromised the result of the whole project, and the work that went into them made it possible to obtain good results.

Finishing with the setup of the simulations, the choice of testing three different types of vehicles, truck, car and motorbike against what is usually done in this area of study, which is to study the behaviour of heavy and large vehicles, has proved to be very useful since in the final results it has been seen that for different vehicle sizes the efficiency of a wind fence is different.

Therefore, from the above, it can be concluded that the setup of the numerical model has been correct for the objectives that were intended. It is stressed that it has been the right one for what was intended to be extracted from the beginning of the simulations, which were average forces, but as research has progressed it has been found that wind barriers produce a vortex behind the vehicle to be protected (Figure 26) that can create instabilities for vehicles further away from the barrier, and in the same vehicle to be protected. Vortex that can be seen below:

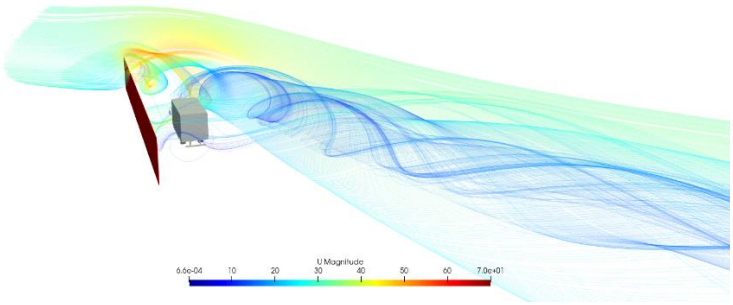

Figure 44: Vortex created by the windbreak fence

Therefore, if the influence that this vortex has on the behavior of the vehicle was wanted to be known, the simulations to be carried out would have had to be transient instead of steady state.

Talking now about the methodology that has been followed for the development of the fence in point 5.1 it can be affirmed that the steps that have been followed were correct, since it has been possible to develop a prototype capable of almost annulling the side force and roll moment coefficients of the truck, which was the priority of this study. It is considered that all the variables have been studied at the time of designing a windbreak fence, that have influence on the aerodynamic coefficients, and this influence of each parameter has been studied and understood in order to be able to configure the fence as more correct has been considered.

At the beginning of the fence design it was hypothesized that if a fence is able to protect the larger vehicle from the wind it will also be able to protect the other vehicles from the wind. This hypothesis has been confirmed, but what was not expected when it was formulated is that there would be such a remarkable negative lateral force for the rest of the vehicles. This situation has been given by focusing the development of the fence on optimizing it for the truck, which could have been solved by checking for each decision taken in the configuration of the fence its influence on the aerodynamic behaviour of the car and the motorbike.

At the beginning of the fence design it was hypothesized that if a fence is able to protect the larger vehicle from the wind it will also be able to protect the other vehicles from the wind. This hypothesis has been confirmed, but what was not expected when it was formulated is that there would be such a remarkable negative lateral force for the rest of the vehicles. This situation has been given by focusing the development of the fence on optimizing it for the truck, which could have been solved by checking for each decision taken in the configuration of the fence its influence on the aerodynamic behaviour of the car and the truck.

6.2 Conclusions on results

Several conclusions can be drawn from the results obtained, the first and most obvious being the great effectiveness that windbreaks can have in reducing the overturning moment and the lateral

force to which a vehicle is subjected when facing a cross wind. With the results obtained in section 5.2 Efficiency of the wind-break fence for the truck it has been clearly demonstrated how a wind fence is capable of reducing to a practical cancellation the lateral forces suffered by the vehicle for any yaw angle that the wind may take, thus demonstrating with these results that the study of wind fences must be continued and not only in an academic way, but also its study for implementation on roads, especially in areas heavily exposed to wind.

In addition, the results obtained have demonstrated the additional efficiency that wind fences can have in reducing the drag coefficient of a vehicle when it is subjected to a cross wind. What is another argument in favor of studying this technology and incorporating it into roads.

Another conclusion that could be drawn from the results obtained throughout the development of the prototype wind fence is that there is no single solution for this technology. Thanks to the extensive study that has been carried out on the influence of each variable to be chosen in the design of a windbreak fence, it can be stated that there are numerous configurations for the fence that can provide good results when it comes to reducing roll moment, side force and drag coefficients.

Firstly in point 5.1.1 it has been observed that instead of a better geometry and porosity to reduce the aerodynamic coefficients, as was thought at the beginning of this work, there is a porosity for each fence geometry for which the roll moment and side force coefficients can be almost cancelled out simultaneously. On this basis then it can also be stated that for any height and distance for which the roll moment and side force coefficients of a vehicle using an opaque fence change their signs, meaning that the roll would be towards the fence and the side force pushes the vehicle towards the fence, it can be achieved for a certain porosity to cancel these coefficients for these heights and distances with the vehicle. Since it has been demonstrated that the greater the porosity, the less protection there is from lateral forces.

Therefore, the prototype windbreak that has finally been reached shown in Figure 40 is only one of the possible configurations with good results in reducing the aerodynamic coefficients of the vehicle that could have been reached.

A conclusion or observation that can be made seeing the results of the wind fence for the car for a yaw angle of 50 (5.4 Efficiency of the wind-break fence for the car) is that a punctual phenomenon can occur by which the drag coefficient of a vehicle is almost cancelled thanks to the action of the fence, phenomenon of which it would be necessary to study in depth its peculiarities since by means of its study the efficiency of the wind fences in the reduction of the drag coefficient could be improved.

Another important conclusion reached when checking the efficiency of the selected fence for all vehicle types is that the efficiency of the fence is not the same for all geometries. Therefore, having focused the development of the wind fence on the truck has allowed to achieve an enormous efficiency for this vehicle but poorer for the rest.

Finally, the last aspect to comment on the results that have been obtained is in the behavior of the lift coefficient due to the incorporation of the windbreak fences. The reduction of this coefficient has not been an objective of this work, but its variations have been observed in front of different wind fences and yaw angles. It has been observed that, just as without wind fences the variation curve of the lift coefficient is the most complex of those of the coefficients when varying the yaw angle, the behaviour of the lift coefficient is difficult to predict when incorporating wind fences. Therefore, in the absence of conclusive data, it must be assumed that wind fences are not a technique with which to reduce the lift coefficient of a vehicle.

6.3 Future researches

The work that has been presented throughout this report is only a first stage in the development of the technique in question, the study of the efficiency of wind barriers can be much more extensive and requires many future works, which can be based on the work presented here.

As already mentioned in the conclusions, focusing the development of the fence on protecting the truck as much as possible has made possible, as was originally hypothesized, to protect smaller vehicles from the action of cross winds, but with a lower efficiency for them than for the truck. Therefore, based on the results obtained in this research on the influence of each parameter of the wind fence design on the efficiency of the same, a more extensive study could be made on the efficiency for each of the three vehicles in order to find the configuration that provides the maximum efficiency for all three together.

In this work, the optimal distance between the vehicle and the wind fence has been studied, but the efficiency obtained from this study only considers vehicles that are in the lane of the road adjacent to the wind fence. Therefore it would have to be studied how this efficiency would be for the lanes furthest from the fence, and also to make a fully realistic study in addition to the study of the influence of the multi-lane fence the influence of having a fence on each side of the road on the behaviour of the vehicles should be studied.

Another study that should be carried out based on the present work is, as already mentioned, the study of the vortex created by the fence that can be seen in Figure 44. It has been seen in the post-processor study shown in Figure 26 that the airflow over the fence is accelerated and creates a vortex, this event must be studied experimentally or with transient simulations to determine how this accelerated flow and the turbulence of the vortex affect the behavior of vehicles on the road where the fence is located. This accelerated flow and vortex event can lead to instabilities in the behaviour of road vehicles due to the turbulence of the phenomenon. These turbulences could compromise the results in terms of fence effectiveness shown in this work. Therefore, the influence of this event must be studied and also the technique to decrease its impact on the behavior of the vehicles.

Many are the future studies that can be based on this work, only some of those that would be the natural continuation of the research that has been carried out with the results obtained have been mentioned.

CHAPTER 7: Sustainable Development Goals

In 2015 the UN presented the Sustainable Development Goals (SDGs), an action plan and targets to be reached by 2030 to make the planet a better place in every corner of it and to try to save the planet from the damage it is subjected to by human action.

SDGs are defined by the UN as follows: The Sustainable Development Goals are the blueprint to achieve a better and more sustainable future for all. They address the global challenges we face, including those related to poverty, inequality, climate change, environmental degradation, peace and justice. The 17 Goals are all interconnected, and in order to leave no one behind, it is important that we achieve them all by 2030.

These being the 17 objectives:

Figure 45: Sustainable Development Goals.

As a person, one must try to collaborate and do one's bit to try to collaborate in all the goals, even if it is only minimally in some of them, in order to help fulfill them. But looking closely at these objectives, not only as a citizen of the world, but also as engineers, it can be seen that many of these objectives are difficult to achieve without the support of the engineering sector. Therefore, as the engineer's work is crucial to achieve these goals to help the planet and its inhabitants, every project that will be carried out must look at how to contribute to reach these objectives, as well as projects should be carried out only with the aim of achieving these goals.

Therefore, with the work that has been done in this thesis it has been sought to contribute in some way to achieving the SDGs by 2030. With targets 3 (Good health and well-being) and 12 (Responsible consumption and production) where the inclusion of wind barriers on roads can make the most difference.

As mentioned in the introduction to this thesis, road accidents are a global health problem, where 1.3 million people die on the roads each year and between 20 and 50 million people suffer non-fatal injuries. Therefore, in view of these worrying figures, objective 3.6 reads as follows: By 2020, halve the number of global deaths and injuries from road traffic accidents (Health – United Nations Sustainable Development n.d.). A goal that wind fences cannot achieve, but they can at least contribute to it.

The report of this thesis begins by listing the numbers of accidents and deaths on the roads due to wind. In the UK 3.7% of road accidents are strongly wind related, which means 6000 accidents per year. In the European Union in 2017 there were 25300 deaths and 135000 people seriously injured in traffic accidents. Therefore, if we assume that the percentage of accidents strongly related to wind is the same for all Europe as for the UK, the action of the wind produces 936 deaths and almost 5000 people seriously injured per year in Europe.

With the results presented throughout this work in which the action of the side forces and the roll moment in the behaviour of a vehicle due to the action of the wind can be seen almost cancelled out by the effect of the wind-break fences, therefore it can be said that thanks to this technology traffic accidents strongly related to wind can be practically annulled. Thus, reducing the 3.7% of accidents (assuming the percentage of UK equal to the rest of countries).

The 3.7% is not 50% as intended by goal number 3 of the Sustainable Development Goals but it is a significant contribution that can be made with only one technique and save thousands of lives, although there would still be 46.3% to reduce in the number of accidents by 2030.

The second objective of the SDGs to which this work on the efficiency of windbreak fences in the aerodynamic behaviour of a vehicle can directly contribute is number 12, specifically, point 12.2 of this goal reads: By 2030, achieve the sustainable management and efficient use of natural resources (Sustainable consumption and production – United Nations Sustainable Development n.d.). In the case of the automotive sector, this can lead to a reduction in the consumption of fuel produced by fossil fuels, which also leads directly to a reduction in greenhouse gas emissions from the road transport sector. That, as already indicated in the introduction, the transport sector is the largest contributor of greenhouse gas emissions in the EU, generating 27% of emissions, which is 1205 million tons of CO2 equivalent, with cars and vans being responsible for half of these. Consumption that can be reduced by reducing the air resistance that a vehicle must overcome.

In this thesis it has been demonstrated how wind barriers can reduce the drag coefficient of a vehicle, having achieved with the proposal of the final prototype a reduction of drag coefficient of 38.3% for the case of the truck, 7.4% for the case of the motorcycle and 33.4% for the case of the car.

Since air resistance is one of the forces that a vehicle has to overcome in order to move, this resistance requires power and therefore fuel consumption. Thus, a reduction in the drag coefficient of a vehicle, which is an indicator of the air resistance that the vehicle has to overcome, translates into a reduction in fuel consumption. According to (Fontaras, Zacharof and Ciuffo 2017), work in which fuel consumption of a vehicle is studied, a 20% reduction in the drag coefficient, compatible with the proven efficiency of wind fences for this coefficient, produces a reduction in a vehicle's fuel consumption of 3-7%.

Taking a 5% reduction in consumption by reducing the drag coefficient by 20%, this reduction in the consumption of a small 16,000 kg truck that consumes an average of 25 litres per 100 km would mean a reduction in consumption of 1.25 litres per 100 km. For the case of a petrol car that is assumed to consume an average of 8 litres per 100 km, the reduction would be 0.4 litres. Finally, in the case of a motorbike with an average consumption of 4.5 litres per 100 km, the reduction would be 0.225 litres. These data do not seem to make much difference when talking about the consumption of each vehicle, but when talking about an overall reduction, this is very significant.

There are 1200 million vehicles in the world, assuming that only half of these pass through roads with wind barriers for half the time they are on the road, this would be equivalent to the reduction in consumption that has been calculated to apply to 25% of the cars on the road in the world. Now applying the reduction of 0.4 litres per 100 km of a car applied to this percentage of total vehicles would mean a fuel saving of 120 million litres per 100 km.

Assuming that the greenhouse gas emissions produced by a vehicle are proportional to the liters of fuel it consumes, this reasoning can also be made for emissions savings.

As mentioned above, emissions from the transport sector in Europe are 1205 million tons of CO2 equivalent, with cars and vans being responsible for 602.5 million tons of CO2 equivalent. Therefore, applying a 5% reduction in emissions, the same as the reduction in fuel consumption, by reducing the drag coefficient by 20% of the 25% of the total vehicles that produce these emissions, the reduction in greenhouse gas emissions in Europe thanks to the windbreaks would be 7.53 million tons of CO2 equivalent. All this without taking into account the difficult to calculate consumption due to the constant need to rectify the trajectory of the car when it is subjected to the cross wind, consumption that would be eliminated thanks to the wind fences.

With all the data that have just been presented, being suppositions not real data, it is possible to conclude the great efficiency of wind fences in the care of the environment and the responsible consumption of natural resources, thus helping to achieve goal 12 of the Sustainable Development Goals.

CHAPTER 8: Bibliography

Alonso-Estébanez, A., J. J. Del Coz Díaz, F. P. Álvarez Rabanal, and P. Pascual-Muñoz. 2017. "Performance analysis of wind fence models when used for truck protection under crosswind through numerical modeling." *Journal of Wind Engineering and Industrial Aerodynamics* 168 (April): 20-31.

Amaral, G., J. Bushee, U. G. Cordani, KOJI KAWASHITA, J. H. Reynolds, Fernando FLÁVIO MARQUES De E ALMEIDA, F. F.M. de Almeida, et al. 2013. "No 主観的健康感を中心とした在宅高齢者における　　健康関連指標に関する共分散構造分析Title." *Journal of Petrology* 369 (1): 1689-1699.

Avadiar, T., M. C. Thompson, J. Sheridan, and D. Burton. 2018. "Characterisation of the wake of the DrivAer estate vehicle." *Journal of Wind Engineering and Industrial Aerodynamics* (Elsevier Ltd) 177 (March): 242-259.

Baker, C J, and S Reynolds. 1992. "Wind-induced accidents of road vehicles." *Accident Analysis & Prevention* 24 (6): 559-575.

Bocciolone, Marco, Federico Cheli, Roberto Corradi, Sara Muggiasca, and Gisella Tomasini. 2008. "Crosswind action on rail vehicles: Wind tunnel experimental analyses." *Journal of Wind Engineering and Industrial Aerodynamics* 96 (5): 584-610.

2005. "Cab Chassis." (October).

Cheli, F., F. Ripamonti, E. Sabbioni, and G. Tomasini. 2011. "Wind tunnel tests on heavy road vehicles: Cross wind induced loads-Part 2." *Journal of Wind Engineering and Industrial Aerodynamics* 99 (10): 1011-1024.

Cheli, F., R. Corradi, E. Sabbioni, and G. Tomasini. 2011. "Wind tunnel tests on heavy road vehicles: Cross wind induced loads-Part 1." *Journal of Wind Engineering and Industrial Aerodynamics* (Elsevier) 99 (10): 1000-1010.

Chen, Ning, Yongle Li, Bin Wang, Yang Su, and Huoyue Xiang. 2015. "Effects of wind barrier on the safety of vehicles driven on bridges." *Journal of Wind Engineering and Industrial Aerodynamics* (Elsevier) 143: 113-127.

Chu, Chia Ren, Chao Yen Chang, Chih Jung Huang, Tso Ren Wu, Chung Yue Wang, and Ming Yi Liu. 2013. "Windbreak protection for road vehicles against crosswind." *Journal of Wind Engineering and Industrial Aerodynamics* (Elsevier) 116: 61-69.

2018. "CO 2 EMISSIONS FROM CARS: the facts A report by Transport & Environment Acknowledgements."

Çoşkun, Şemsi, Hooman Amiri Hazaveh, Oğuz Uzol, and Özgür Kurç. 2017. "Experimental investigation of wake flow field and wind comfort characteristics of fractal wind fences." *Journal of Wind Engineering and Industrial Aerodynamics* (Elsevier B.V.) 168: 32-47.

n.d. *DrivAer*. https://www.mw.tum.de/en/aer/research-groups/automotive/drivaer/.

Edwards, Julia B. 1999. "The temporal distribution of road accidents in adverse weather." *Meteorological Applications* (John Wiley & Sons, Ltd) 6 (1): 59-68.

n.d. *File:HRNvsLRN.png -- CFD-Wiki, the free CFD reference.* https://www.cfd-online.com/Wiki/File:HRNvsLRN.png.

Fintelman, D., H. Hemida, M. Sterling, and F. X. Li. 2015. "A numerical investigation of the flow around a motorbike when subjected to crosswinds." *Engineering Applications of Computational Fluid Mechanics* 9 (1): 528-542.

Fontaras, Georgios, Nikiforos Georgios Zacharof, and Biagio Ciuffo. 2017. "Fuel consumption and CO2 emissions from passenger cars in Europe – Laboratory versus real-world emissions." *Progress in Energy and Combustion Science.* Vol. 60. Elsevier Ltd. 97-131.

Gillespie, Thomas D. 1992. *Fundamentals of vehicle dynamics.* Vol. 400. Society of automotive engineers Warrendale, PA.

Giuseppe, Via, and La Masa. 2005. "W . P . 2 . 2 . 1 (October 2005) Report describing the experimental set-up and the wind-tunnel tests methodology." (October): 1-13.

Gopal Shinde Kishor Nikann, Aniruddha Joshi. 2013. "Numerical Investigations of the DrivAer Car Model using Opensource CFD Solver OpenFOAM." *Conference Paper OSCIS 13, Hamburg,Germany* (October): 12.

Gu, Houyu, Tanghong Liu, Zhiwei Jiang, and Zijian Guo. 2020. "Research on the wind-sheltering performance of different forms of corrugated wind barriers on railway bridges." *Journal of Wind Engineering and Industrial Aerodynamics* (Elsevier Ltd) 201 (March): 104166.

n.d. *Health – United Nations Sustainable Development.* https://www.un.org/sustainabledevelopment/health/.

Heft, A.I., T. Indinger, and N.A. Adams. 2012. "Experimental and numerical investigation of the drivaer model." *American Society of Mechanical Engineers, Fluids Engineering Division (Publication) FEDSM.* 41-51.

Heft, Angelina I, Thomas Indinger, and Nikolaus A Adams. 2012. "Introduction of a New Realistic Generic Car Model for Aerodynamic Investigations." *SAE 2012 World Congress & Exhibition.* SAE International.

Hong, Se Woon, In Bok Lee, and Il Hwan Seo. 2015. "Modelling and predicting wind velocity patterns for windbreak fence design." *Journal of Wind Engineering and Industrial Aerodynamics* (Elsevier) 142: 53-64.

n.d. *Introduction to turbulence/Reynolds averaged equations -CFD-Wiki.* https://www.cfd-online.com/Wiki/Introduction_to_turbulence/Reynolds_averaged_equations.

Kozmar, Hrvoje, Lorenzo Procino, Alessandra Borsani, and Gianni Bartoli. 2012. "Sheltering efficiency of wind barriers on bridges." *Journal of Wind Engineering and Industrial Aerodynamics* (Elsevier) 107-108: 274-284.

Kramer, C, R Grundmann, and H J Gerhardt. 1991. "Testing of road vehicles under cross wind conditions." *Journal of Wind Engineering and Industrial Aerodynamics* 38 (1): 59-69.

Menter, Florian R. 1993. "AIAA 93·2906 Zonal Two Equation k·co Turbulence Models for Aerodynamic Flows. ZONAL TWO EQUATION k-w TURBULENCE MODELS FOR AERODYNAMIC FLOWS."

OpenFOAM User Guide. 2011. "OpenFOAM The OpenFOAM Foundation User Guide."

n.d. *OpenFOAM: User Guide: potentialFoam.* https://www.openfoam.com/documentation/guides/latest/doc/guide-applications-solvers-basic-potentialFoam.html.

Peters, Brett C, Mesbah Uddin, Jeremy Bain, Alex Curley, and Maxwell Henry. 2015. "Simulating DrivAer with Structured Finite Difference Overset Grids." SAE International.

Rüttgers, Mario, Junshin Park, and Donghyun You. 2019. "Large-eddy simulation of turbulent flow over the DrivAer fastback vehicle model." *Journal of Wind Engineering and Industrial Aerodynamics* (Elsevier Ltd) 186 (January): 123-138.

Salati, L., P. Schito, D. Rocchi, and E. Sabbioni. 2018. "Aerodynamic Study on a Heavy Truck Passing by a Bridge Pylon under Crosswinds Using CFD." *Journal of Bridge Engineering* 23 (9): 1-14.

Speziale, C G. 1991. "Analytical Methods for the Development of Reynolds-Stress Closures in Turbulence." *Annual Review of Fluid Mechanics* (Annual Reviews) 23 (1): 107-157.

n.d. *Sustainable consumption and production – United Nations Sustainable Development.* https://www.un.org/sustainabledevelopment/sustainable-consumption-production/.

n.d. *Two equation turbulence models - CFD-Wiki.* https://www.cfd-online.com/Wiki/Two_equation_models.

W.P.2.2.1. 2005. "W.E.A.T.H.E.R-W.P.2.2.1." (October): 1-13.

W.P.2.3.2. 2005. "W.E.A.T.H.E.R-W.P.2.3.2." (October).

Wang, Shibo, Terence Avadiar, Mark C. Thompson, and David Burton. 2019. "Effect of moving ground on the aerodynamics of a generic automotive model: The DrivAer-Estate." *Journal of Wind Engineering and Industrial Aerodynamics* (Elsevier Ltd) 195 (February): 104000.

n.d. *What is Aerodynamics? I Computational Fluid Dynamics I SimScale.* https://www.simscale.com/docs/simwiki/cfd-computational-fluid-dynamics/what-is-aerodynamics/.

Appendix A: Meshes for each yaw angle

- **10° yaw angle**

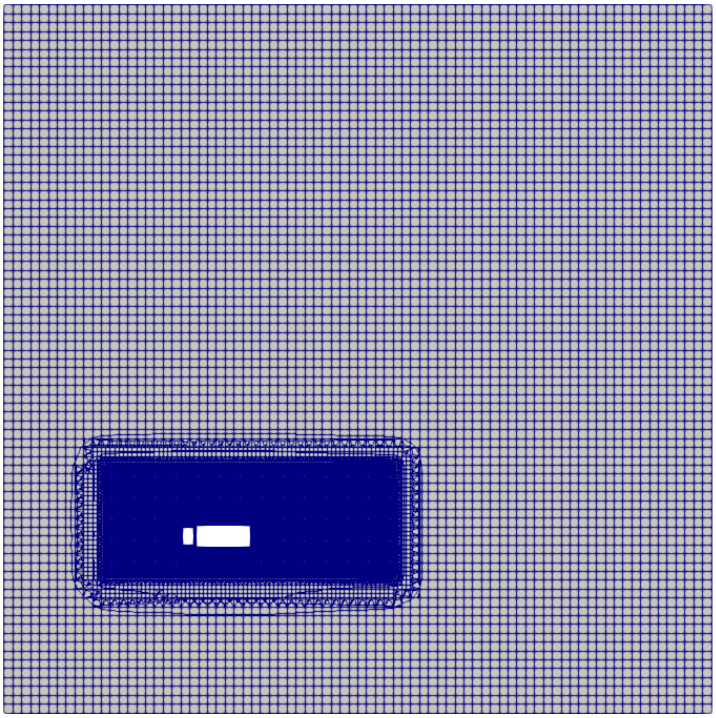

Figure 46: View of the mesh in the x-y plane for z=2 for 10° yaw angle.

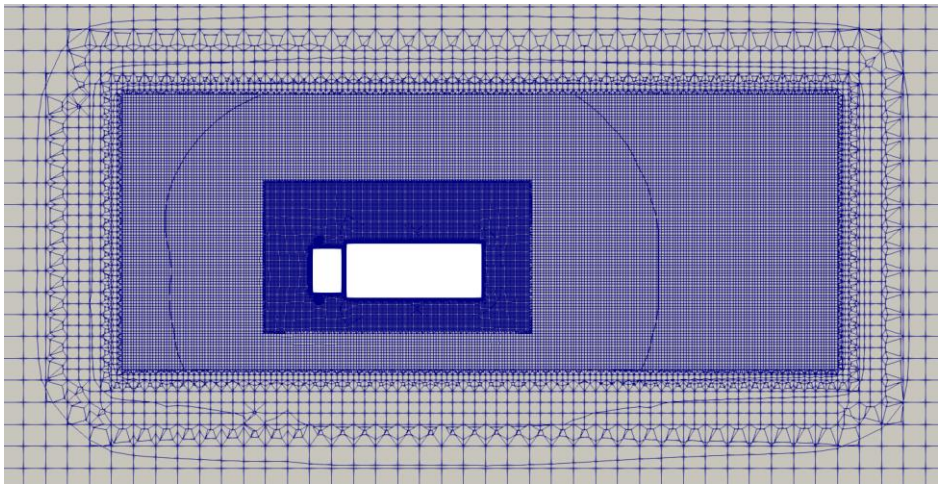

Figure 47: Detailed view of the mesh in the x-y plane for z=2 for 10° yaw angle.

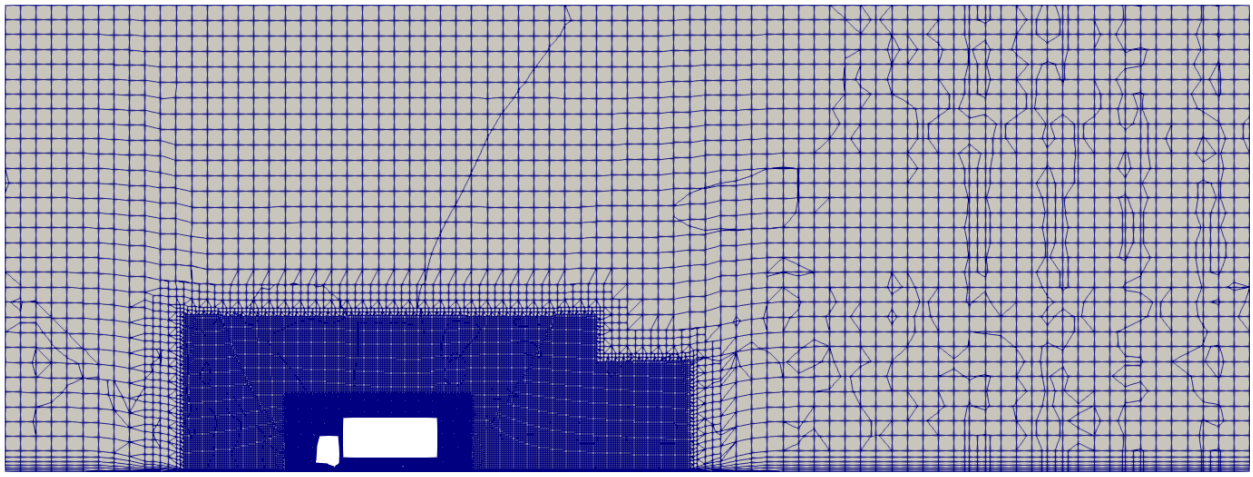

Figure 48: View of the mesh in the x-z plane for y=0 for 10° yaw angle.

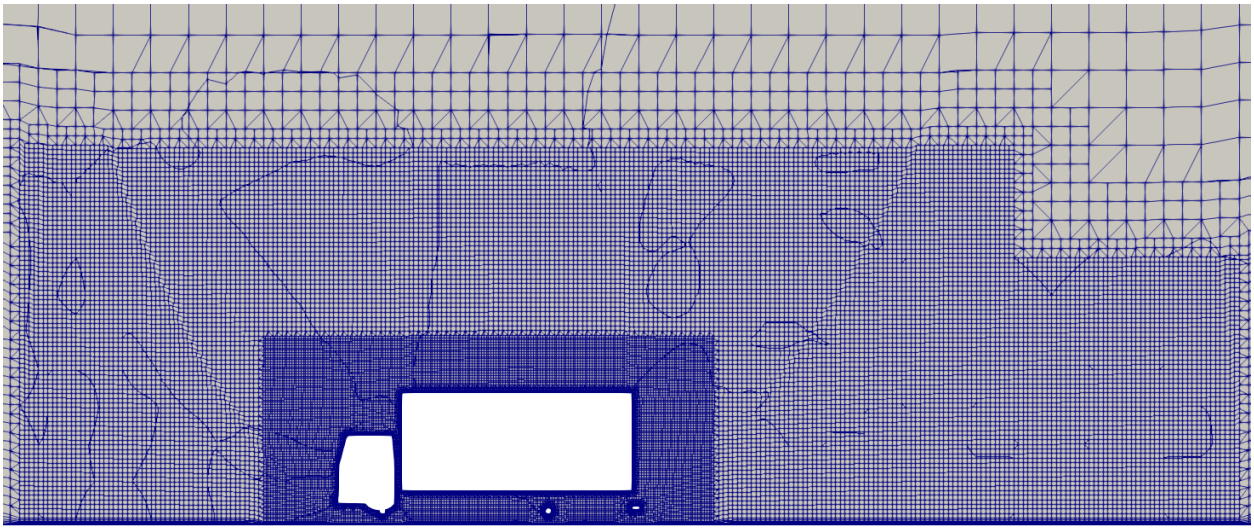

Figure 49: Detailed view of the mesh in the x-z plane for y=0 for 10° yaw angle.

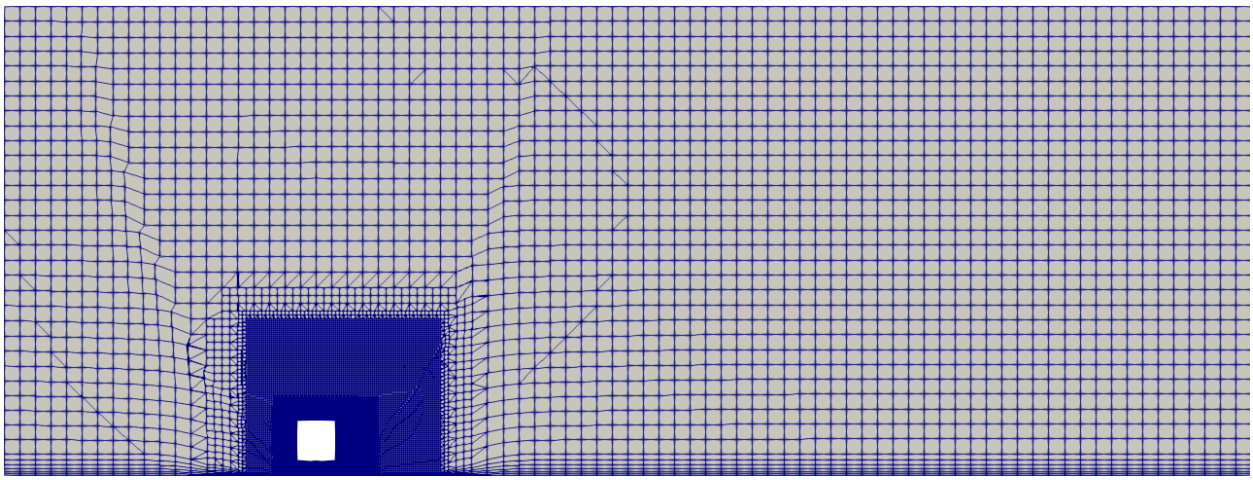

Figure 50: View of the mesh in the y-z plane for x=2 for 10° yaw angle.

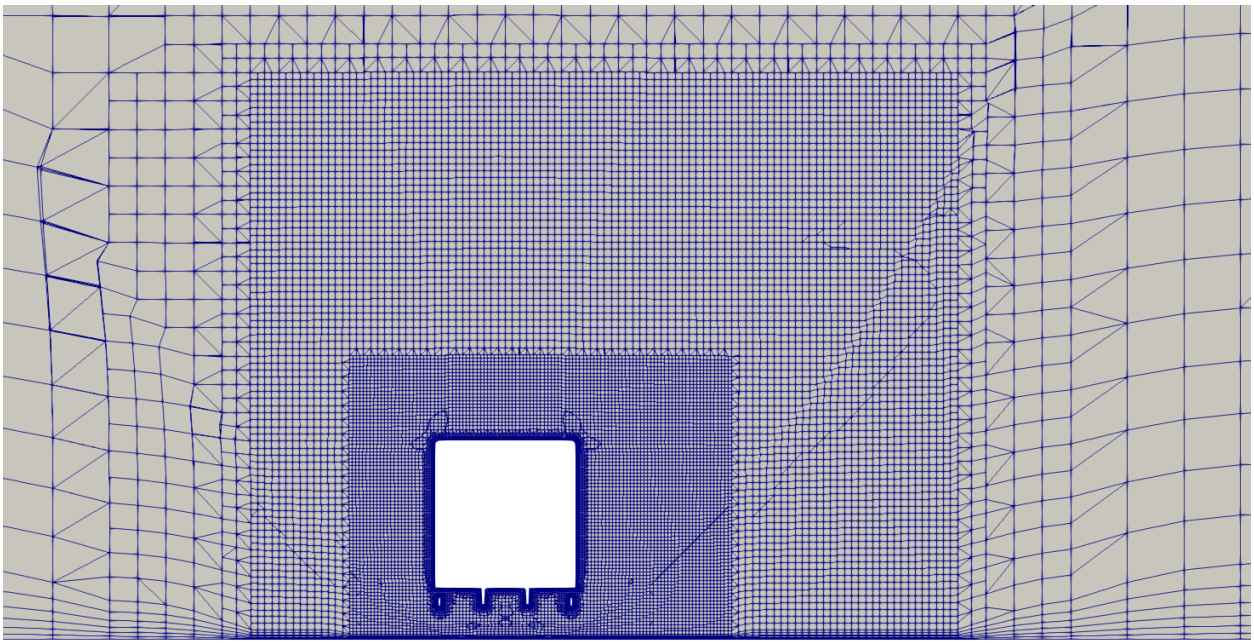

Figure 51: Detailed view of the mesh in the y-z plane for x=0 for 10° yaw angle.

- Refinement boxes:

```
refinementBox1
    {
        type searchableBox;
        min (-2 -2.8 0.0);
        max ( 10.0 4.0 5.0);
    }
    refinementBox2
    {
        type searchableBox;
        min (-8.5 -4.5 0.0);
        max ( 18 8 10.0);
    }
    refinementBox3
    {
        type searchableBox;
        min (-8.5 -4.5 0.0);
        max ( 24 8 7.0);
    }
```

- **20° yaw angle**

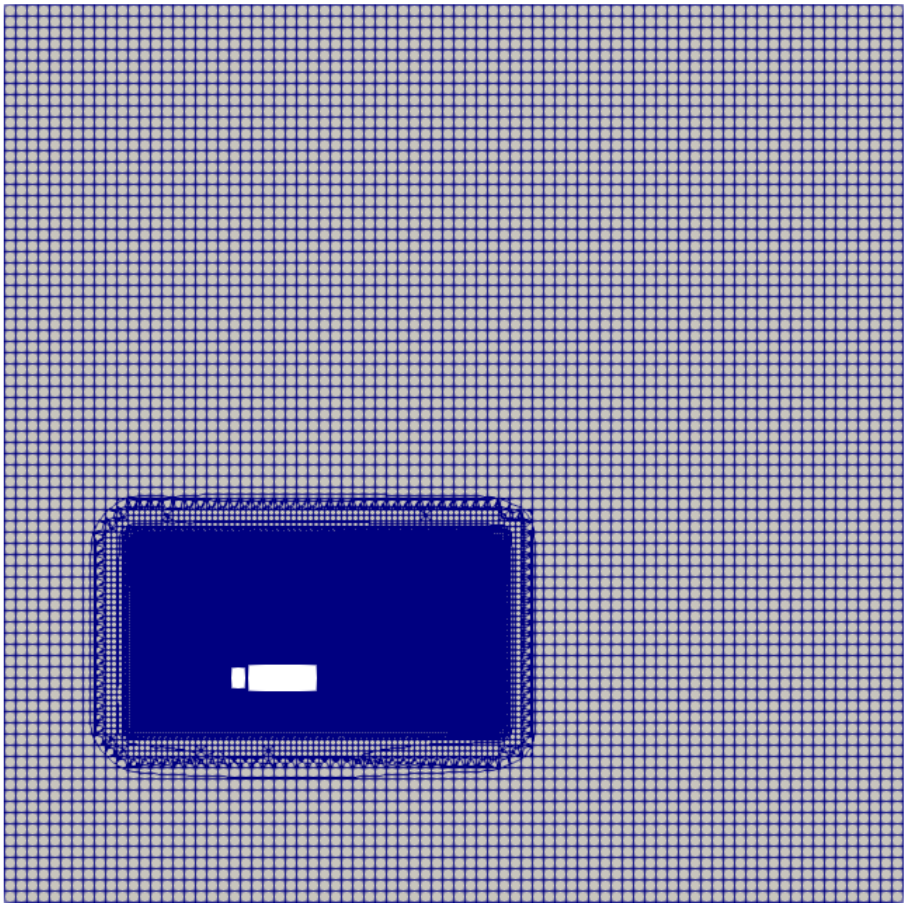

Figure 52: View of the mesh in the x-y plane for z=2 for 20° yaw angle.

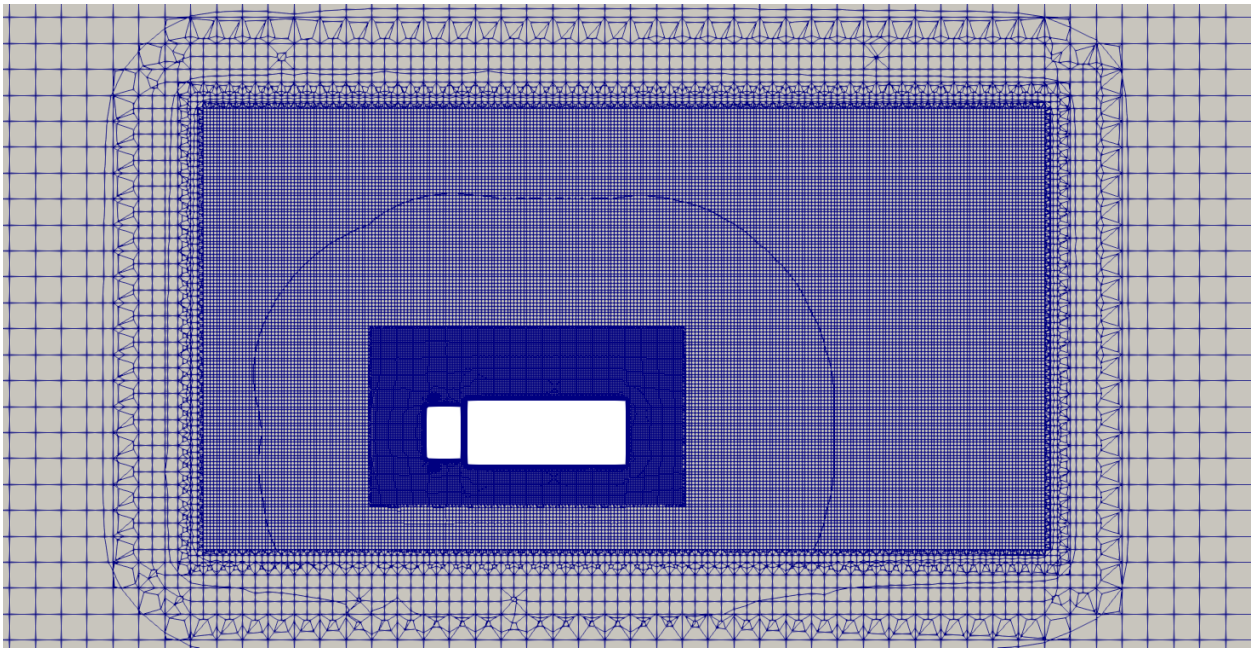

Figure 53: Detailed view of the mesh in the x-y plane for z=2 for 20° yaw angle.

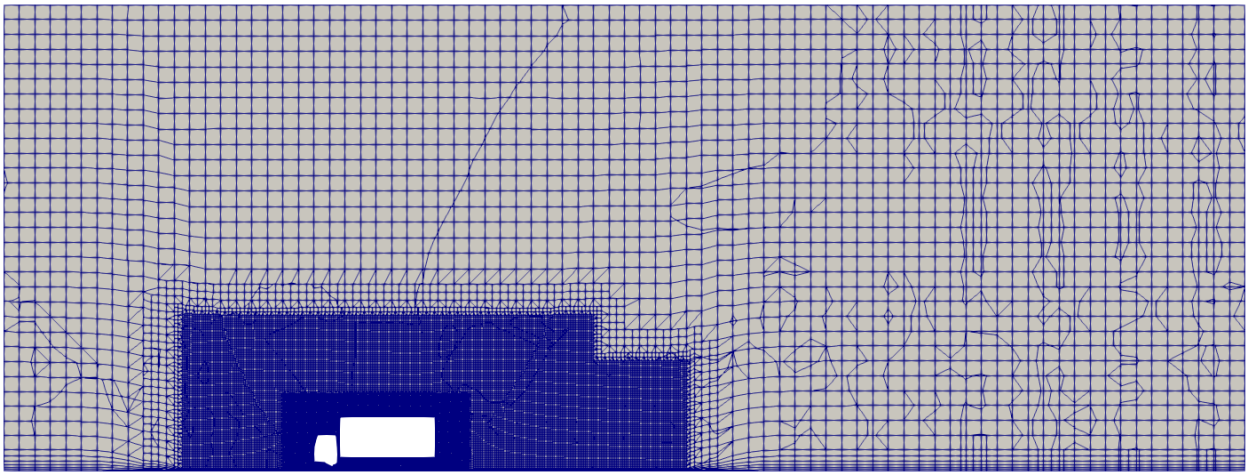

Figure 54: View of the mesh in the x-z plane for y=0 for 20° yaw angle.

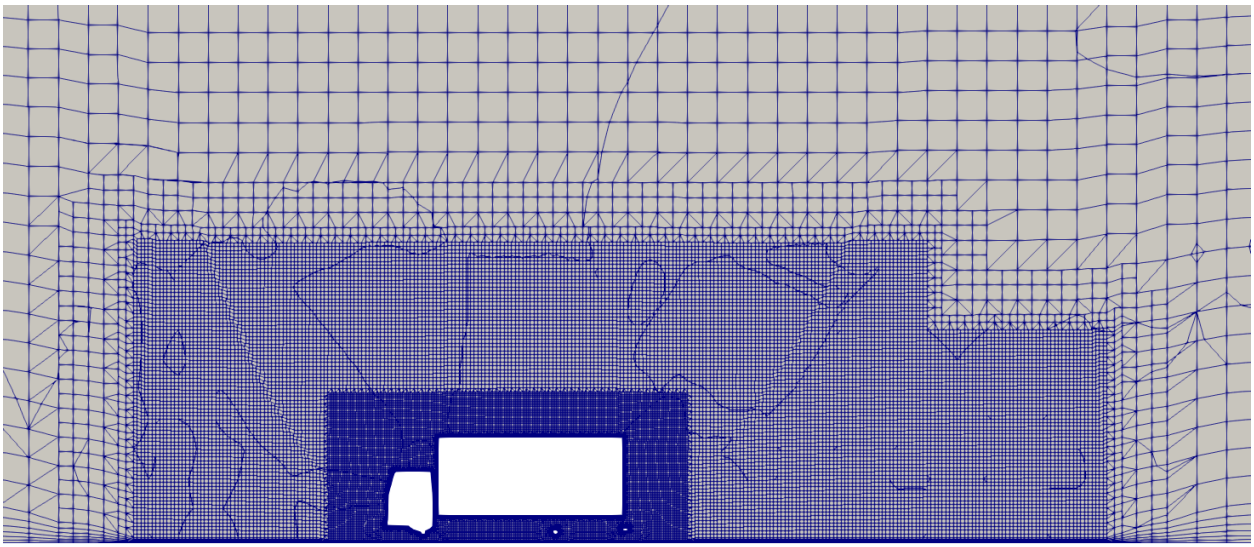

Figure 55: Detailed view of the mesh in the x-z plane for y=0 for 20° yaw angle.

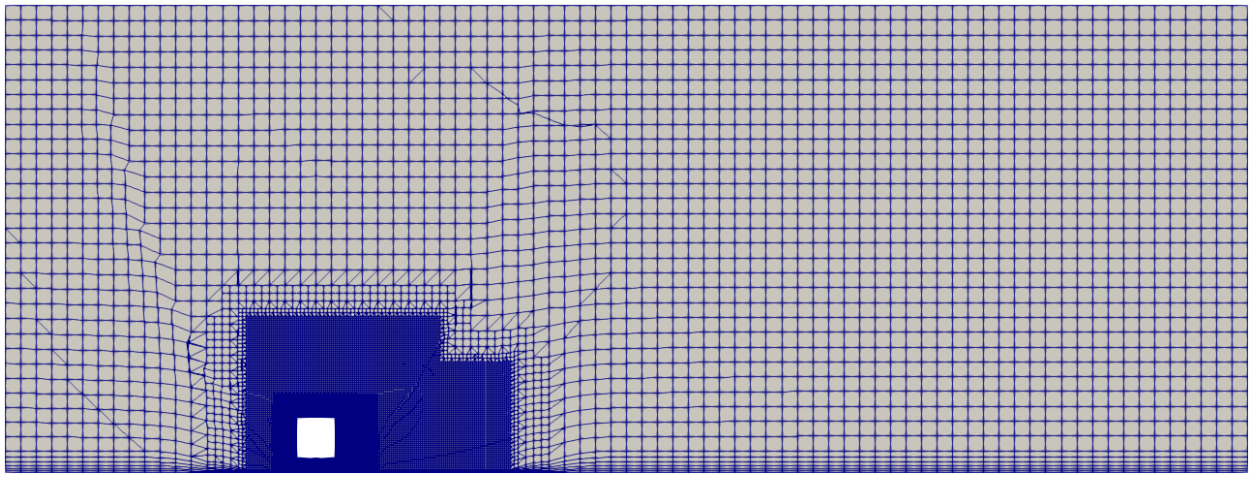

Figure 56: View of the mesh in the y-z plane for x=2 for 20° yaw angle.

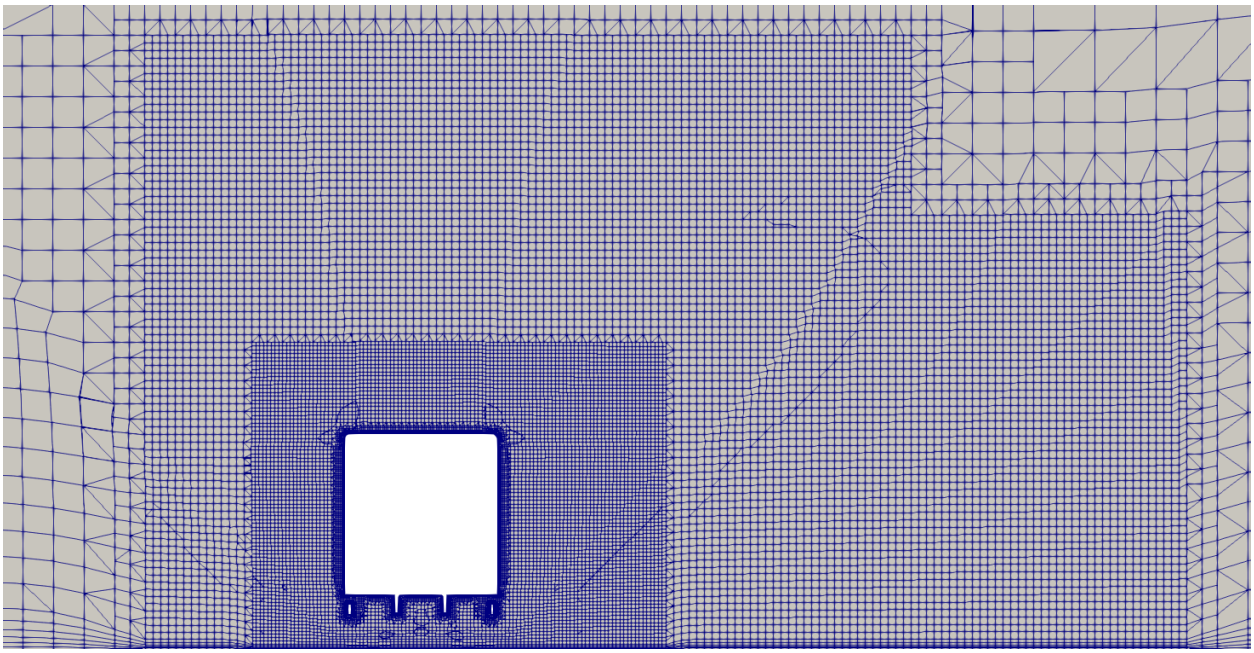

Figure 57: Detailed view of the mesh in the y-z plane for x=2 for 20° yaw angle.

- Refinement boxes:

```
refinementBox1
    {
        type searchableBox;
        min (-2 -2.8 0.0);
        max ( 10.0 4.0 5.0);
    }
    refinementBox2
    {
        type searchableBox;
        min (-8.5 -4.5 0.0);
        max ( 18 8 10.0);
```

```
    }
    refinementBox3
    {
        type searchableBox;
        min (-8.5 -4.5 0.0);
        max ( 24 12.5 7.0);
    }
```

- **30° yaw angle**

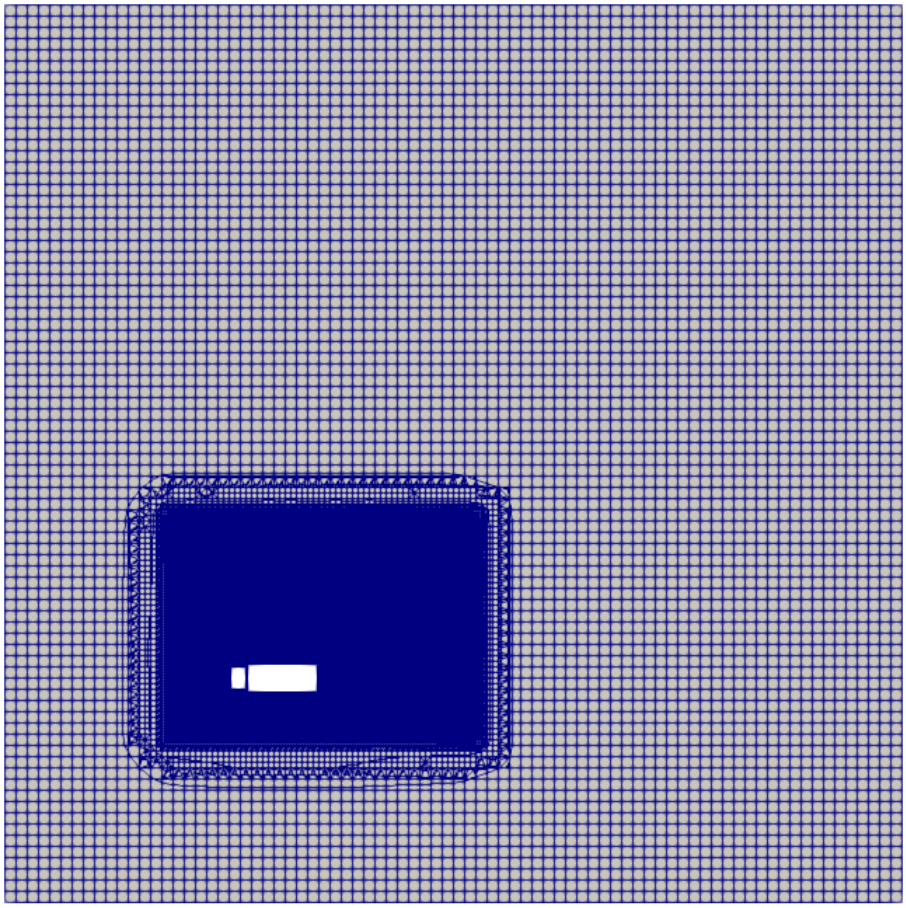

Figure 58: View of the mesh in the x-y plane for z=2 for 30° yaw angle.

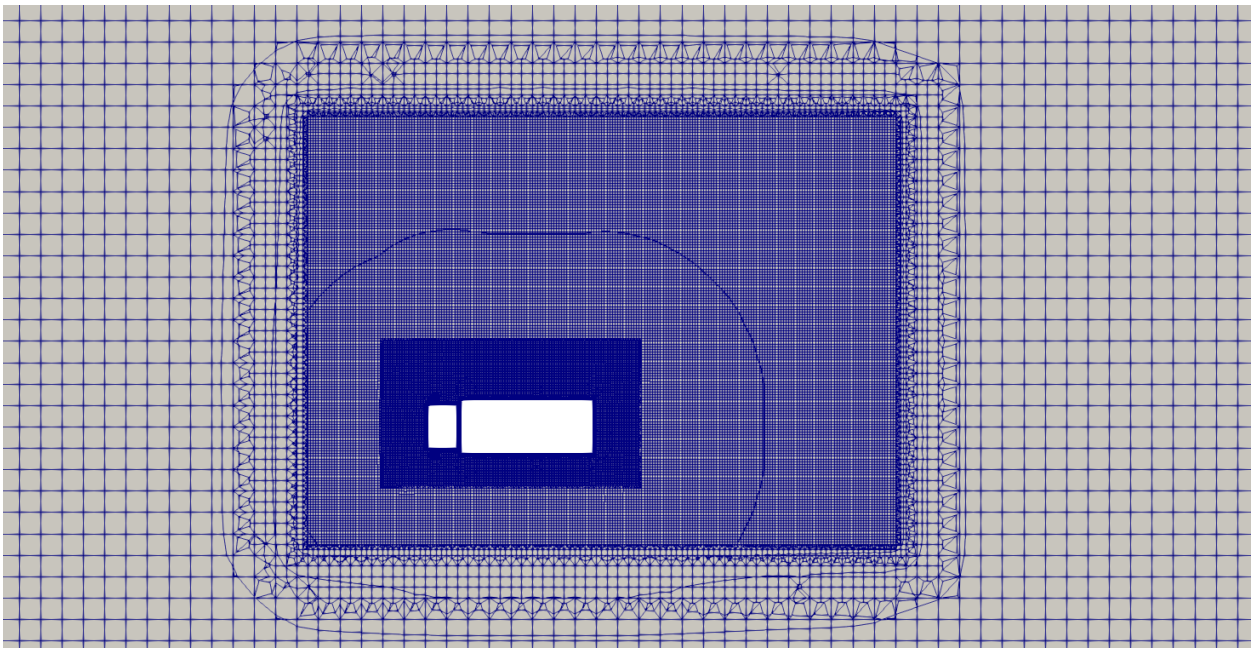

Figure 59: Detailed view of the mesh in the x-y plane for z=2 for 30° yaw angle.

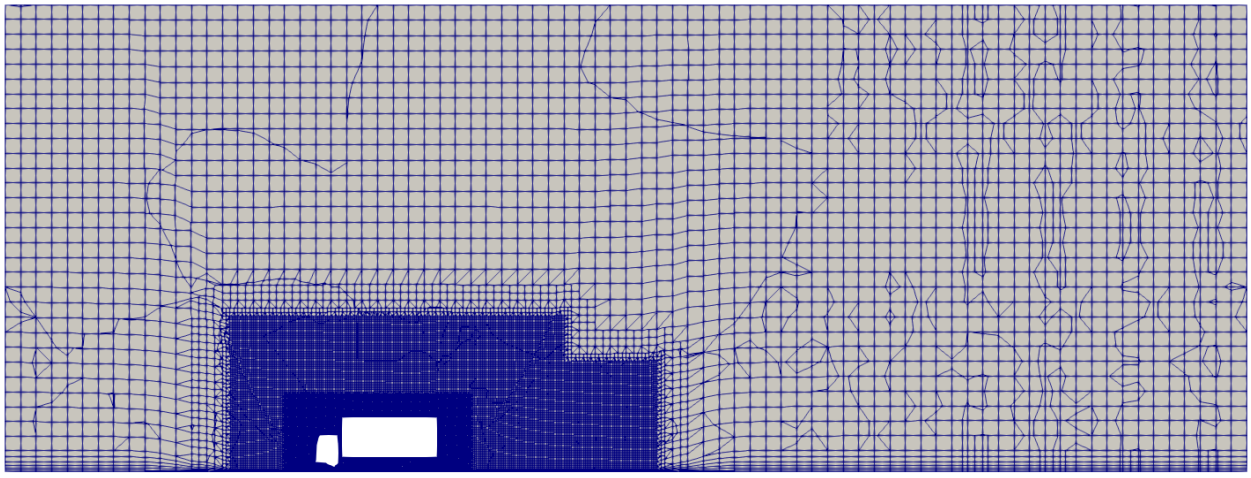

Figure 60: View of the mesh in the x-z plane for y=0 for 30° yaw angle.

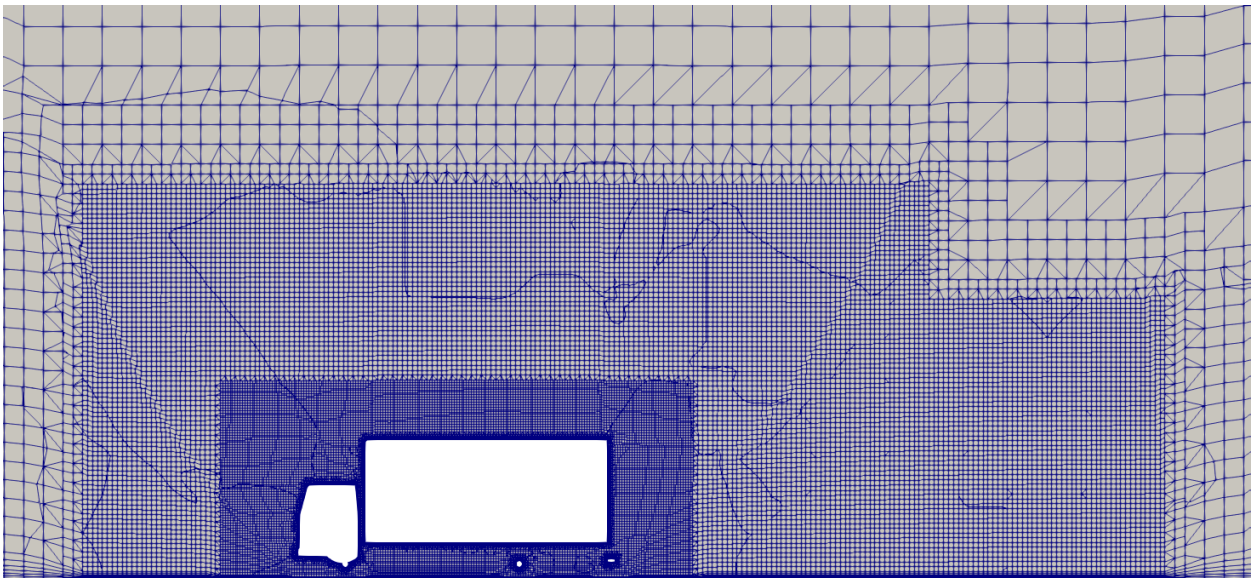

Figure 61: Detailed view of the mesh in the x-z plane for y=o for 30° yaw angle.

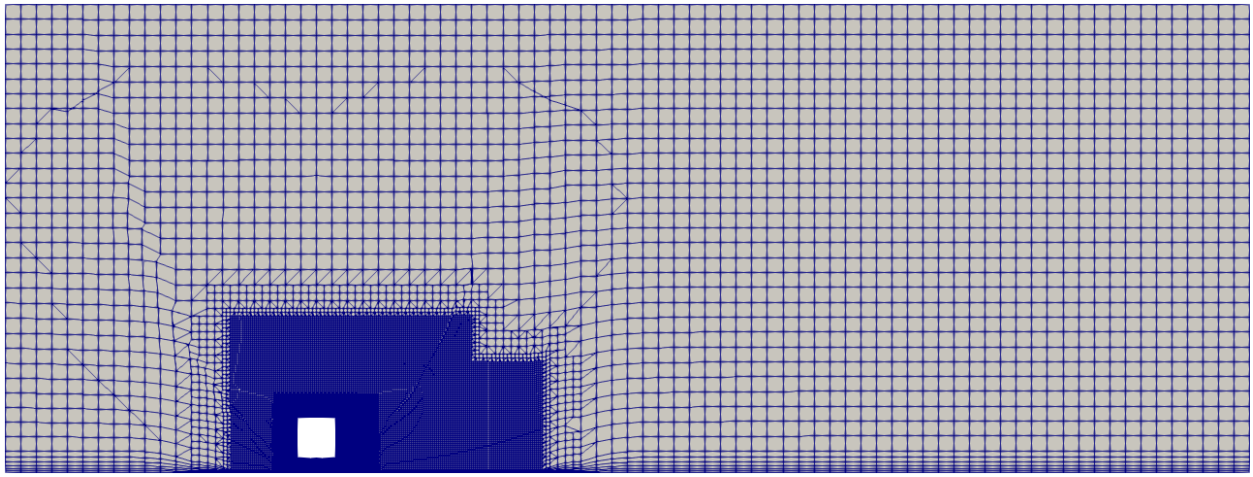

Figure 62: View of the mesh in the y-z plane for x=2 for 30° yaw angle.

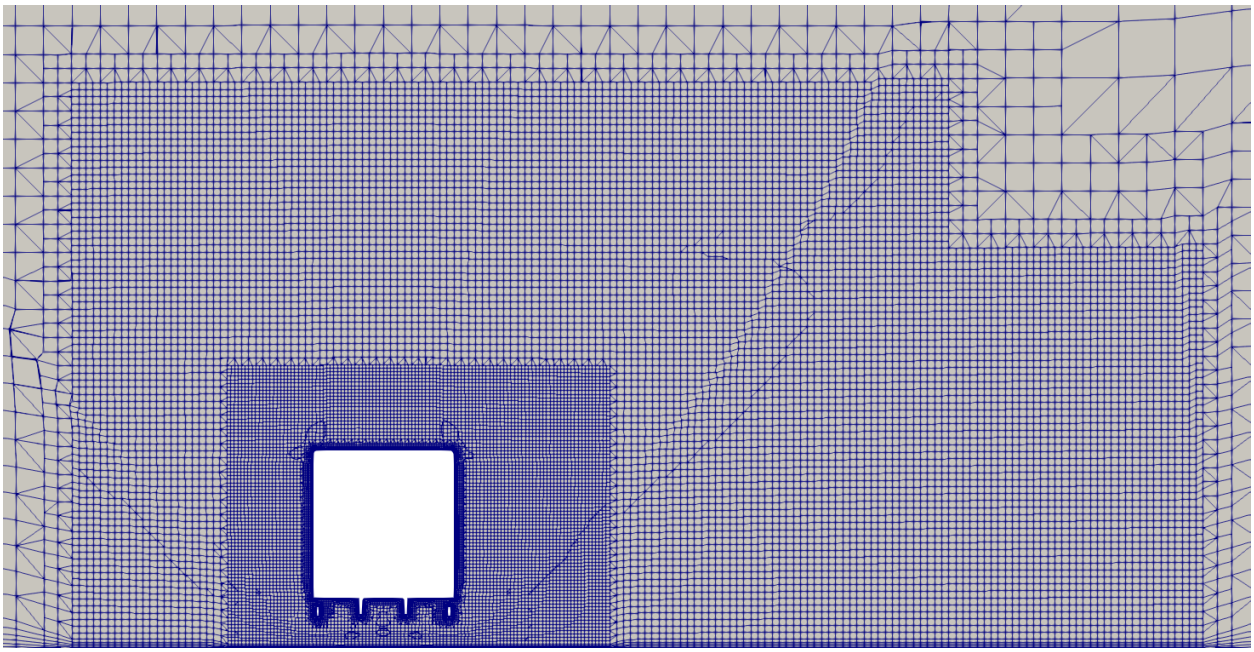

Figure 63: Detailed view of the mesh in the y-z plane for x=2 for 30° yaw angle.

- Refinement boxes:

```
refinementBox1
    {
        type searchableBox;
        min (-2 -2.8 0.0);
        max ( 10.0 4.0 5.0);
    }
    refinementBox2
    {
        type searchableBox;
        min (-5.5 -5.5 0.0);
        max ( 16 10 10.0);
    }
    refinementBox3
    {
        type searchableBox;
        min (-5.5 -5.5 0.0);
        max ( 22 14.5 7.0);
    }
```

- **40° yaw angle**

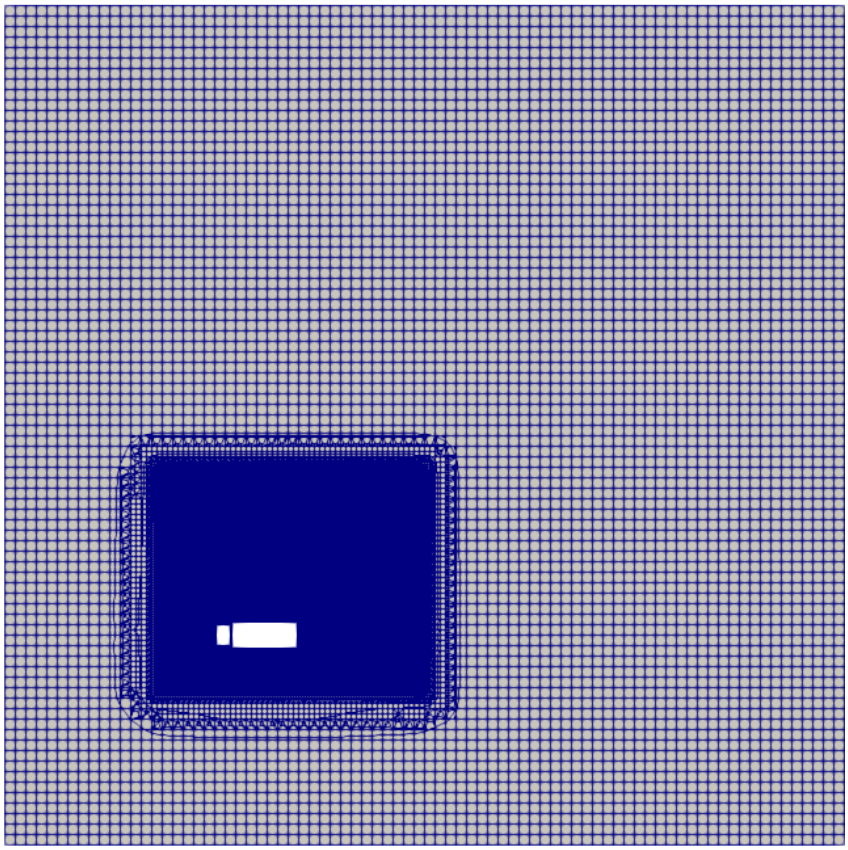

Figure 64: View of the mesh in the x-y plane for z=2 for 40° yaw angle.

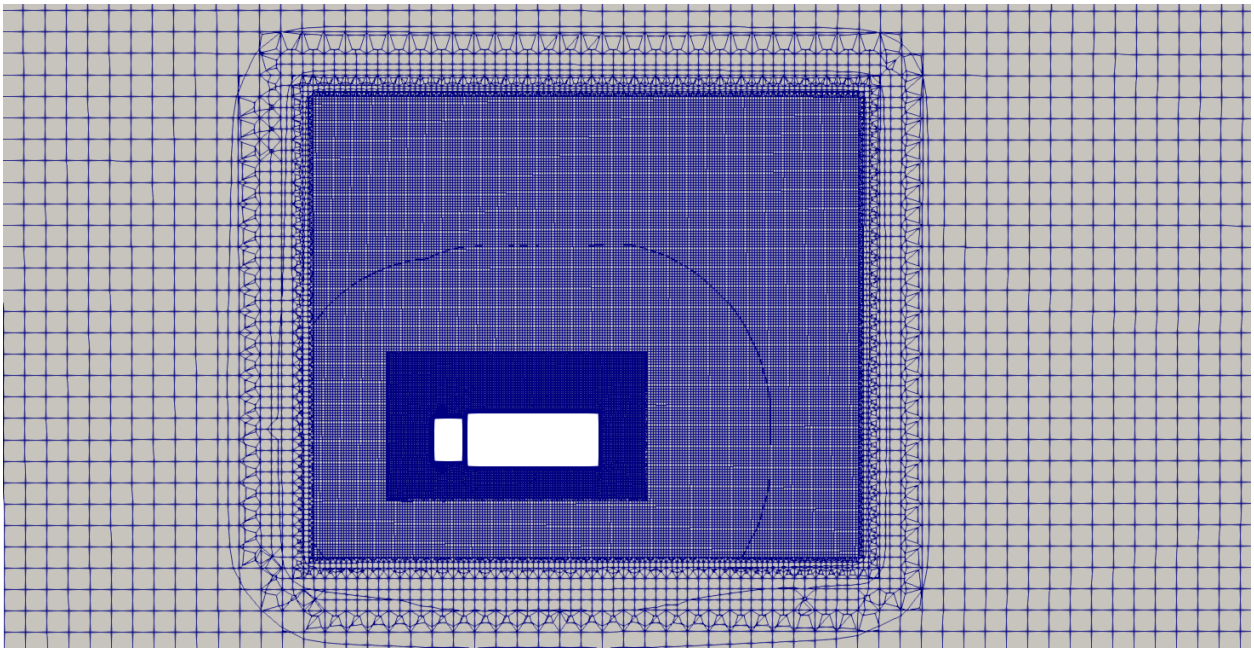

Figure 65: Detailed view of the mesh in the x-y plane for z=2 for 40° yaw angle.

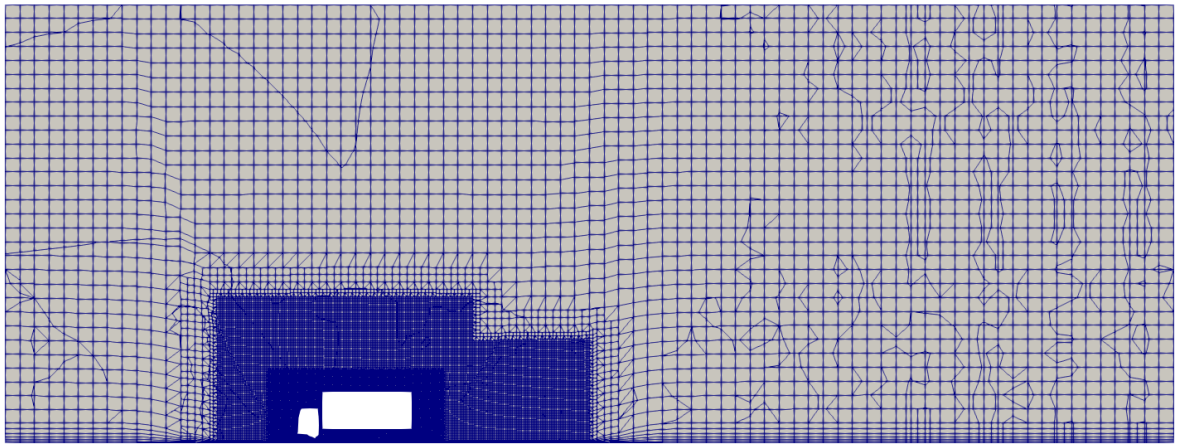

Figure 66: View of the mesh in the x-z plane for y=0 for 40° yaw angle.

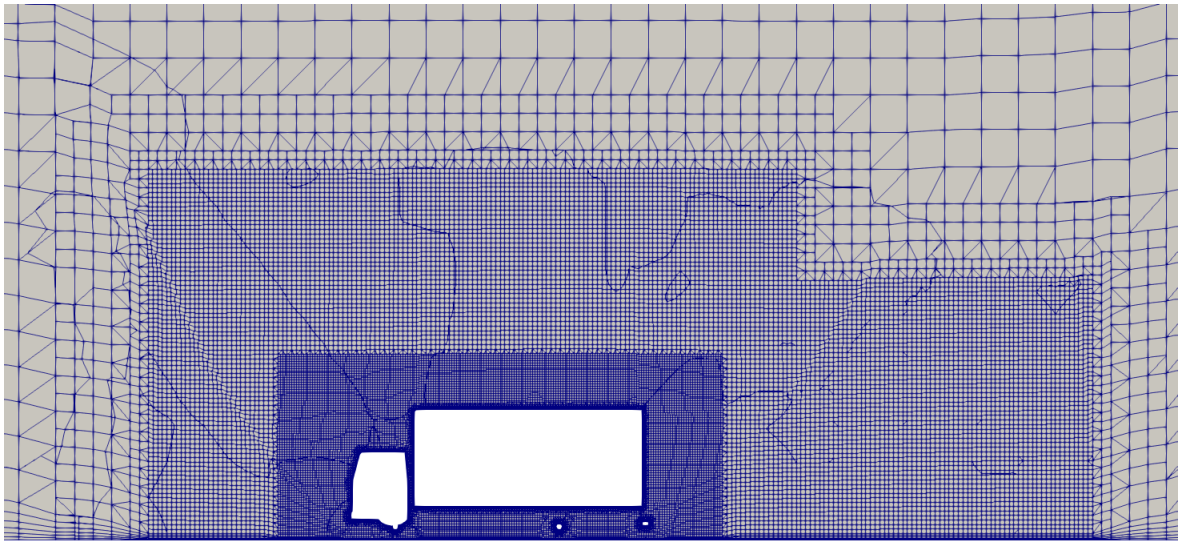

Figure 67: Detailed view of the mesh in the x-z plane for y=0 for 40° yaw angle.

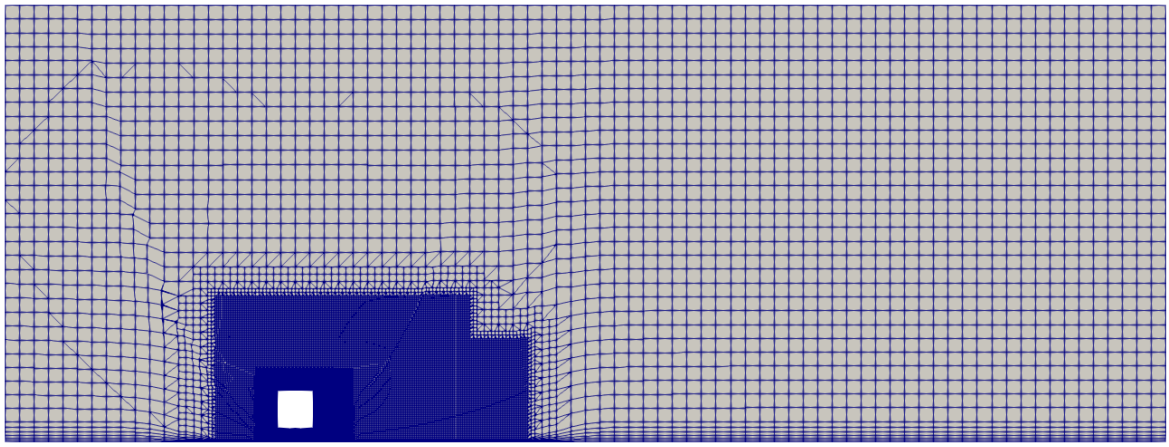

Figure 68: View of the mesh in the y-z plane for x=2 for 40° yaw angle.

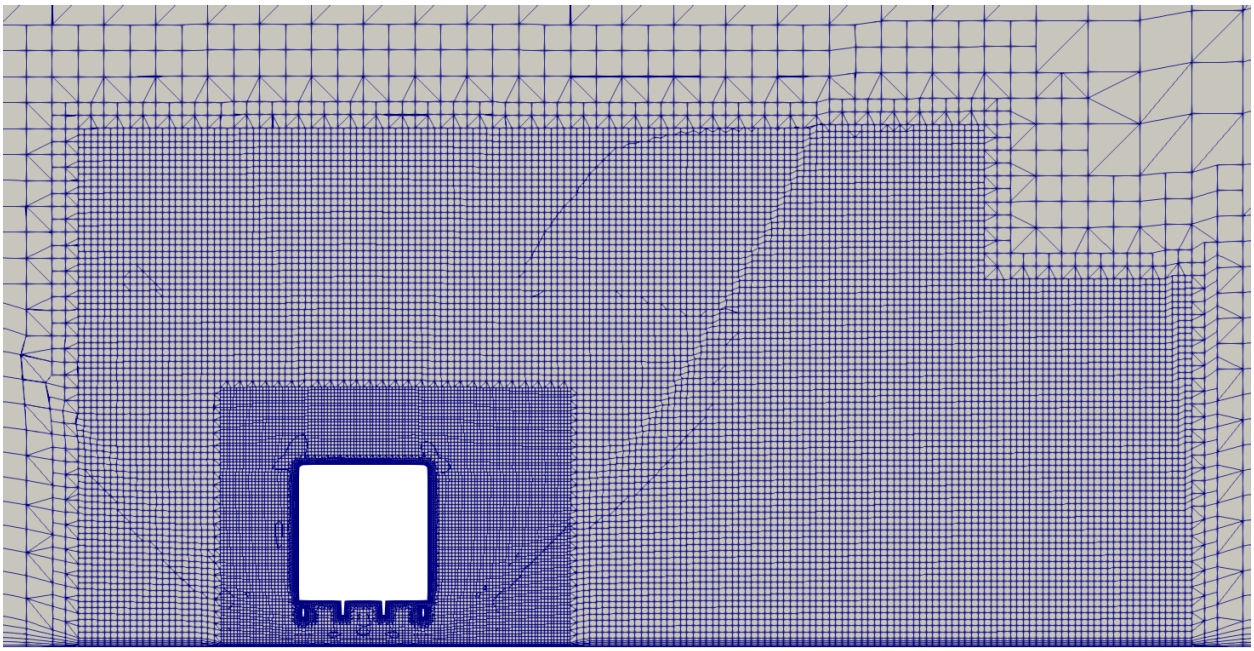

Figure 69: Detailed view of the mesh in the y-z plane for x=2 for 40° yaw angle.

- Refinement boxes:

```
refinementBox1
    {
        type searchableBox;
        min (-2 -2.8 0.0);
        max ( 10.0 4.0 5.0);
    }
    refinementBox2
    {
        type searchableBox;
        min (-5.5 -5.5 0.0);
        max ( 12.0 12.0 10.0);
    }
    refinementBox3
    {
        type searchableBox;
        min (-5.5 -5.5 0.0);
        max ( 20.0 16.0 7.0);
    }
```

- **50° yaw angle**

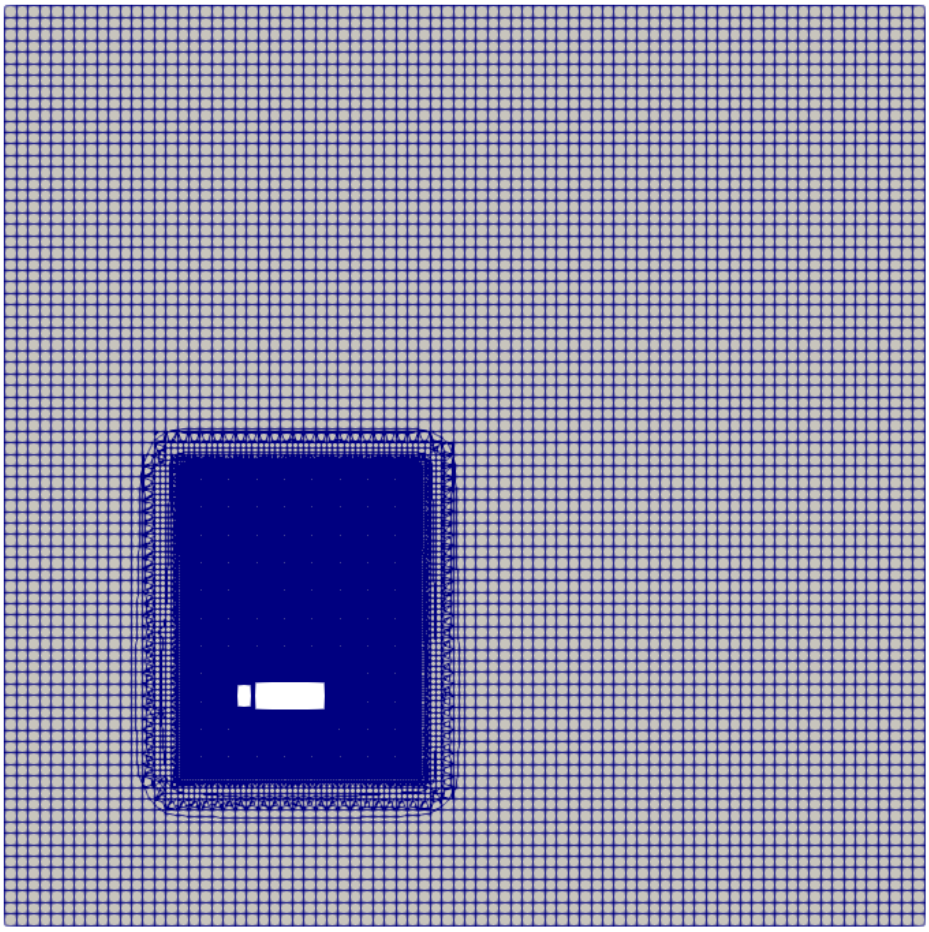

Figure 70: View of the mesh in the x-y plane for z=2 for 50° yaw angle.

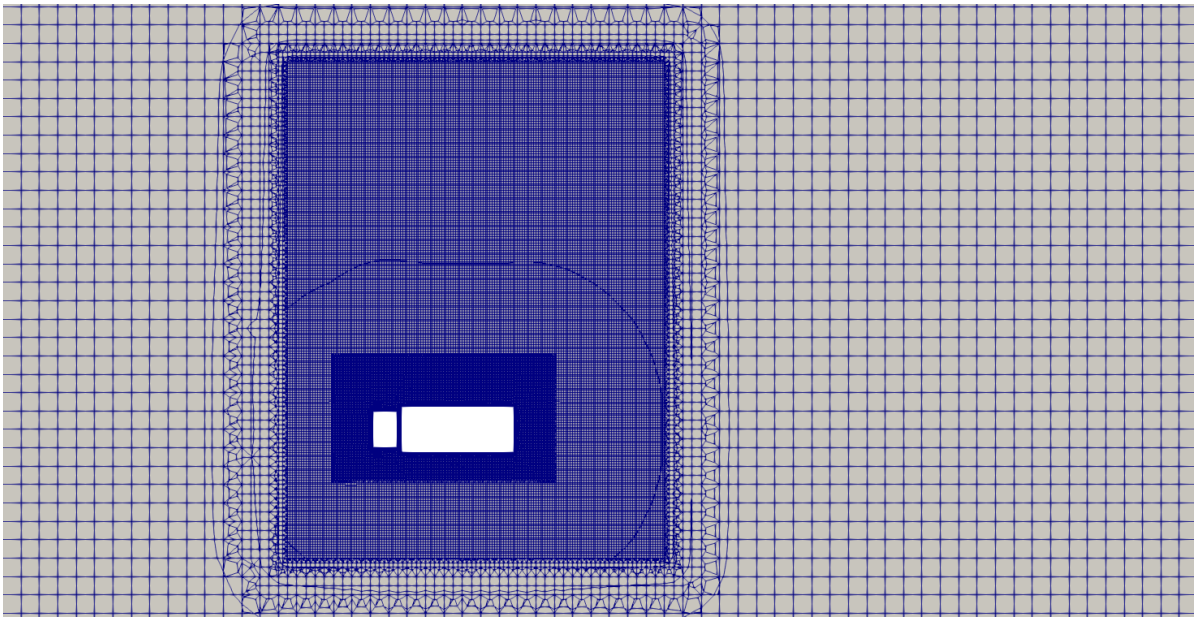

Figure 71: Detailed view of the mesh in the x-y plane for z=2 for 50° yaw angle.

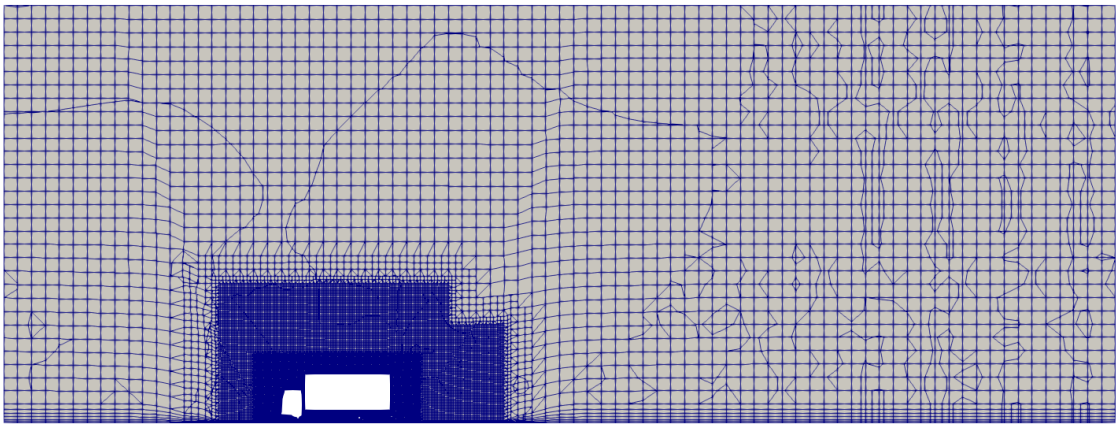

Figure 72: View of the mesh in the x-z plane for y=0 for 50° yaw angle.

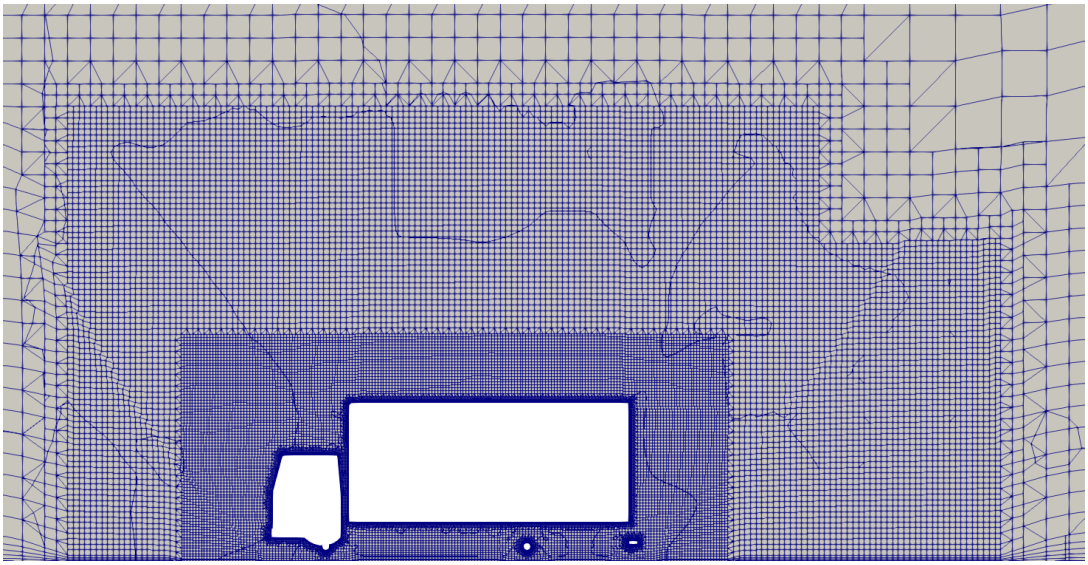

Figure 73: Detailed view of the mesh in the x-z plane for y=0 for 50° yaw angle.

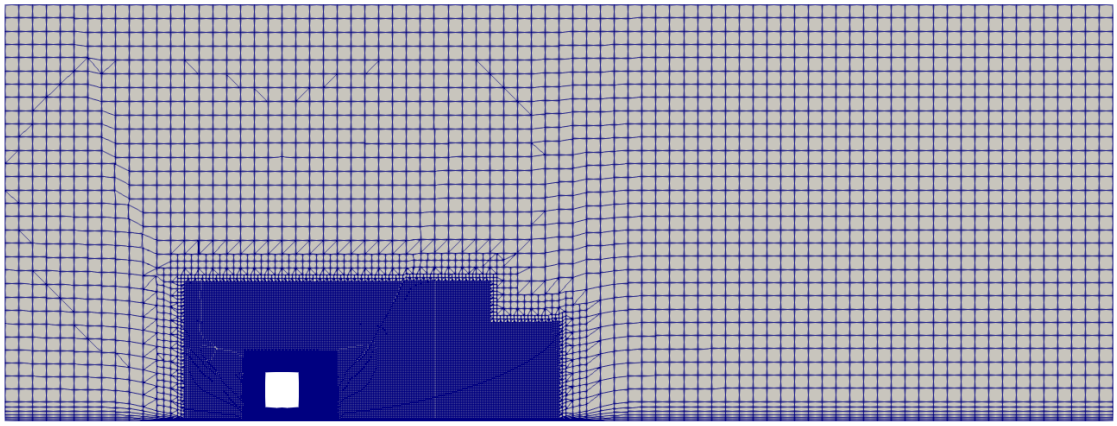

Figure 74: View of the mesh in the y-z plane for x=2 for 50° yaw angle.

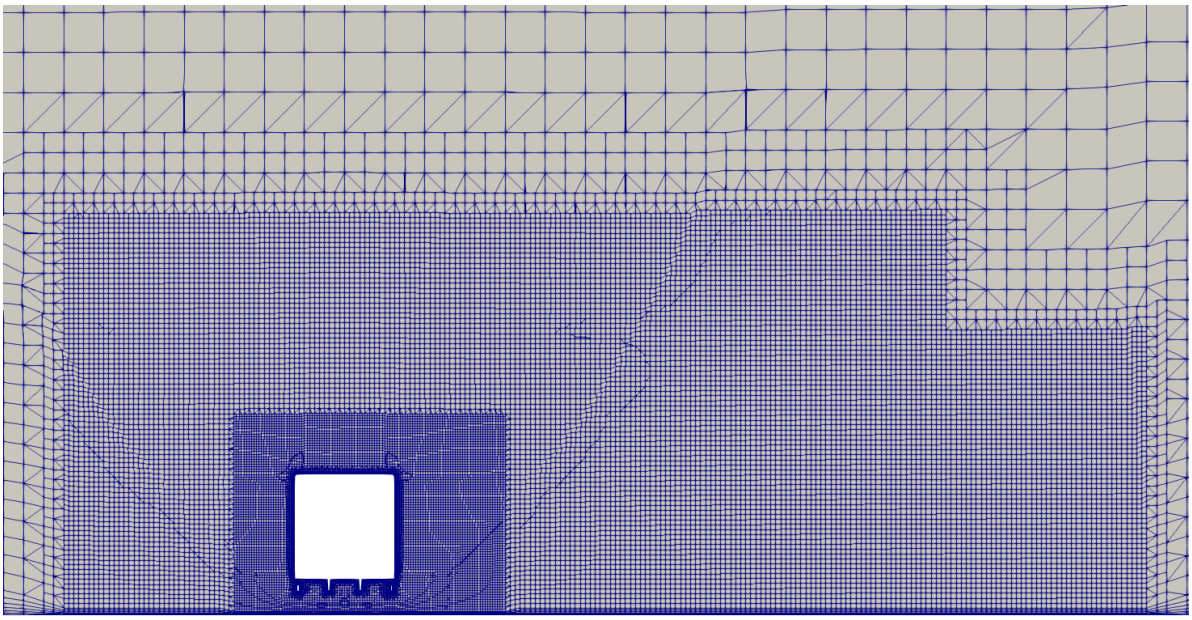

Figure 75: Detailed view of the mesh in the y-z plane for x=2 for 50° yaw angle.

- Refinement boxes:

```
refinementBox1
    {
        type searchableBox;
        min (-2 -2.8 0.0);
        max ( 10 4.0 5.0);
    }
    refinementBox2
    {
        type searchableBox;
        min (-4.5 -7 0.0);
        max ( 12 15 10.0);
    }
    refinementBox3
    {
        type searchableBox;
        min (-4.5 -7 0.0);
        max ( 16.0 20.0 7.0);
    }
```

- **Fences**

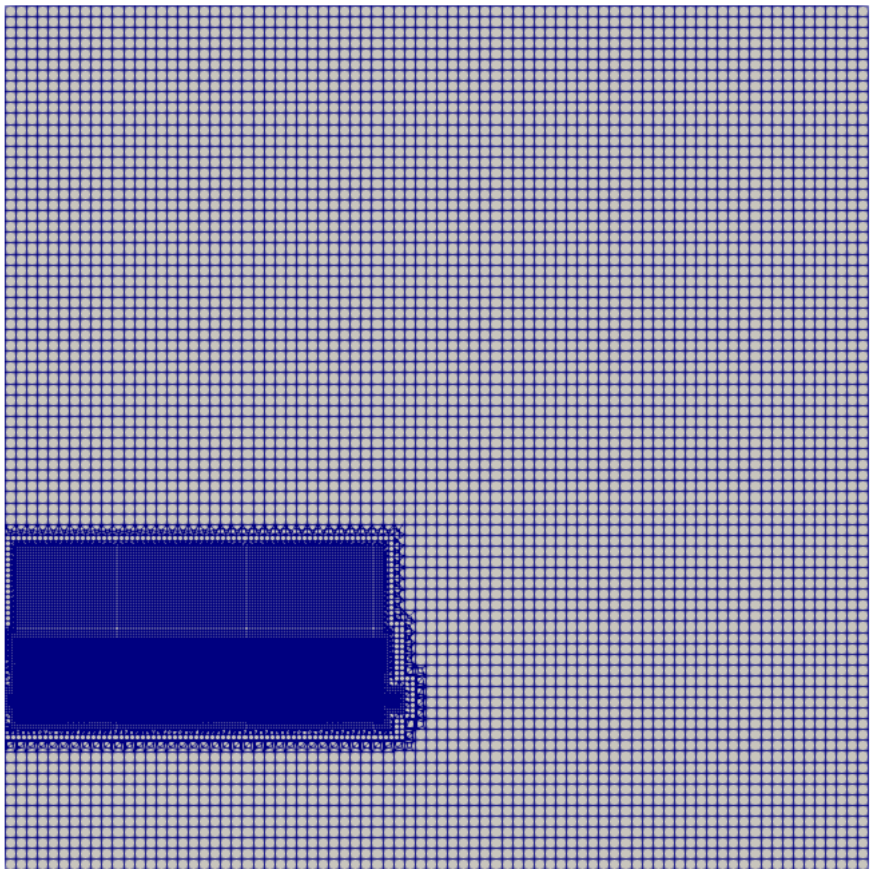

Figure 76: View of the mesh in the x-y plane for z=2 for the fences.

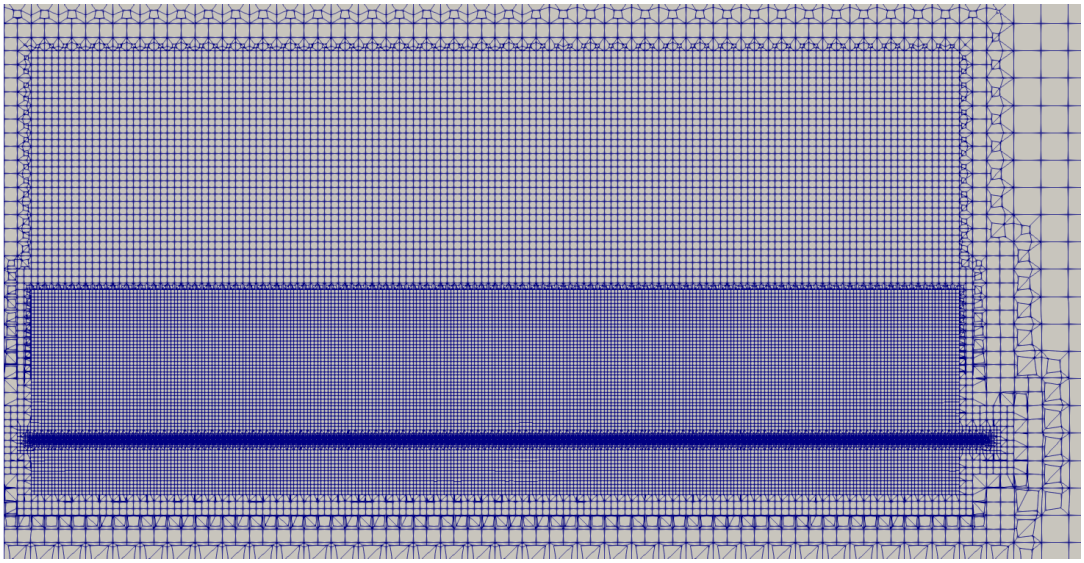

Figure 77: Detailed view of the mesh in the x-y plane for z=2 for the fences.

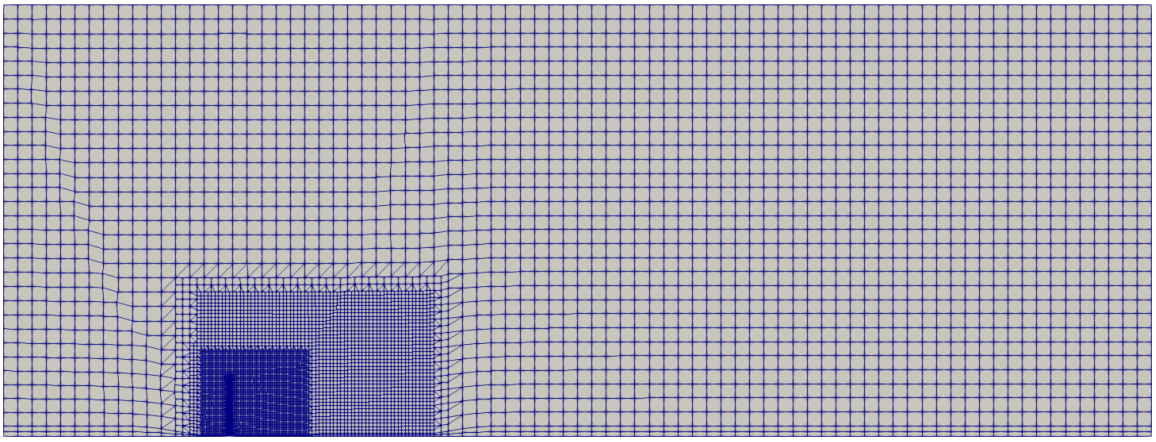

Figure 78: View of the mesh in the y-z plane for x=2 for the fences.

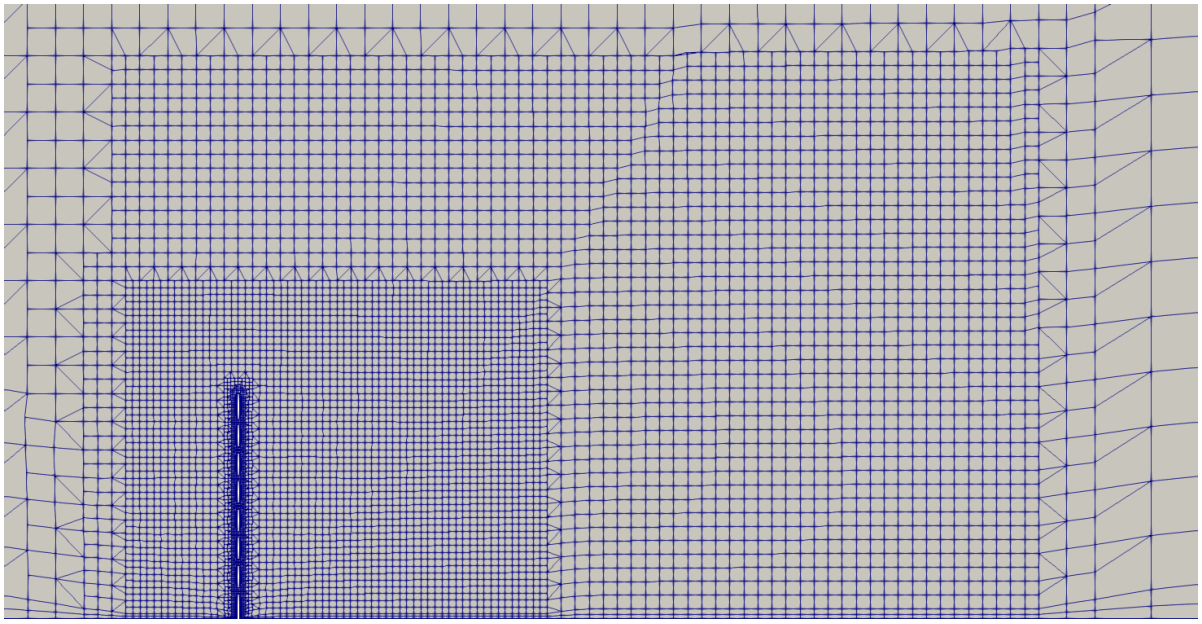

Figure 79: Detailed view of the mesh in the y-z plane for x=2 for the fences.

- Refinement boxes:

```
refinementBox1
    {
        type searchableBox;
        min (-19.0 -6.25 0.0);
        max ( 15 1.25 6.0);
    }
    refinementBox2
    {
        type searchableBox;
        min (-19.0 -6.25 0.0);
        max ( 15.0 10.0 10.0);
    }
```

Appendix B: Case base code

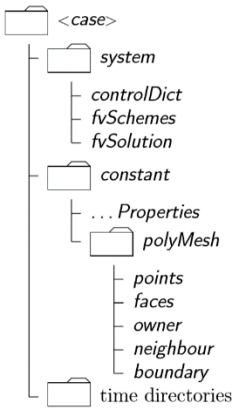

Figure 80: Case directory structure (OpenFOAM User Guide 2011).

- Case\0\k:

```
#include        "include/initialConditions"

dimensions      [0 2 -2 0 0 0 0];

internalField   uniform $turbulentKE;

boundaryField
{
    #includeEtc "caseDicts/setConstraintTypes"

    inlet
    {
        type            fixedValue;
        value           $internalField;
    }
    outlet
    {
        type            inletOutlet;
        inletValue      $internalField;
        value           $internalField;
    }
    front
    {
        type            fixedValue;
        value           $internalField;
    }
    back
```

```
    {
        type            inletOutlet;
        inletValue      $internalField;
        value           $internalField;
    }
    lowerWall
    {
        type            kqRWallFunction;
        value           $internalField;
    }
    upperWall
    {
        type            slip;
    }
    truck
    {
        type            kqRWallFunction;
        value           $internalField;
    }
    fence
    {
        type            kqRWallFunction;
        value           $internalField;
    }
}
```

- Case\0\nut:

```
dimensions      [0 2 -1 0 0 0 0];

internalField   uniform 0;

boundaryField
{
    #includeEtc "caseDicts/setConstraintTypes"

    front
    {
        type            calculated;
        value           uniform 0;
    }
    back
    {
        type            calculated;
        value           uniform 0;
    }
    inlet
    {
        type            calculated;
        value           uniform 0;
    }
    outlet
    {
```

```
        type            calculated;
        value           uniform 0;
    }
    lowerWall
    {
        type            nutkWallFunction;
        value           uniform 0;
    }
    upperWall
    {
        type            calculated;
        value           uniform 0;
    }
    truck
    {
        type            nutkWallFunction;
        value           uniform 0;
    }
    fence
    {
        type            nutkWallFunction;
        value           uniform 0;
    }
}
```

- Case\0\omega:

```
#include        "include/initialConditions"

dimensions      [0 0 -1 0 0 0 0];

internalField   uniform $turbulentOmega;

boundaryField
{
    #includeEtc "caseDicts/setConstraintTypes"

    inlet
    {
        type            fixedValue;
        value           $internalField;
    }
    outlet
    {
        type            inletOutlet;
        inletValue      $internalField;
        value           $internalField;
    }
    front
    {
        type            fixedValue;
        value           $internalField;
```

```
    }
    back
    {
        type            inletOutlet;
        inletValue      $internalField;
        value           $internalField;
    }
    lowerWall
    {
        type            omegaWallFunction;
        value           $internalField;
    }
    upperWall
    {
        type            slip;
    }
    truck
    {
        type            omegaWallFunction;
        value           $internalField;
    }
    fence
    {
        type            omegaWallFunction;
        value           $internalField;
    }
}
```

- Case\0\p:

```
#include        "include/initialConditions"

dimensions      [0 2 -2 0 0 0 0];

internalField   uniform $pressure;

boundaryField
{
    //- Set patchGroups for constraint patches
    #includeEtc "caseDicts/setConstraintTypes"

    front
    {
        type            zeroGradient;
    }
    inlet
    {
        type            zeroGradient;
    }

    back
    {
        type            fixedValue;
```

```
        value           $internalField;
    }

    outlet
    {
        type            fixedValue;
        value           $internalField;
    }

    lowerWall
    {
        type            zeroGradient;
    }

    truck
    {
        type            zeroGradient;
    }
    fence
    {
        type            zeroGradient;
    }

    #include "include/UpperPatches"
}
```

- Case\0\U:

```
#include        "include/initialConditions"

dimensions      [0 1 -1 0 0 0 0];

internalField   uniform $flowVelocity;

boundaryField
{
    //- Set patchGroups for constraint patches
    #includeEtc "caseDicts/setConstraintTypes"

    front
    {
        type               fixedValue;
        value              $internalField;
    }

    inlet
    {
        type               fixedValue;
        value              $internalField;
    }

    back
```

```
    {
        type            inletOutlet;
        inletValue      uniform (0 0 0);
        value           $internalField;
    }

    outlet
    {
        type            inletOutlet;
        inletValue      uniform (0 0 0);
        value           $internalField;
    }

    lowerWall
    {
        type               fixedValue;
        value              uniform (19.4444 0 0);
    }

    truck
    {
        type            noSlip;
    }
    fence
    {
        type               fixedValue;
        value              uniform (19.4444 0 0);
    }

    #include "include/UpperPatches"
}
```

- Case\system\fvSchemes:

```
ddtSchemes
{
    default         steadyState;
}

gradSchemes
{
    default         Gauss linear;
    grad(U)         cellLimited Gauss linear 1;
}

divSchemes
{
    default         none;
    div(phi,U)      bounded Gauss linearUpwindV grad(U);
    div(phi,k)      bounded Gauss limitedLinear 1;;
    div(phi,omega)  bounded Gauss limitedLinear 1;;
    div((nuEff*dev2(T(grad(U))))) Gauss linear;
```

```
}

laplacianSchemes
{
    default         Gauss linear limited 0.333;
}

interpolationSchemes
{
    default         linear;
}

snGradSchemes
{
    default         limited 0.333;
}

wallDist
{
    method meshWave;
}
```

- Case\system\fvSolution:

```
solvers
{
    p
    {
        solver          GAMG;
        smoother        GaussSeidel;
        tolerance       1e-7;
        relTol          0.01;
    }

    Phi
    {
        $p;
    }

    U
    {
        solver          smoothSolver;
        smoother        GaussSeidel;
        tolerance       1e-8;
        relTol          0.1;
        nSweeps         1;
    }

    k
    {
        solver          smoothSolver;
```

```
        smoother        GaussSeidel;
        tolerance       1e-8;
        relTol          0.1;
        nSweeps         1;
    }

    omega
    {
        solver          smoothSolver;
        smoother        GaussSeidel;
        tolerance       1e-8;
        relTol          0.1;
        nSweeps         1;
    }
}

SIMPLE
{
    nNonOrthogonalCorrectors 0;
    consistent yes;
}

potentialFlow
{
    nNonOrthogonalCorrectors 15;
}

relaxationFactors
{
    fields
    {
        p               0.3;
    }
    equations
    {
        U               0.7;
        k               0.7;
        omega           0.7;
    }
}

cache
{
    grad(U);
}
```